ECSS-E-HB-31-01 Part 12A
5 December 2011

EUROPEAN COOPERATION

ECSS

FOR SPACE STANDARDIZATION

Space engineering

Thermal design handbook - Part 12: Louvers

ECSS Secretariat
ESA-ESTEC
Requirements & Standards Division
Noordwijk, The Netherlands

Foreword

This Handbook is one document of the series of ECSS Documents intended to be used as supporting material for ECSS Standards in space projects and applications. ECSS is a cooperative effort of the European Space Agency, national space agencies and European industry associations for the purpose of developing and maintaining common standards.

The material in this Handbook is a collection of data gathered from many projects and technical journals which provides the reader with description and recommendation on subjects to be considered when performing the work of Thermal design.

The material for the subjects has been collated from research spanning many years, therefore a subject may have been revisited or updated by science and industry.

The material is provided as good background on the subjects of thermal design, the reader is recommended to research whether a subject has been updated further, since the publication of the material contained herein.

This handbook has been prepared by ESA TEC MT/QR division, reviewed by the ECSS Executive Secretariat and approved by the ECSS Technical Authority.

Disclaimer

ECSS does not provide any warranty whatsoever, whether expressed, implied, or statutory, including, but not limited to, any warranty of merchantability or fitness for a particular purpose or any warranty that the contents of the item are error-free. In no respect shall ECSS incur any liability for any damages, including, but not limited to, direct, indirect, special, or consequential damages arising out of, resulting from, or in any way connected to the use of this document, whether or not based upon warranty, business agreement, tort, or otherwise; whether or not injury was sustained by persons or property or otherwise; and whether or not loss was sustained from, or arose out of, the results of, the item, or any services that may be provided by ECSS.

Published by: ESA Requirements and Standards Division
ESTEC, P.O. Box 299,
2200 AG Noordwijk
The Netherlands

Table of contents

Figures

Tables

1 Scope

Thermal louvers are thermal control surfaces whose radiation characteristics can be varied in order to maintain the correct operating temperature of a component subject to cyclical changes in the amount of heat that it absorbs or generates.

The design and construction of louvers for space systems are described in this Part 12 and a clause is also dedicated to providing details on existing systems.

The Thermal design handbook is published in 16 Parts

ECSS-E-HB-31-01 Part 1	Thermal design handbook – Part 1: View factors
ECSS-E-HB-31-01 Part 2	Thermal design handbook – Part 2: Holes, Grooves and Cavities
ECSS-E-HB-31-01 Part 3	Thermal design handbook – Part 3: Spacecraft Surface Temperature
ECSS-E-HB-31-01 Part 4	Thermal design handbook – Part 4: Conductive Heat Transfer
ECSS-E-HB-31-01 Part 5	Thermal design handbook – Part 5: Structural Materials: Metallic and Composite
ECSS-E-HB-31-01 Part 6	Thermal design handbook – Part 6: Thermal Control Surfaces
ECSS-E-HB-31-01 Part 7	Thermal design handbook – Part 7: Insulations
ECSS-E-HB-31-01 Part 8	Thermal design handbook – Part 8: Heat Pipes
ECSS-E-HB-31-01 Part 9	Thermal design handbook – Part 9: Radiators
ECSS-E-HB-31-01 Part 10	Thermal design handbook – Part 10: Phase – Change Capacitors
ECSS-E-HB-31-01 Part 11	Thermal design handbook – Part 11: Electrical Heating
ECSS-E-HB-31-01 Part 12	Thermal design handbook – Part 12: Louvers
ECSS-E-HB-31-01 Part 13	Thermal design handbook – Part 13: Fluid Loops
ECSS-E-HB-31-01 Part 14	Thermal design handbook – Part 14: Cryogenic Cooling
ECSS-E-HB-31-01 Part 15	Thermal design handbook – Part 15: Existing Satellites
ECSS-E-HB-31-01 Part 16	Thermal design handbook – Part 16: Thermal Protection System

2 References

ECSS-S-ST-00-01	ECSS System - Glossary of terms

All other references made to publications in this Part are listed, alphabetically, in the **Bibliography**.

3 Terms, definitions and symbols

3.1 Terms and definitions

For the purpose of this Standard, the terms and definitions given in ECSS-S-ST-00-01 apply.

3.2 Symbols

A	Clause 5: bellows effective area, [m^2]
	Clause 7: contact surface (bourdon sensing element), [m^2]
B	radiosity, [W.m^{-2}]
B*	dimensionless radiosity, $B^* = B/\sigma T^4$
D_i	bellows innermost diameter, [m]
D_o	bellows outermost diameter, [m]
E	modulus of elasticity, [N.m^{-2}]
F	flexibility, [m.Pa^{-1}]
F_c	coil force constant, [N.m^{-2}.Angular degrees^{-1}]
H	energy flux impinging on the unit area, [W.m^{-2}]
J	heat flux to the skin arriving from outside, [W.m^{-2}]
K	bellows spring rate, [N.m^{-1}]
K_c	coil deflection constant, [angular degrees, K^{-1}]
L	Clause 5: coil active length, [m]
	Clause 5: length of all convolutions in bellows, [m]
	Clause 6: louver blade spacing, [m]

L_c	length of a single convolution in bellows measured along the surface, [m]
M	torsional moment of a coil, [N.m]
P	fluid pressure, [Pa]
P_t	proportionality limit pressure in a bourdon, [Pa]
Q	heat transfer to the fluid within the bourdon, [J]
Q_0	heat transfer to the fluid within the bourdon after an infinitely large time, [J]
R(θ)	equivalent thermal resistance of the louver system, it is a function of the optical properties of blades, and inner skin surface, but for a given system *R* depends only on the blade angle
R_0	coiling radius of a bourdon, [m]
R_m	mean radius of the bellows, [m]
S	heat flux from the space to the skin, [W.m^{-2}]
S_0	solar constant, $S_0 = 1353$ W.m^{-2}
T	temperature, [K]
T_C	bourdon filling fluid temperature, [K]
T_0	reference temperature, [K]
ΔT	temperature differential, [K], $\Delta T = T - T_0$
T_{0L}	starting fluid temperature, [K]
T_S	skin temperature, [K]
T*	local dimensionless temperature, $T^* = T^4/T^4_{BP}$
V	inside volume of bellows, [m^3]
X	sensitivity of a bimetal, [angular degrees, K^{-1}]
a	semi-major axis of the bourdon tube cross section, [m]
b	Clause 5: semi-minor axis of the bourdon tube section, [m] Clause 6: louver blade width, [m]

c	Clause 5: numerical coefficient given in Table 5-7 under additional data
	Clause 7: fluid specific heat, [J.kg⁻¹.K⁻¹]
f(θ)	defined as $f(\theta) = 1 - [1/R(\theta)]$
$f_{n=1}$	fundamental natural frequency, [s⁻¹]
h	total thermal conductance of a bourdon (sensing element plus fluid, [W.m⁻².K⁻¹]
l	length of a given metallic strip when the temperature is T [m]
	live length of the bellows, [m]
l_0	length of a given metallic strip when the temperature is T_0, [m]
m_a	mass of bellows active convolutions, [kg]
m_c	mass of one convolution, [kg]
m_{fa}	mass of fluid trapped in active length at rest, [kg] $m_{fa} = \rho L[0{,}262(D_o^2+D_oD_i)-0{,}524D_i^2]$
m_l	mass of liquid within the bellows, [kg]. $m_l = \rho Al$
m_1	mass on bellows free end, [kg]
m_2	bellows mass, [kg]
q	louver heat rejection capability, [W.m⁻²]
q_{shadow}	heat rejection capability for zero solar input, [W.m⁻²]
t	thickness of the strip of the coil, [m]
	wall thickness for bellows or bourdon tube, [m]
w	width of the strip of the coil, [m]
x	coordinate along the louver baseplate, [m]
y,z	Coordinates along the outer and inner faces of the blade, [m]
Φ	sun angle, [angular degrees]
α	absorptance

	numerical coefficient which appears in the expression of bourdon flexibility
α_s	solar absorptance
α_λ	spectral absorptance
β	Clause 5: linear thermal expansion coefficient, [K^{-1}]
	Clause 5: numerical coefficient which appears in that expression of bourdon flexibility
	Clause 6: Dimensionless coordinate along the louver baseplate, $\beta = x/L$
β_H	linear thermal expansion coefficient of the high expansibility component of a bimetal, [K^{-1}]
β_L	linear thermal expansion coefficient of the low expansibility component of a bimetal, [K^{-1}]
ε	hemispherical total emittance
ε_I	emittance of the skin inner surface
ε_s	emittance of the skin outer surface
η,ζ	dimensionless coordinates, $\eta = y/L$, $\zeta = z/L$
θ	Clause. 5: angular deflection of a coil, [angular degrees]
	Clause 6: louver blade angle, [angular degrees]
ν	poisson's ratio
ρ	Clauses 5 and 7: fluid density, [$kg.m^{-3}$]
	Clause 6: reflectance
ρ_λ	spectral reflectance
ρ^s	specular reflectance
ψ_0	initial coiling angle in a bourdon, also called mechanical preload angle, [angular degrees]
σ	Stefan-Boltzmann constant, $\sigma = 5{,}6697 \times 10^{-8}$ $W.m^{-2}.K^{-4}$
τ	time, [s]

Subscripts

B	concerns louver blades
B_I	concerns the inner face of the louver blade
B_0	concerns the outer face of the louver blade
B_P	concerns louver baseplate
eff	effective value

4 General introduction

Thermal louvers are thermal control surfaces whose radiation characteristics can be varied in order to maintain the proper temperature of a component which experiences cyclical changes in the amount of heat that it absorbs or generates.

Louvers are constituted by five main components: baseplate, blades, actuators, sensing elements, and structural elements.

The baseplate is a surface of low absorptance to emittance ratio which covers the critical set of components whose temperature is being controlled.

The blades, driven by the actuators, are the elements of the louvers which give variable radiation characteristics at the baseplate. When the blades are closed, they shield the baseplate from the surroundings, while when they are fully open, the coupling by radiation of the baseplate to the surroundings is the largest.

The radiation characteristics of the baseplate can be varied in the range defined by these two extreme positions of the blades.

The actuators are the elements of the louvers which drive the blades according to the temperature sensed by sensors placed in the baseplate. Up to now, the actuators of the louvers flown on satellites have been bimetal spirals or bellows, although other types could be used, such as Bourdon spirals, and electrical devices.

In a single actuation system all the blades are driven by the same actuator. In the multiple blade actuator system several actuators are required to operate the system. Generally, bimetals are used as multiple blade actuation system, and bellows as single blade systems.

The sensing element senses the temperature of the baseplate and activates the actuators, which drive the blades according to this temperature. The type of sensing element depends on the kind of actuator. When the actuator is a bimetal, the sensing element is the bimetal itself. If the actuators are bellows or Bourdon, the sensing element can be a tank or a tube, containing a liquid or a liquid-vapor mixture, and soldered to the baseplate.

The different components of the louver system are supported by means of a frame. When bimetallic actuators are used, they are enclosed in a housing to shield the bimetal from the environment. This actuator housing may be a structural part of the frame.

Louver systems can be made for shadow or sunlight operation. In the first case heat is radiated through the louver to the outer skin of the spacecraft, while in the second the excess heat is transferred from the emitting baseplate to the outer space.

Louvers do not consume power except those that are electrically actuated.

5 Components of a louver

5.1 Blades

Louver blades are normally of rectangular plan form. Trapezoidal plan forms are preferred for circular assemblies.

Each blade is mounted around a shaft. This provides the torsional stiffness required to transmit the actuator torque:

Characteristics of blades used in several existing configurations are given in Table 5-1.

Table 5-1: Blade Characteristics of Existing Louver Assemblies
R: Rectangular, T: Trapezoidal

<table>
<tr><th rowspan="2">PRODUCER</th><th>SPACECRAFT</th><th>α_s</th><th rowspan="2">BLADE MATERIAL</th><th>CONFIGURATION</th></tr>
<tr><th>LAUNCH DATE</th><th>ε</th><th>DIMENSIONS x10³ [m]</th></tr>
<tr><td rowspan="2"></td><td>MARINER 2</td><td>0,12</td><td rowspan="2">0,508x10^{-3} m thick Polished Aluminium</td><td>R</td></tr>
<tr><td>8/26/1962</td><td>0,04</td><td></td></tr>
<tr><td colspan="5">COMMENTS: Louver blades are center pivoted.</td></tr>
<tr><td rowspan="2"></td><td>O.G.O.</td><td>0,12</td><td rowspan="2">Two layers of 0,127x10^{-3} m thick Polished Aluminium</td><td>R</td></tr>
<tr><td>9/4/1964</td><td>0,04</td><td>500x45</td></tr>
<tr><td colspan="5">COMMENTS: The blade is a rectangular center-rotating member constructed of two formed aluminium sheets spot-welded together along the two edges. Plastic end fittings are provided at each end of the blades.</td></tr>
<tr><td rowspan="2"></td><td>MARINER 4</td><td>0,12</td><td rowspan="2">Two layers of 0,127x10^{-3} m thick Polished Aluminium</td><td>R</td></tr>
<tr><td>11/28/1964</td><td>0,04</td><td>150x30</td></tr>
<tr><td colspan="5">COMMENTS: Each louver blade is a rectangular center-pivoted member consisting of an aluminium tube whose square cross section has a side of 3,5x10^{-3} m.</td></tr>
<tr><td rowspan="2">Fairchild Hiller</td><td>PEGASUS II</td><td>0,11</td><td rowspan="2">Polished Aluminium 5052</td><td>R</td></tr>
<tr><td>5/25/1965</td><td>0,05</td><td>200x50</td></tr>
<tr><td colspan="5">COMMENTS: Each louver blade is a rectangular center-pivoted member constructed from Aluminium Alloy 5052.
Louver for shadow operation.</td></tr>
</table>

PRODUCER	SPACECRAFT / LAUNCH DATE	α_s / ε	BLADE MATERIAL	CONFIGURATION / DIMENSIONS $x10^3$ [m]
GENERAL ELECTRIC	NIMBUS 1 & 2 (SENSORY SUBSYSTEM)	0,15	32 Layers of $6{,}35x10^{-6}$ m thick embossed preshrunk aluminized Mylar	R
	1-8/28/1964 2-5/15/1966	0,03		
COMMENTS: The blades are side pivoted and are covered by a layer of Mylar $2{,}54x10^{-5}$ m thick not embossed, to maintain specular external surface.				
GENERAL ELECTRIC	NIMBUS 1 & 2 (CONTROL SUBSYSTEM)	0,20	11 Layers of $6{,}35x10^{-6}$ m thick matted glass fiber paper	R
	1-8/28/1964 2-5/15/1966	0,80		
COMMENTS: The blades are covered on both sides by an additional layer of glass fiber paper, and are enclosed with a $5{,}08x10^{-5}$ m thick woven glass fiber fabric that is impregnated with Teflon. The blades are diffuse.				
Fairchild Hiller	ATS	0,17 [a]	Polished Aluminium with a whitepaint strip (6% of area)	R
	5/30/1974	0,05 [a]		
COMMENTS: Blades are sandwiched with a BR-34 polyimide adhesive bond. A white paint strip (DC 92-007) was added to the top of each blade along its entire length to lower the blade temperature during operation in a solar environment. [a] Values measured before the white strip was added.				
Fairchild Hiller	O.A.O.	0,12	Two stamped sheets of Polished Aluminium	R
		0,06		
COMMENTS: Louver for shadow operation.				
TRW-Systems	PIONNER IV	0,15-0,20	$0{,}076x10^{-3}$ m Aluminium foil sheets (1100-H 18)	T
	3/3/1959	0,04		Length = 267. Width at the large end = 76,2. Width at the narrow end = 25,4.
COMMENTS: To obtain the appropriate stiffness and longitudinal rigidity, sheet blades are formed into $6{,}35x10^{-3}$ m thick rectangular cross section, containing a hollow-internal shaft. Circular system.				
SNIAS		0,10	Polished Aluminium (A 9)	R
		0,04		123x38
COMMENTS:				
ERNO	HELIOS		Uncoated Aluminium	T

PRODUCER	SPACECRAFT	α_s	BLADE MATERIAL	CONFIGURATION
	LAUNCH DATE	ε		DIMENSIONS $x10^3$ [m]
	12/10/1974		Sandwich	Length = 220 Width at the large end = 100
COMMENTS:				
RCA			Foam with glued aluminized Mylar	R
COMMENTS: Louver made per blade, actuated by bimetal. Price: US $ 2100 per blade.				

5.2 Actuators

5.2.1 Bimetals

5.2.1.1 Introduction

Bimetal is a composite material having two or more metallic layers of different thermal expansion coefficients, that are permanently bonded together. If the bimetal temperature raises, the metal layer with the higher thermal expansion coefficient (high expansion component) tends to expand more than the one with the lower coefficient (low expansion component). The differences in thermal expansion cause the bending of the bimetal. If one end of the bimetal is fixed, the displacement at the free end can be used for operating electrical contacts or tripping a mechanism.

In order to achieve large deflections, the bimetal is frequently used in the form of helicoidal spring. If this spring is fixed at its outer extremity, the inner end may be attached to a shaft which will then rotate when the temperature changes. The available forces will depend both on the material mechanical and thermal characteristics, and on the spring dimensions.

Bimetals have been used in many spatial louver systems such as: Mariner, ATS, OGO, Pegasus, Pioneer, etc.. In these systems the bimetal is thermally coupled to the nearest portion of the radiator plate, and is, therefore, used as actuator and as sensing element.

5.2.1.2 Materials

Materials which are used in the manufacture of the bimetals for low expansion components or for high expansion components are given in Table 5-2.

Table 5-2: Materials Used

	MATERIAL	ALLOYS WITH LARGEST β / ALLOYS WITH SMALLEST β
LOW EXPANSION COMPONENT	INVAR, Also called; NILO 36, NILEX, NILVAR, and INDILATANS	
HIGH EXPANSION COMPONENT	BRASSES	CARTRIDGE BRASS
		RED BRASS
	AUSTENITIC ALLOY STEELS	STAINLESS STEEL 347
		STAINLESS STEEL 310
	NICKEL-MANGANESE-CHROMIUM ALLOYS	NIMONIC ALLOY PE 16
		NIMONIC ALLOY PK 33

Thermal Expansion Coefficient

Values of the relative linear thermal expansion of the above alloys are plotted as functions of temperature in Figure 5-1 to Figure 5-4.

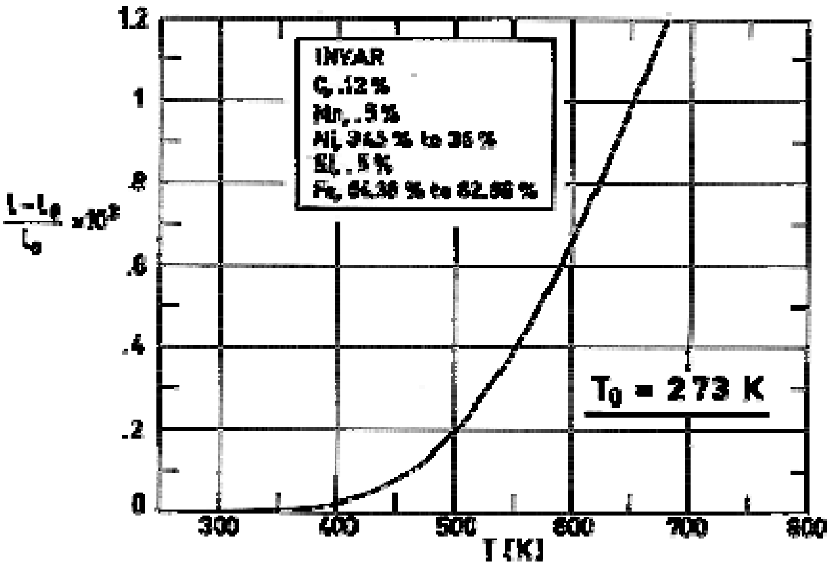

Note: non-si units are used in this figure

Figure 5-1: Relative linear thermal expansion vs. temperature in the case of Invar. T_0 = 273 K. From THE MOND NICKEL CO [35].

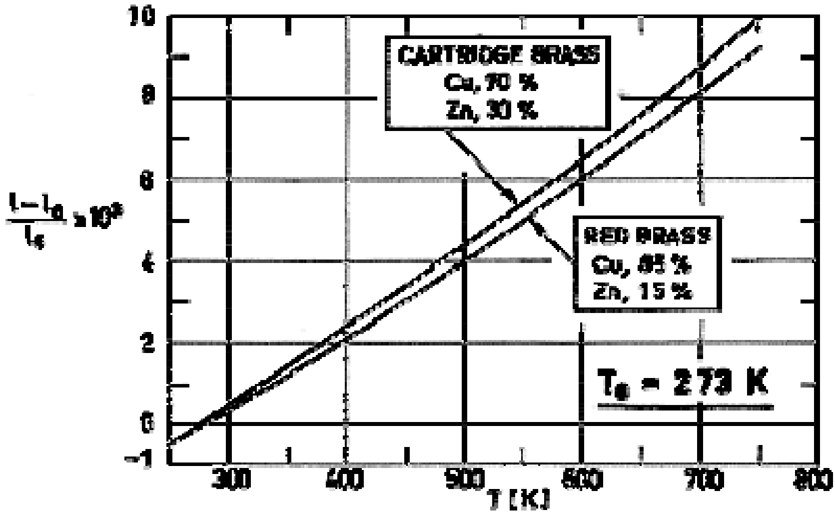

Figure 5-2: Relative linear thermal expansion vs. temperature in the case of brasses. T_0 = 273 K. After Baldwin (1961) [3].

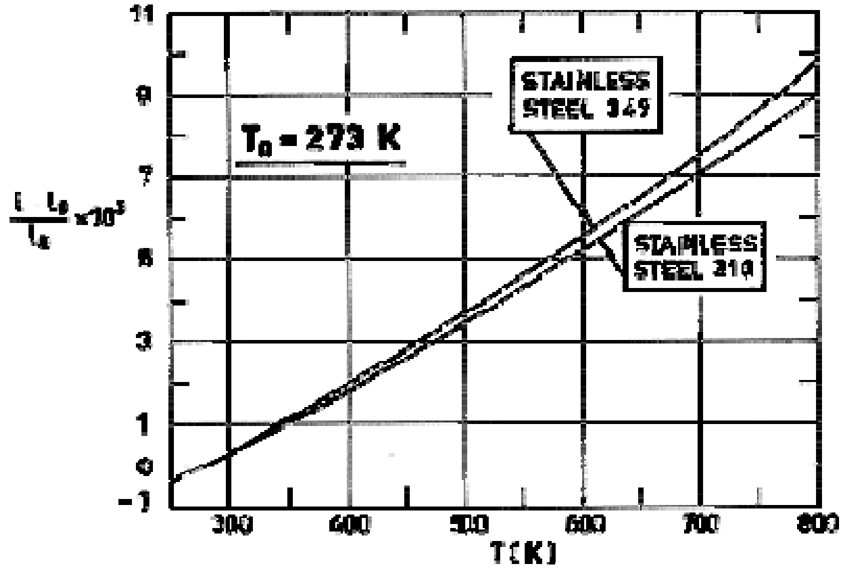

Figure 5-3: Relative linear thermal expansion vs. temperature in the case of austenitic steels. T_0 = 273 K. After Zapffe (1961) [39].

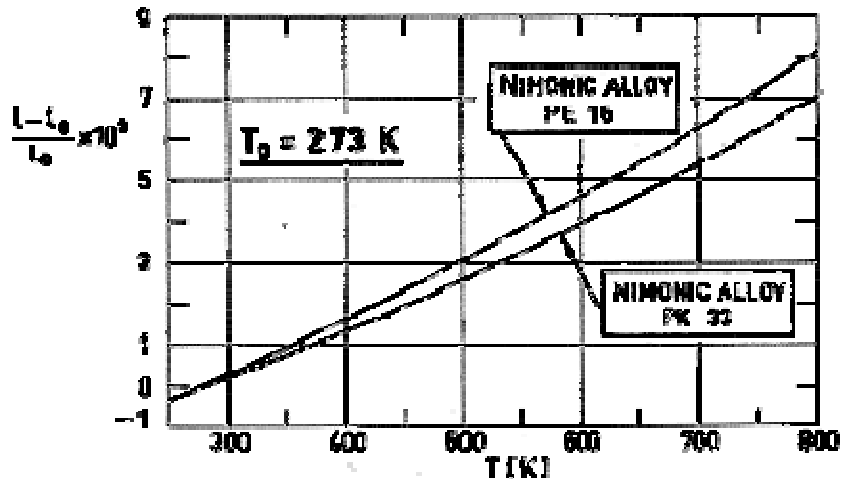

Figure 5-4: Relative linear thermal expansion vs. temperature in the case of Nimonic alloys. T_0 = 273 K. After WIGGIN & Co. (1967) [38].

This relative linear thermal expansion is defined as

$(l-l_0)/l_0 = \beta\,\Delta T$

Figure 5-5 is a summary of the data given in the four foregoing figures.

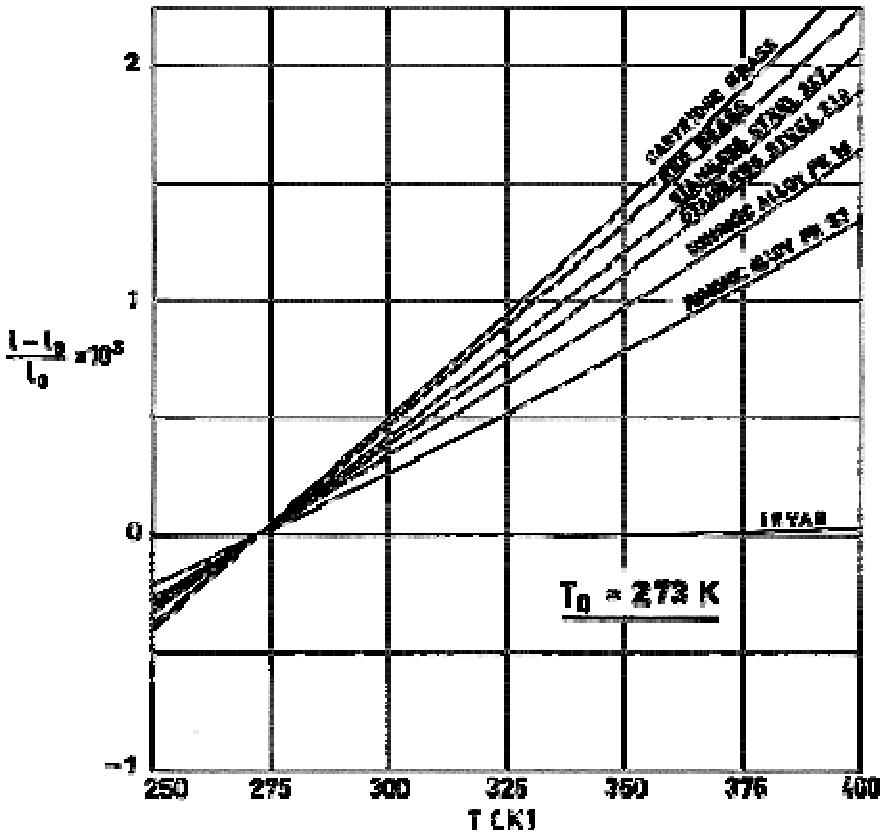

Figure 5-5: Relative linear thermal expansion vs. temperature for different alloys. T_0 = 273 K. After Baldwin (1961) [3], Zapffe (1961) [39], WIGGIN Co. (1967) [38].

5.2.1.3 Deflection of spirals and helical coils. sensitivity

Bimetalic spirals and helical coils deflected rotationally when the temperature changes. The deflection is given by

$$\theta = \frac{K_c \Delta T L}{t} \quad [5\text{-}1]$$

where the coil deflection constant, K_c, may be written as:

$$K_c = \frac{3}{4}\frac{360}{\pi}\left(\beta_H - \beta_L\right) = \frac{270}{\pi}\left(\beta_H - \beta_L\right) \quad [5\text{-}2]$$

The sensitivity, X, of spirals and helical coils is:

$$X = \frac{\theta}{\Delta T} = \frac{K_c L}{t} \quad [5\text{-}3]$$

Although the above expressions are always valid, it should be pointed out that K_c depends on the temperature and it is really constant only when the relative linear thermal expansion is a linear function of temperature.

Typical values of K_c for different bimetals are from $5\text{x}10^{-4}$ to $25\text{x}10^{-4}$ Angular Degrees.K^{-1}.

Figure 5-6 gives the ΔT required to achieve a given rotation θ, for different sensitivities, X, while Figure 5-7 shows X as a function of the bimetal slenderness, L/t, for different values of the deflection constant K_c.

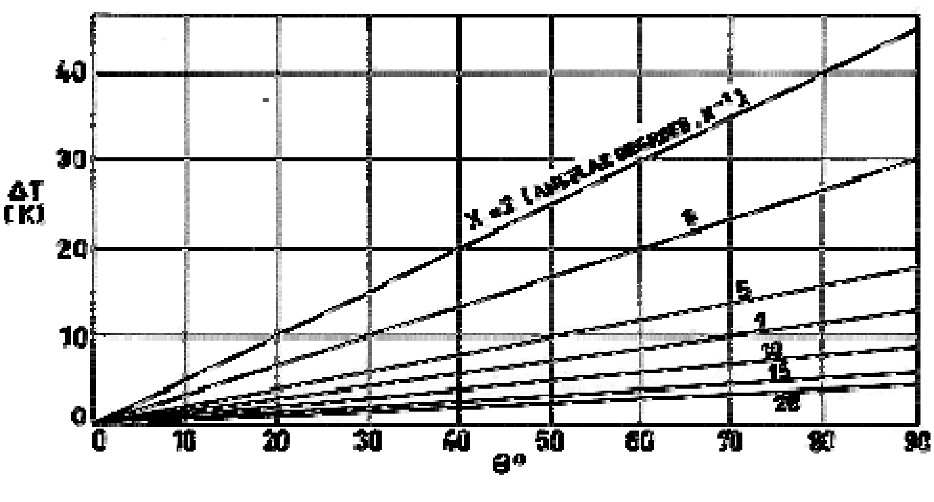

Figure 5-6: Difference of temperature, ΔT, vs. angle of rotation of the free end, θ, for several values of the sensitivity, X. After Martin & Yarworth (1961) [21], KAMMERER (1971) [16].

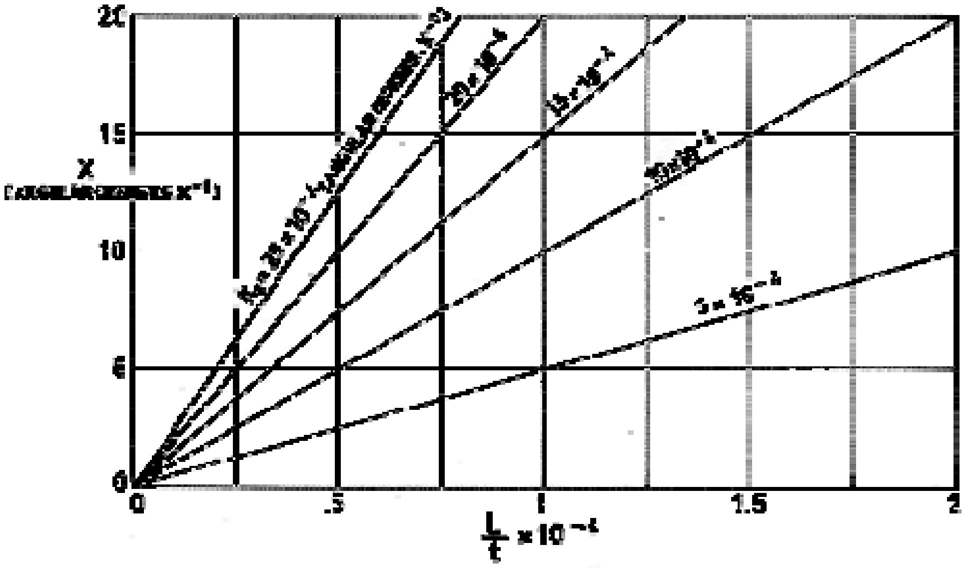

Note: non-si units are used in this figure

Figure 5-7: Sensitivity vs. ratio *L*/*t*, for different values of K_c. After Martin & Yarworth (1961) [21], KAMMERER (1971) [16].

References: Martin & Yarworth (1961) [21], KAMMERER (1971) [16], Trylinski (1971) [37].

5.2.1.4 Torsional moment of spirals and helical coils

The Torsional Moment of spirals and helical coils is given by

$M = K_c F_c \, \Delta T \, w \, t^2$

where the so called thermal force of the spiral, $K_c F_c$, is:

$$K_c F_c = \frac{37}{216} E(\beta_H - \beta_L) \qquad [5\text{-}4]$$

Typical values of $K_c F_c$, for different bimetals are of order of 1×10^5 to 5×10^5 $N.m^{-2}.K^{-1}$.

The Figure 5-8 gives the ratio $M / K_c F_c \Delta T L^3$ versus *L*/*t*, for different values of *w*/*t*.

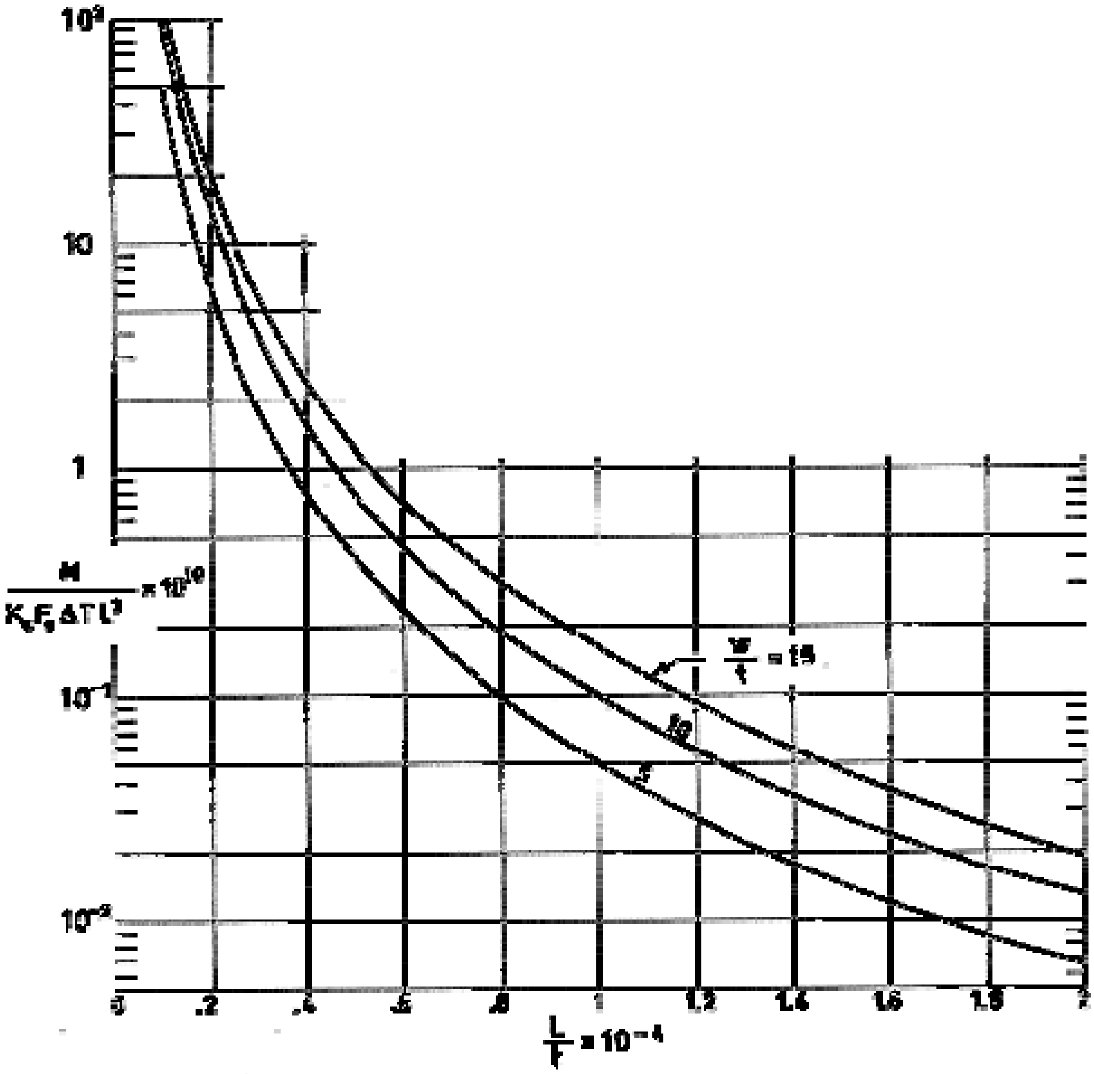

Note: non-si units are used in this figure

Figure 5-8: Dimensionless ratio $M/K_cF_c\Delta TL^3$ vs. L/t, for several values of w/t. After Martin & Yarworth (1961) [21], KAMMERER (1971) [16].

5.2.2 Bellows

5.2.2.1 Introduction

Bellows are flexible, thin-walled, circumferentially corrugated cylinders with open or closed ends.

The principle of operation of the bellows is simple: an inner to outer pressure difference causes a change in the bellow length, unless both ends are clamped. If an end is clamped while the other is free, the bellows can behave as an actuator.

Bellows serve many different functions, either as independent units or as integral parts of more complex components. Filled with a liquid they are used as measuring devices. Louvers of the NIMBUS spacecraft are actuated by bellows containing a liquid-vapor mixture of Freon (Freon-11 for the louvers of the control subsystem and Freon-114 for those of the sensory subsystem).

Bellows constituted by one or more layers of materials are called respectively one-ply or multi-ply bellows.

5.2.2.2 Materials

Both metallic and non-metallic materials can be used to manufacture the bellows. Metallic bellows can be either formed, welded, machined, or deposited. In the last method the metal is deposited by electroplating or chemically onto machined aluminium mandrels which are later dissolved.

The characteristics of the metallic and non-metallic materials more used in the manufacture of bellows are summarized in the following pages.

Table 5-3: Typical Alloy Used in Bellows
D: Deposited, F: Formed, W: Welded

MATERIAL			TYPE	OUTSTANDING CHARACTERISTICS
COPPER ALLOYS	BRASS, BRONZE		F D	HIGH PROPORTIONAL LIMIT. GOOD TOUGHNESS.
	BERYLLIUM COPPER			
	ZIRCONIUM COPPER			
ALUMINIUM ALLOYS	5083		F	HIGH STRENGTH-WEIGHT RATIOS. GOOD TOUGHNESS AT LOW AND INTERMEDIATE STRESS LEVELS AT TEMPERATURES AS LOW AS 20 K.
	6061			
	7075			
NICKEL AND CUPRO-NICKEL ALLOYS	NICKEL 200		F D	GOOD CORROSION RESISTANCE. LOW MAGNETIC PERMEABILITY.
	MONELS	400 404 K 500		
TITANIUM ALLOYS	Ti - 75 A		F	HIGH STRENGTH AND STRENGTH TO WEIGHT RATIO. GOOD CREEP STRENGTH FROM 530 K TO 640 K.
	Ti - 6 Al - 4 V			
LOW-ALLOY STEELS	4130		F	EXTREMELY HIGH STRENGTH. HIGH PROPORTIONAL LIMIT. HIGH FATIGUE STRENGTH. GOOD CREEP RESISTANCE.
STANDARD AUSTENITIC STAINLESS STEELS	304, 304 L 310, 316 321, 347		F W	EXCELLENT TOUGHNESS TO 20 K. GOOD FATIGUE AND CREEP STRENGTH. GOOD NEUTRON RADIATION RESISTANCE. GOOD CORROSION AND OXIDATION RESISTANCE.

MATERIAL		TYPE	OUTSTANDING CHARACTERISTICS
PRECIPOTATION-HARDENING STAINLESS STEELS	17-4 PH, 17-7 PH	F W	HIGH STRENGTH. GOOD CREEP STRENGTH. HIGH FATIGUE STRENGTH.
	PH-15-7 Mo, AM350		
OTHER IRON-BASE ALLOYS	19 - 9 DL	F W	HIGH STRENGTH. GOOD CREEP STRENGTH. HIGH FATIGUE STRENGTH PLUS SEALABILITY TO HARD GLASS (KOVAR).
	A - 286		
	KOVAR		
NICKEL-BASE ALLOYS GROUP I	INCOELS 600, 625, X-750, 718	F W	GOOD HIGH TEMPERATURE STRENGTH. GOOD FATIGUE STRENGTH. GOOD TOUGHNESS. GOOD CREEP RESISTANCE. GOOD STRENGTH-TO RUPTURE.
	INCOLOY 825		
	HASTELLOY C		
NICKEL-BASE ALLOYS GROUP II	M252: WASPALOY	W	
	UDIMET 700		
	RENE 41 AND 62		
COBALT-BASE ALLOYS	L 605	W	
REFRACTORY METALS	COLUMBIUM	W	GOOD STRENGTH AT EXTREME TEMPERATURES. HIGH PROPORTIONAL LIMIT. EXCELLENT FATIGUE STRENGTH ABOVE TRANSITION TEMPERATURE. EXCELLENT CREEP STRENGTH.
OTHER ALLOYS	INVAR, (Ni-Span-C)	W	ZERO THERMAL EXPANSION COEFFICIENT OR CONSTANT ELASTIC MODULUS.

NOTE From TRW (1970) [36].

Table 5-4: Typical Nonmetallic Materials Used in Bellows

	BUNA-N	NEOPRENE	RUBBER COMPOUNDS		SILICONE RUBBER	TEFLON
			MODIFIED ISOMERIZED RUBBER	CHLORINATED		
Temperature Range without significant changes in Properties [K]	200-500	250-360				200-525
Density [kg.m^{-3}]	1000	1230	1060	1640	1666	2160
Specific Heat [J.kg^{-1}.K^{-1}]	2000	1674	2092	1550 to 1800		1670
Thermal Conductivity [W.m^{-1}.K^{-1}]	0,158 to 0,213	0,209	0,109 to 0,121	0,126	0,177 to 0,277	0,242
Thermal Expansion Coefficient [K^{-1}]	9x10^{-5} to 2x10^{-4}	9x10^{-5} to 2x10^{-4}	7,5x10^{-5}	1,2x10^{-4}	3,6x10^{-4}	(1,6±0.2) x10^{-5}
Solar Radiation Effects	NONE	NONE		DARKENS	NONE	NONE
Acid Effects	None except strong acids	None	None for weak acids, and ClH, SO_4H_2	None	None except strong acids	None
Organic Dissolvent Effects	None except ketones and esters	None except oxygenated dissolvents and aromatic hydrocarbons	None except aromatic and aliphatic hydrocarbons	None except ketones, esters, and aromatic hydrocarbons	None except esters, and aromatic and aliphatic hydrocarbons	None
Alcali Effects	None		None	None	None except strong alkalies	None
Mineral Oil and Fuel Effects	None	None	Attacked	None	None	None

NOTE References: Burton (1949) [5], Stern (1954) [34].

Actuating Fluids

Table 5-5: Typical Fluids Used in Bellows

NAME	FORMULA	DENSITY [kg.m^{-3}]	MELTING POINT [K]	BOILING POINT [K]
Butane	$CH_3(CH_2)_2CH_3$	600 (T = 273 K)	138	272,6 to 272,9
Ethyl Chloride (Chloroethane)	CH_3CH_2Cl	921,4 (273 K)	134,5	285,3
Freon 11	$CClF_3$		162	248
Freon 21	$CHCl_2F$	1421 (273 K)	146	282
Methyl Chloride (Chloromethane)	CH_3Cl	1008 (243 K) 960 (273 K)	175,5	249

NOTE From Hodgman (1953) [14].

5.2.2.3 Convolutions and characteristics

Table 5-6: Bellows Convolutions and Relevant Characteristics

	CONVOLUTION SHAPE	AXIAL SPRING RATE	LONG STROKE CAPABILITY	RESISTENCE TO DIFFERENTIAL PRESSURE
FORMED				
SEMITOROIDAL		VERY HIGH	VERY POOR	VERY GOOD
U-SHAPED, STRAIGHT WALL		MEDIUM	FAIR	FAIR
U-SHAPED, EXTERNAL RING SUPPORT		HIGH	FAIR	VERY GOOD
U-SHAPED, INTERNAL RING SUPPORT		HIGH	FAIR	VERY GOOD
U-SHAPED, EXTERNAL T-RING SUPPORT		HIGH	FAIR	VERY GOOD
S-SHAPED		MEDIUM	FAIR	FAIR
S-SHAPED EXTERNAL RING SUPPORT		HIGH	FAIR	VERY GOOD

	CONVOLUTION SHAPE	**AXIAL SPRING RATE**	**LONG STROKE CAPABILITY**	**RESISTENCE TO DIFFERENTIAL PRESSURE**
TOROIDAL EXTERNAL PRESSURE		VERY HIGH	POOR	EXCELLENT
TOROIDAL INTERNAL PRESSURE		VERY HIGH	POOR	EXCELLENT
NESTING (SINGLE SWEEP)		MEDIUM	GOOD	GOOD
WELDED				
FLAT CONICAL PLATE		MEDIUM	FAIR	GOOD
STEPPED FLAT PLATE		LOW	GOOD	FAIR
CURVED (SINGLE SWEEP)		MEDIUM	GOOD	GOOD
CORRUGATED (NESTING)		VERY LOW	EXCELLENT	POOR
CORRUGATED (NON-NESTING)		LOW	GOOD	POOR
TOROIDAL		VERY HIGH	POOR	EXCELLENT
DEPOSITED				
U-SHAPED (CAN BE VARIED)		LOW	GOOD	FAIR
MACHINED				
RECTANGULAR		HIGH	FAIR	EXCELLENT

NOTE From TRW (1970) [36].

5.2.2.4 Spring rate

The spring rate, *K*, is the ratio of the applied force to the resulting deflection. In the case of bellows the spring rate ranges from 2x10³ N.m⁻¹ to 3x10⁵ N.m⁻¹. Formulae to calculate *K* in several cases can be found in Table 5-7 below.

Table 5-7: Spring Rate for Several Bellows

SHAPE	SPRING RATE	ADDITIONAL DATA
ELLIPTICAL 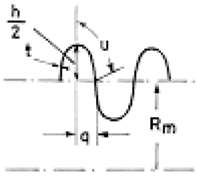	$k = 6{,}92\frac{ER_m t^3}{uh^2}\frac{q}{L_c}\left(\frac{1}{c}\right)\cdot \left[\frac{q+h/2}{2q+h/2}\right]$ $L_c = 4u$	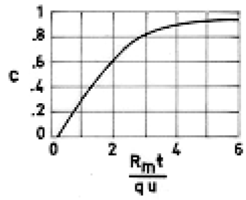 $m_c = 6{,}63\rho t D_m \sqrt{3{,}3h^2 + 2qh + 3{,}3q^2}$
CONICAL FLAT PLATE 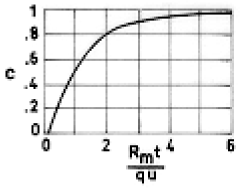	$k = 6{,}92\frac{ER_m t^3}{uh^2}\frac{q}{L_c}\left(\frac{1}{c}\right)$ $L_c = 4u$	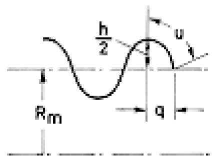 $m_c = 6{,}28\rho t D_m \sqrt{h^2 + 4q^2}$
SINE WAVE 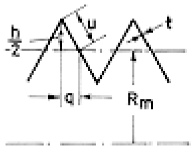	$k = 6{,}92\frac{ER_m t^3}{uh^2}\frac{q}{L_c}\left(\frac{1}{c}\right)\cdot \left[\frac{q+h/2}{1{,}6q+h/2}\right]$ $L_c = 4u$	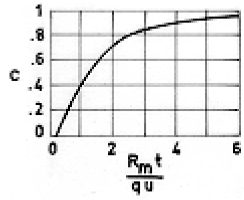 $m_c = 12{,}57\rho t D_m u$

NOTE From TRW (1970) [36].

The flexibility, *F*, is the ratio of the deflection to the applied pressure difference.

5.2.2.5 Effective area

Effective area of a bellows is the equivalent surface area on which pressure acts to produce the axial force. Typical range of effective area of the bellows is from 6x10⁻⁴ to 30x10⁻⁴ m².

Effective area on both formed and welded bellows can be approximated to an accurancy of 3 percent by the following relationship:

$A = \pi/16(D_0 + D_i)^2$

References: FIAT (1970) [12], TRW (1970) [36], Trylinski (1971) [37].

5.2.2.6 Volume

The inner volume of the bellows may be obtained from the following expression:

$V = 0{,}262\, L\, (D_0^2 + D_0 D_i + D_i^2)$

Reference: TRW (1970) [36].

5.2.2.7 Response

Response of a bellows is the time required to move it against its own inertia and spring force, through its operating stroke.

Typical values of gas filled bellows response vary from $3x10^{-3}$ to $50x10^{-3}$ s, depending on the bellows geometry. Bellows with large effective areas and low spring rates have faster response times. Bellows that require long deflections are generally slow. Liquid filled bellows may have response times of one to three seconds.

Reference: TRW (1970) [36].

5.2.2.8 Vibrations

Life of the bellows under vibration depends upon the stresses induced, the level and frequency of vibration, and the amount of damping within the system.

The vibration frequency can be estimated by use of the following formulae.

Table 5-8: Frequency of Bellows Vibration

FREQUENCY MODE	FORMULA	CONDITIONS OF CALCULATION	APPROXIMATION TO EXACT VALUE
LONGITUDINAL	$f_{n=1} = 3{,}13\sqrt{\dfrac{K}{m_1 + \dfrac{m_2}{3}}}$	BELLOW EMPTY. ONE END FREE.	GOOD
LONGITUDINAL (ACCORDION)	$f_{n=1} = 19{,}825\sqrt{\dfrac{K}{m_{fa} + m_a}}$	BOTH ENDS CLAMPED. DIFFERENTIAL PRESSURE LESS THAN $6{,}9x10^3$ Pa.	GOOD
LATERAL (TRANSVERSE OR BEAM)	$f_{n=1} = 2{,}22\sqrt{\dfrac{KD_o^2}{l^2(m_a + m_l)}}$	BOTH ENDS CLAMPED. DIFFERENTIAL PRESSURE LESS THAN $6{,}9x10^3$ Pa.	POOR
TORSIONAL	VERY HIGH FREQUENCY AND VERY LOW AMPLITUDE IT IS NOT A PROBLEM.		
FLOW-INDUCED	THEY ARE NOT SIGNIFICANT UNDER SPACE CONDITIONS.		

NOTE From TRW (1970) [36].

5.2.2.9 Summary table concerning existing bellows

Table 5-9: Characteristics of Convoluted Bellows

D_0x10² [m]	D_ix10² [m]	Lx10² [m]	tx10⁴ [m]	Ax10⁴ [m²]	Vx10⁶ [m³]	N [a]	Kx10⁻⁴ [N.m⁻¹]	Fx10² [m.Pa⁻¹]	Stroke x10³ [m]	P_{max} x10⁻³ [Pa]	ΔP_{max} x10⁻³ [Pa]
STAINLESS STEEL. ONE-PLY.											
1,19	0,83	1,64		0,77	1,27	14	2,000	0,39	1,42	4269	364,1
1,39	0,91	2,50		1,03	2,57	20	1,953	0,53	2,03	4221	383,0
1,67	1,15	2,31		1,55	3,58	14	2,315	0,67	2,13	3628	317,9
1,83	1,23	1,82		1,87	3,40	11	2,612	0,72	2,51	3697	348,6
1,90	1,27	3,25		2,00	6,50	16	1,051	1,90	4,47	2311	253,3
1,90	1,23	2,47		1,93	4,79	12	1,460	1,32	3,66	2511	277,3
2,46	1,83	2,42		3,61	8,74	14	6,132	0,59	1,78	3869	301,7
2,58	1,63	2,87		3,48	10,00	13	0,267	13,03	11,88	793	91,2
2,86	1,87	2,90		4,45	12,89	12	0,384	11,59	10,06	800	86,8
2,86	1,87	2,08		4,45	9,27	10	4,642	0,96	3,30	3311	343,8
3,41	2,46	2,80		6,90	19,36	12	3,283	2,10	4,57	2828	217,6
3,49	2,30	2,24		6,65	14,89	9	0,837	7,96	7,09	841	89,1
3,81	2,46	3,19		7,81	24,86	11	5,495	1,42	4,19	2724	295,1
3,81	2,50	3,56		7,94	28,22	10	0,368	21,58	12,70	559	58,9
3,81	2,54	3,83		8,00	30,62	11	2,707	2,96	5,31	1724	179,4
4,05	2,82	2,74		9,35	25,66	12	4,570	2,05	4,57	2366	217,6
4,17	2,82	3,09		9,68	29,89	8	0,508	19,06	8,13	421	42,7
4,46	2,82	3,11		10,45	32,49	9	0,798	13,10	13,72	910	104,7
5,08	3,41	3,91		14,32	56,02	14	5,005	2,86	8,18	2724	286,0

D_0x10^2 [m]	D_ix10^2 [m]	Lx10^2 [m]	tx10^4 [m]	Ax10^4 [m^2]	Vx10^6 [m^3]	N [a]	Kx10^{-4} [N.m^{-1}]	Fx10^2 [m.Pa^{-1}]	Stroke x10^3 [m]	P_{max} x10^{-3} [Pa]	ΔP_{max} x10^{-3} [Pa]
5,08	3,81	7,32		15,68	114,68	20	0,345	45,45	17,78	497	39,1
5,48	3,81	5,72		17,03	97,34	15	0,397	42,90	22,86	552	53,3
6,91	5,60	4,36		30,77	134,13	13	11,455	2,69	4,29	2704	159,5
7,54	6,23	3,09		37,68	116,56	7	1,602	23,52	6,93	524	29,5
10,08	7,62	3,86		62,13	239,71	7	0,250	248,52	17,78	117	7,2
19,69	17,46	11,32		270,97	3066,18	15	3,971	68,24	8,38	338	12,3
23,77	21,75	7,89		406,90	3212,22	14	7,758	52,45	6,40	407	12,2
STAINLESS STEEL. TWO PLY											
1,71	1,11	1,80		1,55	2,79	10	2,348	0,66	2,54	3628	384,8
1,91	1,19	2,74		1,94	5,30	13	1,226	1,58	3,96	2262	250,6
2,38	1,55	4,47		3,10	13,84	22	0,597	5,19	11,18	2007	215,4
2,90	1,94	1,79		4,65	8,31	8	4,599	1,01	3,05	3021	302,0
3,41	2,22	5,05		6,32	31,93	14	1,189	5,32	11,38	1980	213,9
3,81	2,54	4,85		8,00	38,83	13	4,447	1,80	6,60	3449	366,7
4,29	2,86	6,90		10,13	69,90	19	1,752	5,78	13,03	2180	225,4
5,08	3,73	4,27		14,19	60,67	11	0,844	16,81	17,04	959	101,4
6,11	3,97	3,77		20,26	76,36	7	0,939	21,58	15,82	676	73,3
6,67	5,08	9,31		27,29	253,98	16	14,672	1,86	3,66	2490	196,8
9,21	7,62	6,90		55,81	384,99	14	24,026	2,32	2,84	2297	122,4
11,75	10,16	10,44		94,26	984,47	16	27,373	3,44	3,25	2200	94,5

D_0x10[2] [m]	D_ix10[2] [m]	Lx10[2] [m]	tx10[4] [m]	Ax10[4] [m²]	Vx10[6] [m³]	N [a]	Kx10[−4] [N.m⁻¹]	Fx10[2] [m.Pa⁻¹]	Stroke x10[3] [m]	P_{max} x10[−3] [Pa]	ΔP_{max} x10[−3] [Pa]
STAINLESS STEEL. THREE-PLY.											
2,89	1,91	7,74		4,52	34,96	24	5,570	0,81	5,49	6677	677,8
3,84	2,62	5,00		8,19	40,96	12	8,176	1,00	3,35	5670	335,0
5,15	3,49	5,94		14,65	87,04	15	3,153	4,65	9,53	2159	204,9
5,84	3,73	4,42		16,65	73,56	10	11,387	1,46	5,59	3904	382,9
6,21	4,45	6,07		22,32	135,51	10	7,884	2,83	6,35	2538	224,4
11,92	9,60	6,05		90,97	549,92	10	7,358	12,36	9,91	1304	419,9
22,65	20,00	4,23		357,16	1797,14	7	6,007	59,46	14,76	662	24,8
BERILLIUM COOPER. ONE-PLY.											
3,33	2,25	2,04	1,00	6,20		8	0,340	20,46	10,86	521	53,0
INCOEL. ONE-PLY											
3,33	2,25	2,80	1,27	6,19		11	0,708	8,77	11,59	1293	131,5
BRASS. ONE-PLY											
4,13	2,79	3,18	1,20	9,52		10	0,215	45,85	11,95	256	25,5
PHOSPHOR BRONZE. ONE-PLY.											
5,08	3,38	5,40	1,84	14,22		15	0,250	46,12	18,05	373	38,3
6,98	4,98	5,48	2,35	28,35		15	0,525	51,23	19,11	407	37,3
MONEL. ONE-PLY.											
5,40	3,51	4,45	1,47	15,82		10	0,253	62,38	18,56	274	29,4

[a] N is the number of active convolutions.

NOTE From FIAT (1970) [12], TRW (1970) [36].

5.2.3 Bourdons

5.2.3.1 Introduction

Bourdons are non-circular cross section tubes, coiled into a circle or spiral. The Bourdon tube is connected to the pressure to be gauged. The difference between internal and external pressures causes a deflection of the closed end of the tube (the free end). Deflections of an end-piece in the free end can drive a mechanism.

Bourdons are mainly used for measuring pressures above 50 kPa. Since their measuring range depends upon the material and cross sectional shape of the tube, they can serve other purposes. A Bourdon, developed by REUSSER, will actuate the SNIAS louver array.

5.2.3.2 Materials and characteristics

Bourdon tubes are metallic. The metals most commonly used are: brass, phosphor bronze, or stainless steel.

The behavior of a Bourdon tube is linear provided that the pressure does not exceed a proportionally limit Pt. The maximum allowable pressure in the tube, Pmax, should be smaller than Pt. Usually, the ratio Pt/Pmax is of the order of 2 in the case of slow pressure variations, 2,5 for rapidly varying pressures, and 3 for tubes working at temperatures above 320 K. The value of Pt rises when either the aspect-ratio, a/b, of the cross section is decreased, the wall thickness, t, is increased, or the coiling radius, R0, is reduced. Pt can be also increased by heat treatment and stabilization of the material forming the tube

Reference: Trylinski (1971) [37].

5.2.3.3 Flexibility

The flexibility of a Bourdon is the ratio between the deflection of a given section of the Bourdon and the increment of applied pressure. The flexibility is constant, provided that the linear range has not been exceeded, and it only depends upon the shape, size, and initial coiling angle of the Bourdon. Flexibility is given by the expression:

$$F = F_0 \sqrt{(\psi_0 - \sin\psi_0)^2 + (1 - \cos\psi_0)^2} \qquad [5\text{-}5]$$

where F_0, which depends on the material and dimensions of the Bourdon, is given by:

$$F_0 = \frac{\alpha(1-\nu^2)}{E} \frac{R_0^3}{bt} \frac{1}{\beta + \left(\frac{R_0 t}{a^2}\right)^2} \qquad [5\text{-}6]$$

α y β are numerical coefficients depending on the ratio a/b and the shape of the cross section.

Figure 5-9 shows the values of α and β versus a/b, in the cases of an elliptical and flat-sided section, respectively. The ratio F/F_0 as a function of the initial coiling angle, ψ_0, in given in Figure 5-10.

Reference: Trylinski (1971) [37].

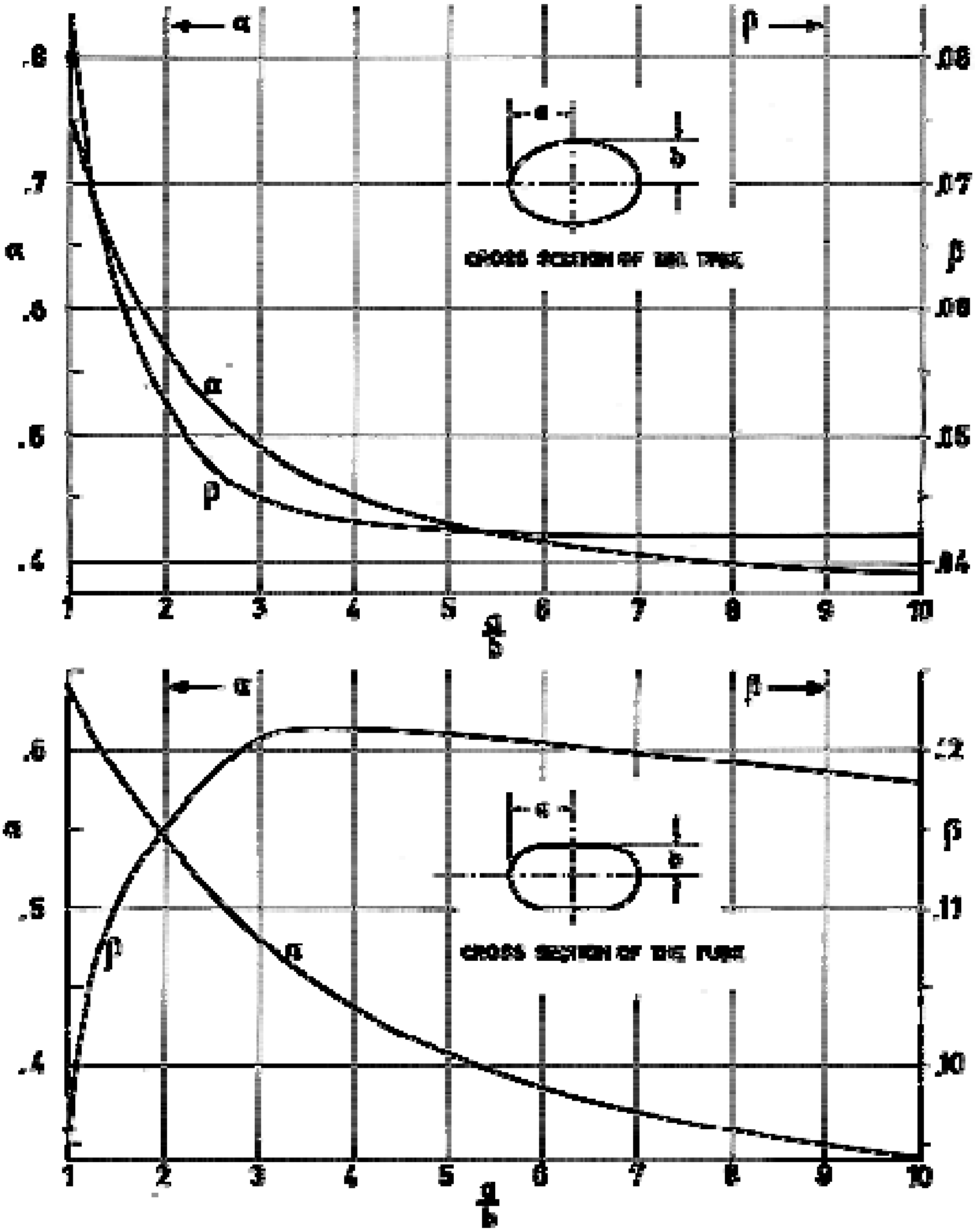

Note: non-si units are used in this figure

Figure 5-9: Values of α and β vs. ratio a/b for different cross sections of the Bourdon tube. After Trylinski (1971) [37].

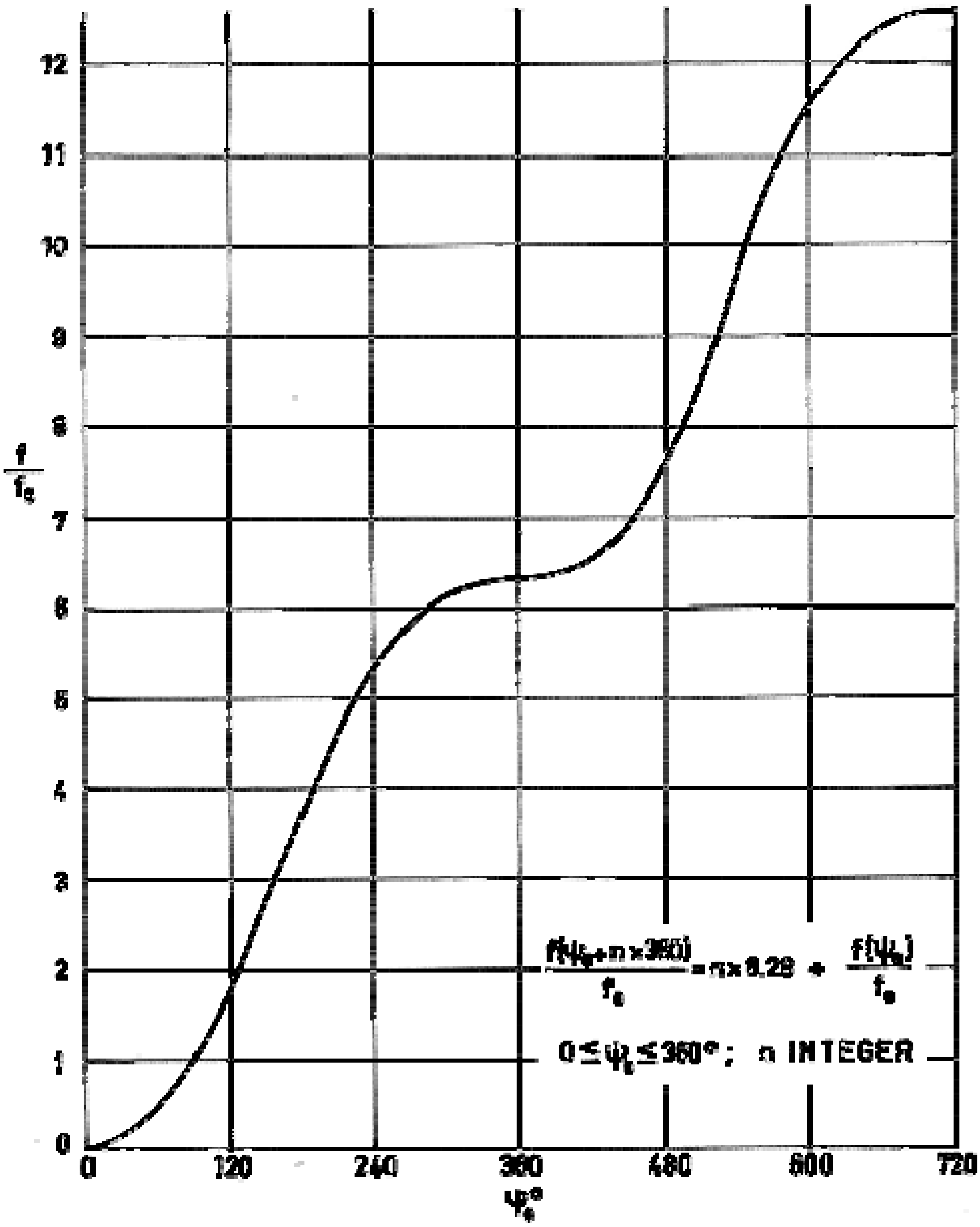

Note: non-si units are used in this figure

Figure 5-10: Ratio F/F_0 vs. Bourdon initial coiling angle, ψ_0. Calculated by the compiler.

5.3 Sensors

5.3.1 Sensor location

In the case of bimetal actuators, the sensor is the proper bimetal, which is thermally coupled to the nearest portion of the radiator plate arranged to be the hot spot.

Vapor-liquid bellows use a sensor tube coupling the bellows to the hottest portion of the radiator plate, as in the case of attitude control subsystem of Nimbus, or to a sensing plate, as in the sensory subsystem of the Nimbus.

Bourdon spirals require a tank of fluid, which is the sensing element.

Hot spot sensing appears superior to average temperature sensing since it gives closer control of the hot side design margin, at the expense of a less accurate control of the cold spot. In general, this solution is preferable since high temperatures may induce permanent failure, while for most electronic components, low temperatures results only in a temporary loss in operability.

When each blade is actuated individually, control problems are mitigated, since each louver can be set to the temperature associated with the portion of the radiator plate which it controls. Thus, the hot spot region will operate with the blades open, while the cold region is operated with the blades closed. The net effect will be as if there were an increase in the conductivity of the radiator plate in the direction normal to the blade rotation axis.

5.3.2 Coupling options

When bimetals or Bourdon spirals are used, it is natural to actuate each blade individually or in couples, since mounting of the actuator is fairly simple and power requirements are low.

On the other hand, liquid-vapor bellows actuators cannot be split into many small individual units without large sacrifices in cost, reliability and weight. Being available the extra power required, it is advisable to operate all the blades at once (ganged system).

5.4 Structural elements

5.4.1 Actuator housing

Although actuator housing may be used as an structural member of the louver system, its main objectives are:

1. Minimization of the temperature difference between the actuators and the baseplate. This requires good radiative and conductive heat transfer between baseplate and actuator housing.
2. Protection of actuators from the external environment (solar radiation, micro-meteorites) and from the radiative heat transfer from the other components.
3. Minimization of heat losses when the blades are in closed position.

The surfaces of the actuator housing which are exposed to the surrounding are usually covered with a reflective surface such as aluminized Mylar (PIONEER spacecraft), highly polished anodized aluminium plus fiberglass (PEGASUS and OAO spacecraft), or as in the case of SNIAS louvers, polished aluminium type A4 on the parts looking towards the baseplate and aluminized Kapton, Kapton outside, in the other parts.

Actuator housing is mandatory when bimetal actuators are used.

5.4.2 Frames

Frames are the structural support of the louver assembly.

In ATS spacecraft, the frames are made of highly polished aluminium, and are spaced away from the mounting surfaces with insulating washers to prevent conduction heat losses.

In OAO and PEGASUS satellites, the structural members constituting the frames are from aluminium, highly polished, with pre-drilled mounting holes whose aim is coupling the assembly to the heat sink.

In the PIONEER the frame is a center support ring containing a Teflon bushing to support the smaller end of the blades.

In the SNIAS louver system, the frames are covered with polished aluminium, type A4, on the parts looking towards the base, and with aluminized Kapton (the Kapton layer being outside) on the others parts.

6
Ideal louvers

6.1 Sun-light operation

6.1.1 Introduction

The following basic assumption are made in this clause:

1. The width of the array and the length of the blades are infinite.
2. Blade angle is identical for all blades.
3. There is no gap between the array and the baseplate.
4. Baseplate temperature is constant.
5. Blade temperature is constant.
6. There is neither conduction nor convection between surfaces.
7. The optical properties of the surfaces are constant.

Additional specific assumptions are made when required.

Angles used are indicated below.

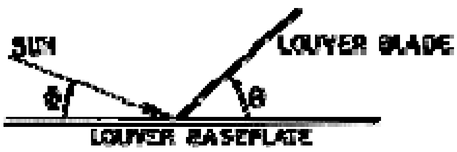

Figure 6-1: Geometry of the blade-baseplate system

6.1.2 Heat rejection capability

Energy balance equation for the louver baseplate can be written as follows:

$q = \varepsilon_{eff}\,\sigma T^4_{BP} - \alpha_{eff} S_0$

where:

S_0,	Solar Constant. S_0 = 1353 W.m^{-2}.
T_{BP},	Baseplate Temperature. [K].

q,	Net Heat Transfer Rate at Louver Baseplate Surface (Heat Rejection Capability). [$W.m^{-2}$].
α_{eff},	Effective Absorptance of the Louver Baseplate.
ε_{eff},	Effective Emittance of the Louver Baseplate.
σ,	Stefan-Boltzmann Constant. $\sigma = 5{,}6697 \times 10^{-8}$ $W.m^{-2}.K^{-4}$.

Other symbols which appear in the following figures are:

ε_B,	Emittance of the Blades.
ε_{BP},	Emittance of the Baseplate
ρ_B,	Reflectance of the Blades.
ρ_{BP},	Reflectance of the Baseplate.

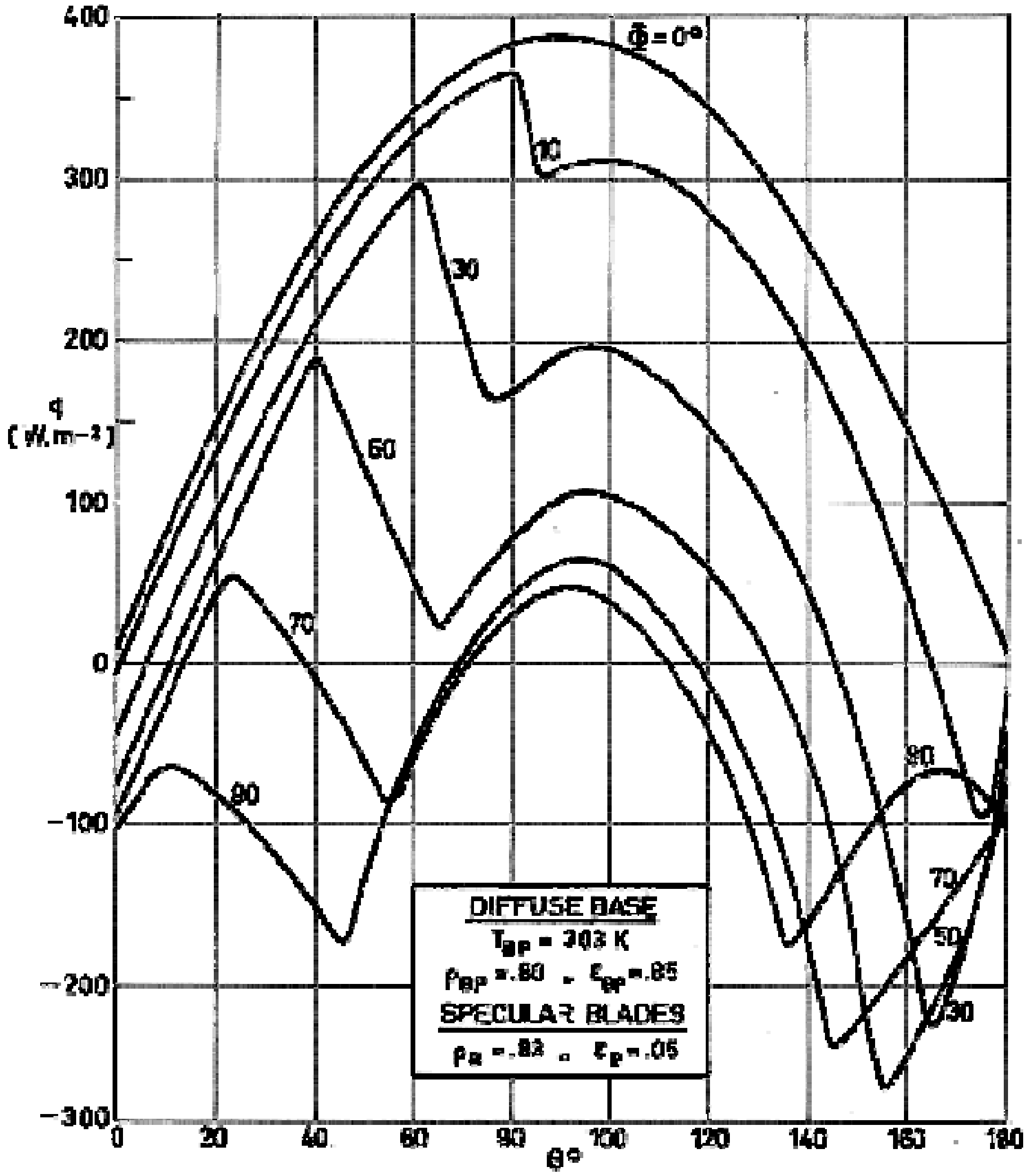

Note: non-si units are used in this figure

Figure 6-2: Heat rejection capability, *q*, vs. blade angle, *θ*, for several values of the sun angle, *ϕ*. From FAIRCHILD HILLER (1972) [10].

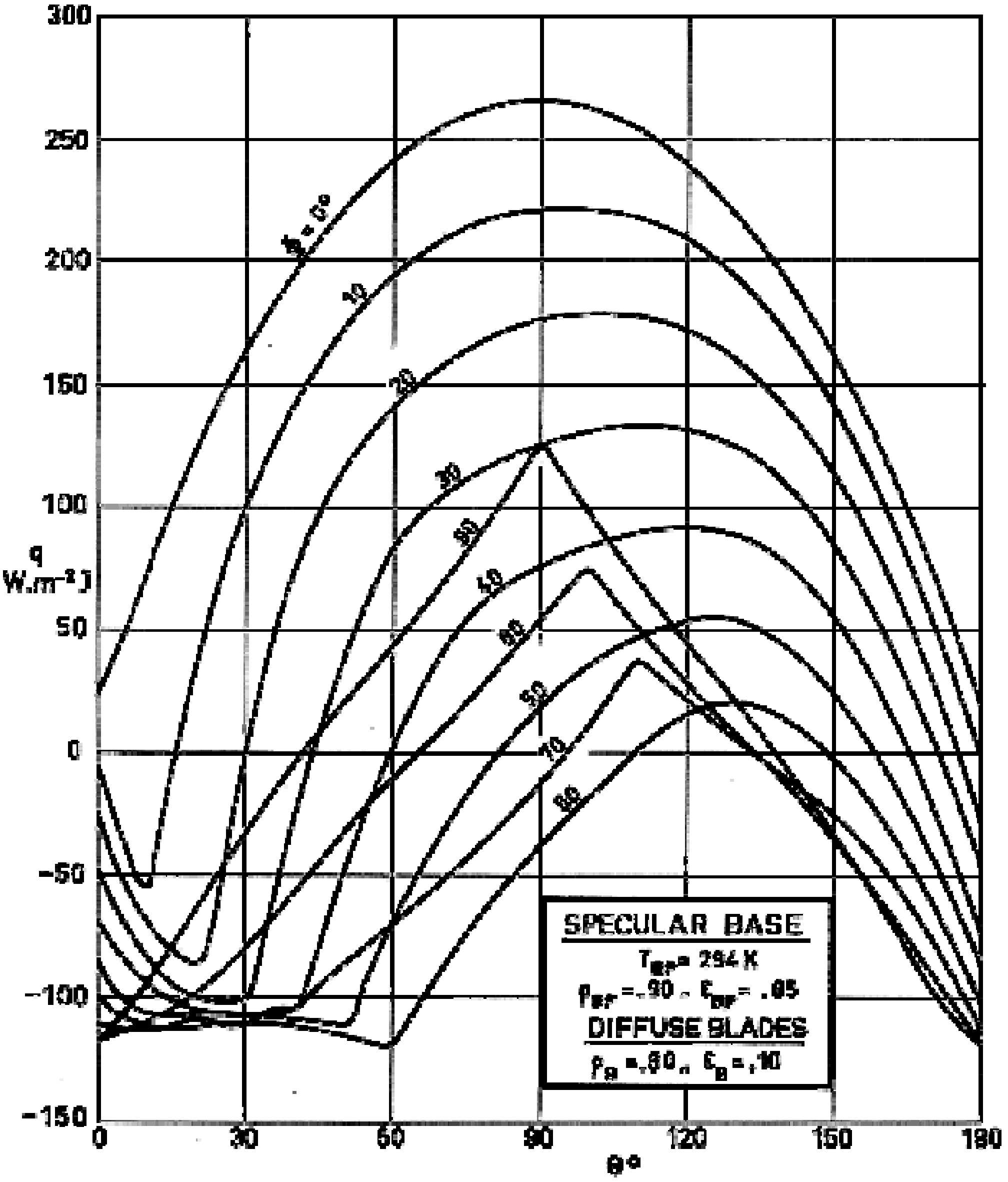

Figure 6-3: Heat rejection capability, *q*, vs. blade angle, *θ*, for several values of the sun angle, *ϕ*. From Parmer & Stipandic (1968) [27].

6.1.3 Effective absorptance

Effective absorptance is defined as

$\alpha_{eff} = (q_{shadow} - q)/S_0$

where:

S_0,	Solar Constant. S_0 = 1353 W.m^{-2}.
q,	Net Heat Transfer Rate at Louver Baseplate Surface (Heat Rejection Capability). [W.m^{-2}].

q_{shadow},	Net Heat Transfer Rate at Louver Baseplate Surface, when Solar Input is zero. [W.m^{-2}].

Other symbols which appear in the following figures are:

T_{BP},	Baseplate Temperature. [K].
ε_{B},	Emittance of the Blades.
ε_{BP},	Emittance of the Baseplate
ρ_{B},	Reflectance of the Blades.
ρ_{BP},	Reflectance of the Baseplate.

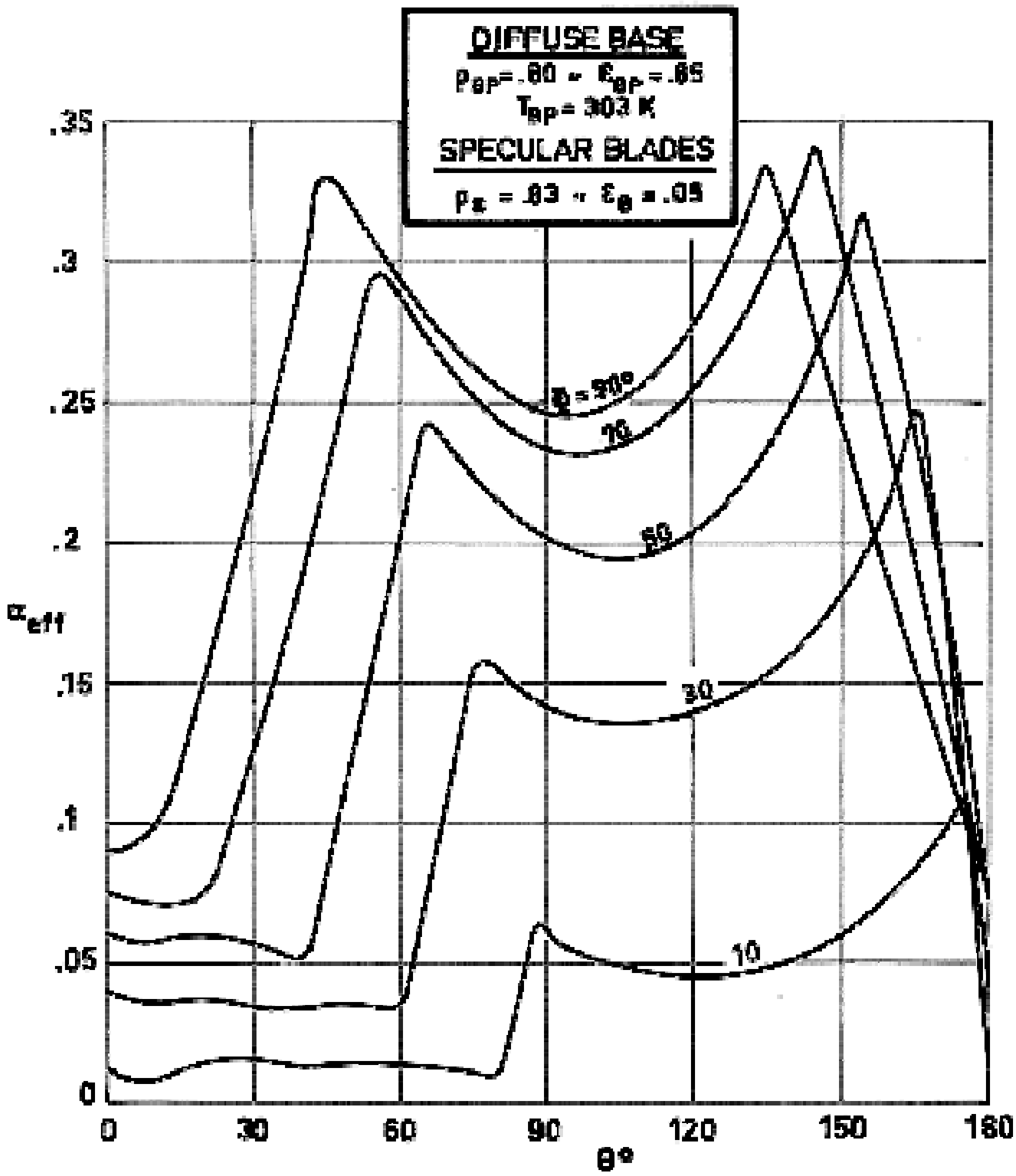

Note: non-si units are used in this figure

Figure 6-4: Effective absorptance, α_{eff}, vs. blade angle, θ, for several values of the sun angle, ϕ. After FAIRCHILD HILLER (1972) [10].

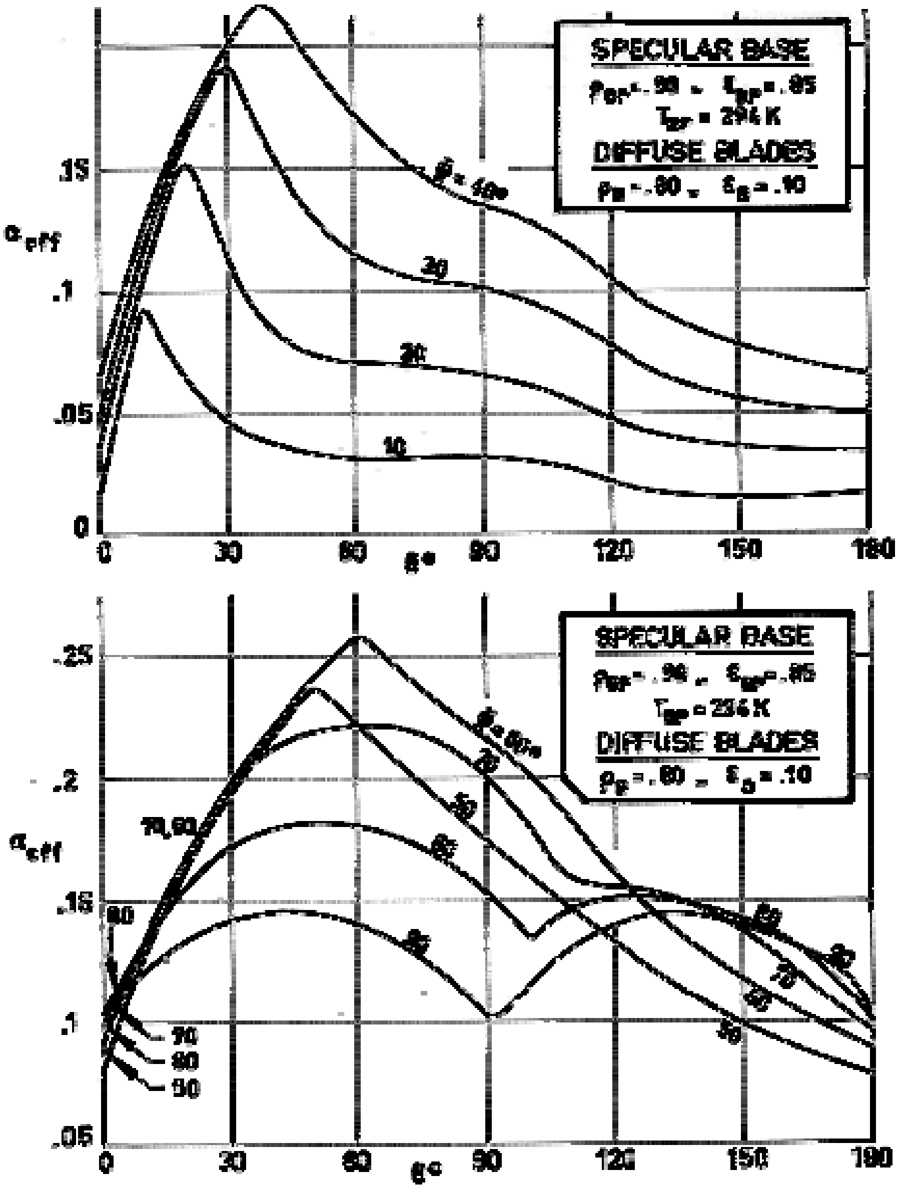

Note: non-si units are used in this figure

Figure 6-5: Effective absorptance, α_{eff}, vs. blade angle, θ, for several values of the sun angle, ϕ. After Parmer & Stipandic (1968) [27].

6.1.4 Effective emittance

Effective emittance of the louver baseplate can be obtained by use of the following expression:

$$\varepsilon_{eff} = q_{shadow} / \sigma T_{BP}^4$$

where:

T_{BP},	Baseplate Temperature. [K].
q_{shadow},	Net Heat Transfer Rate at Louver Baseplate Surface, when Solar Input is zero. [W.m^{-2}].

σ,	Stefan-Boltzmann Constant. $\sigma = 5,6697\text{x}10^{-8}$ $W.m^{-2}.K^{-4}$.

The effective emittance depends on the blade angle θ, and optical properties of the surface, being independent of the sun angle, θ.

Other symbols which appear in the following figures are:

***B*,**	Radiosity of the Baseplate. $[W.m^{-2}]$.
B*,	Dimensionless Radiosity of the Baseplate. $B^* = B / \sigma T_{BP}^4$
***L*,**	Blade Spacing. [m].
***b*,**	Blade Width. [m].
***x*,**	Coordinate along the Baseplate. [m].
***β*,**	Dimensionless Coordinate along the Baseplate. $\beta = x/L$:
ε_B,	Emittance of the Blades.
ε_{BP},	Emittance of the Baseplate
ρ_B,	Reflectance of the Blades.
ρ_{BP},	Reflectance of the Baseplate.

It should be pointed out that data presented in this data item are valid for both sun-light and shadow operation louvers.

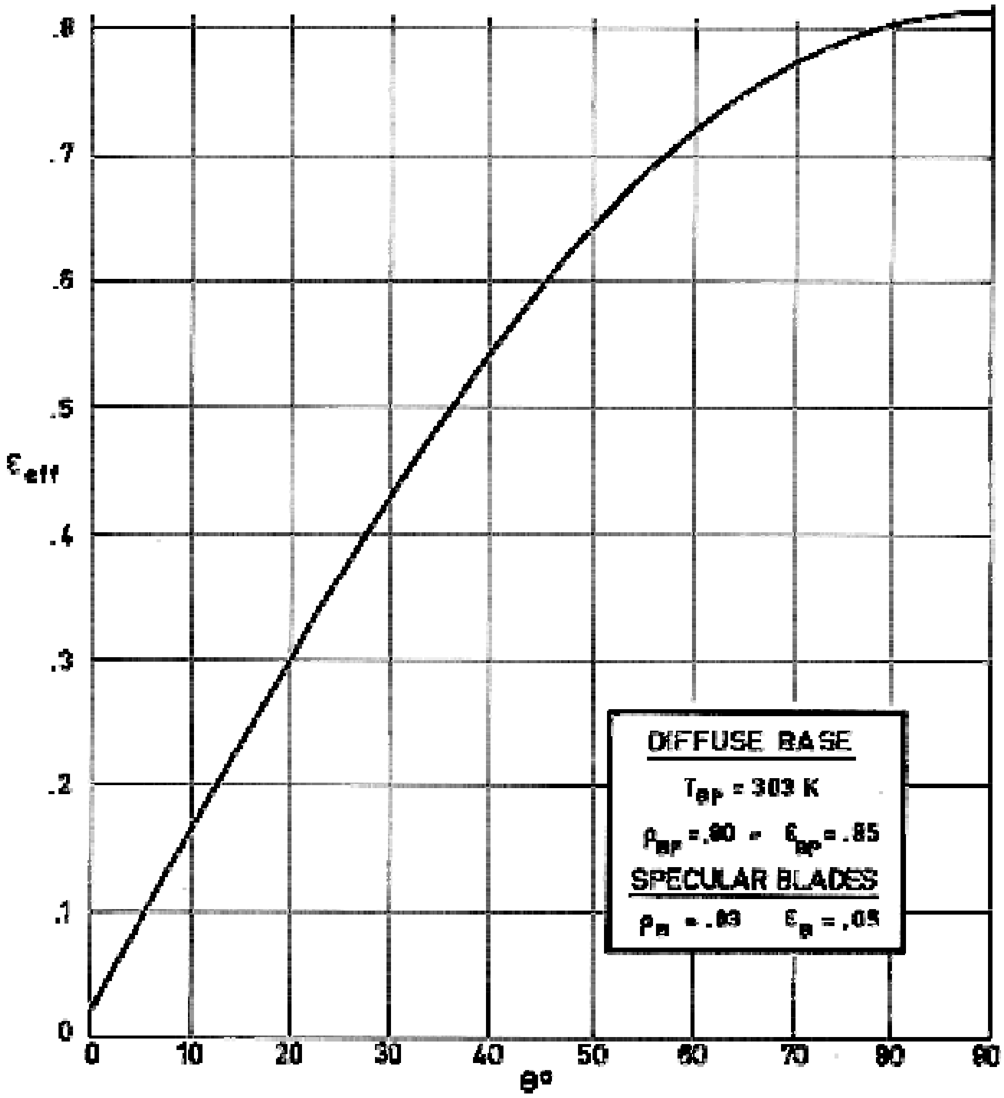

Note: non-si units are used in this figure

Figure 6-6: Effective emittance, ε_{eff}, vs. blade angle, θ. After FAIRCHILD HILLER (1972) [10].

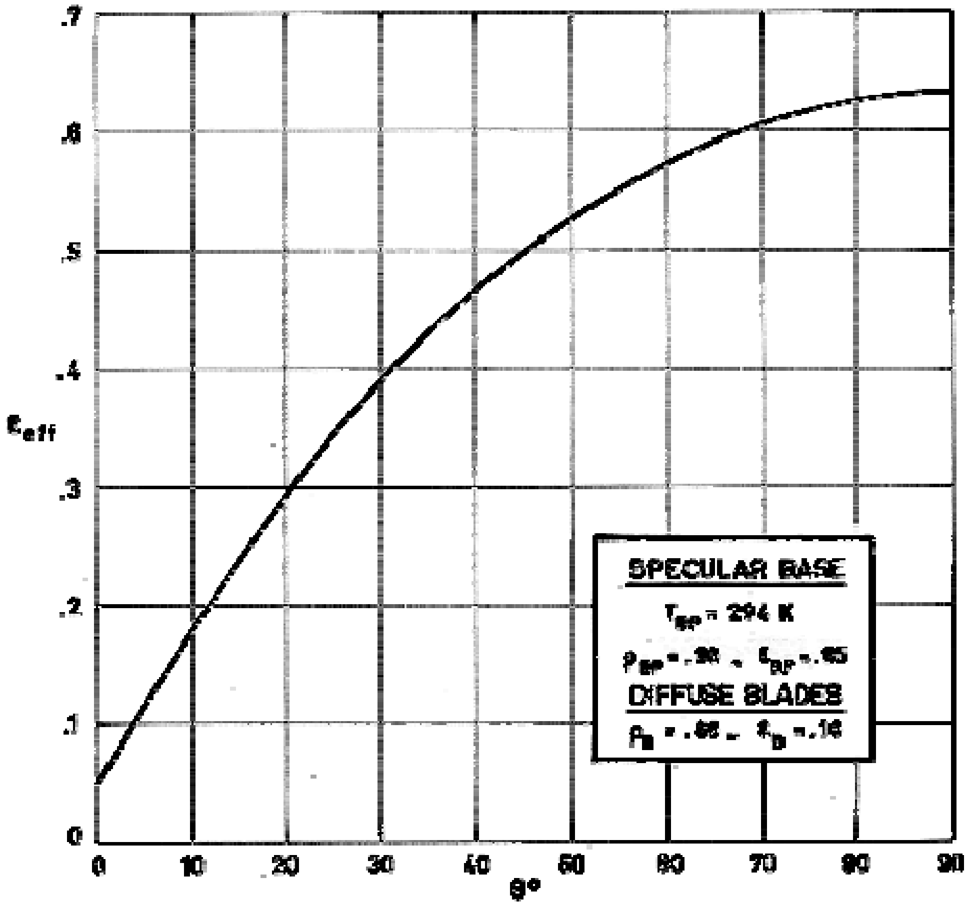

Note: non-si units are used in this figure

Figure 6-7: Effective emittance, ε_{eff}, vs. blade angle, θ. After Parmer & Stipandic (1968) [27].

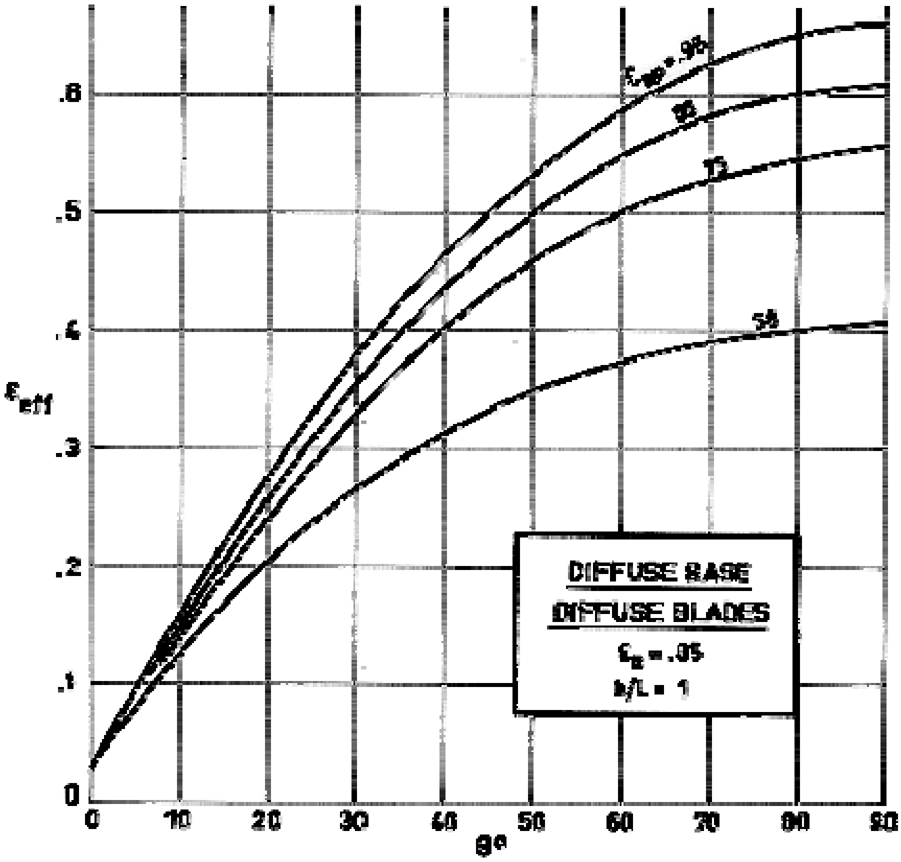

Note: non-si units are used in this figure

Figure 6-8: Effective emittance, ε_{eff}, vs. blade angle, θ, for several values of the baseplate emittance, ε_{BP}. ε_{eff} has been numerically calculated by using the following expression.

$$\varepsilon_{eff} = \frac{\varepsilon_{BP}}{1-\varepsilon_{BP}} \int_0^1 (1 - B^*) d\beta$$

From Plamondon (1964) [28].

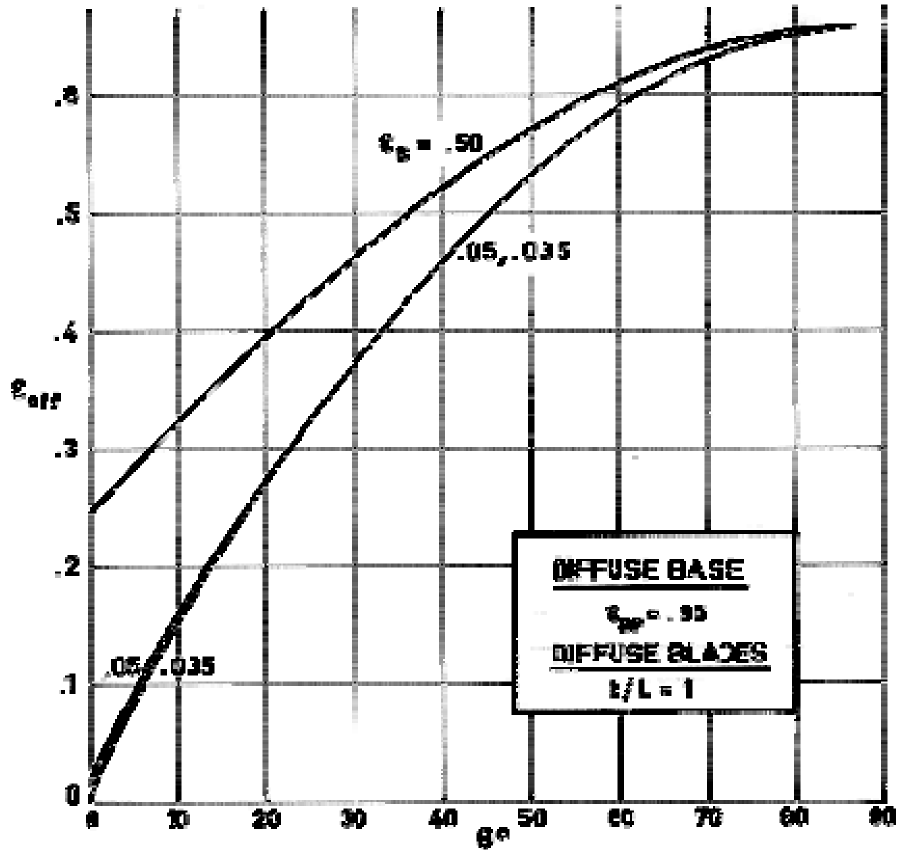

Note: non-si units are used in this figure

Figure 6-9: Effective emittance, ε_{eff}, vs. blade angle, θ, for several values of the blades emittance, ε_B. ε_{eff} has been numerically calculated by using the following expression.

$$\varepsilon_{eff} = \frac{\varepsilon_{BP}}{1-\varepsilon_{BP}} \int_0^1 (1 - B^*) d\beta$$

From Plamondon (1964) [28].

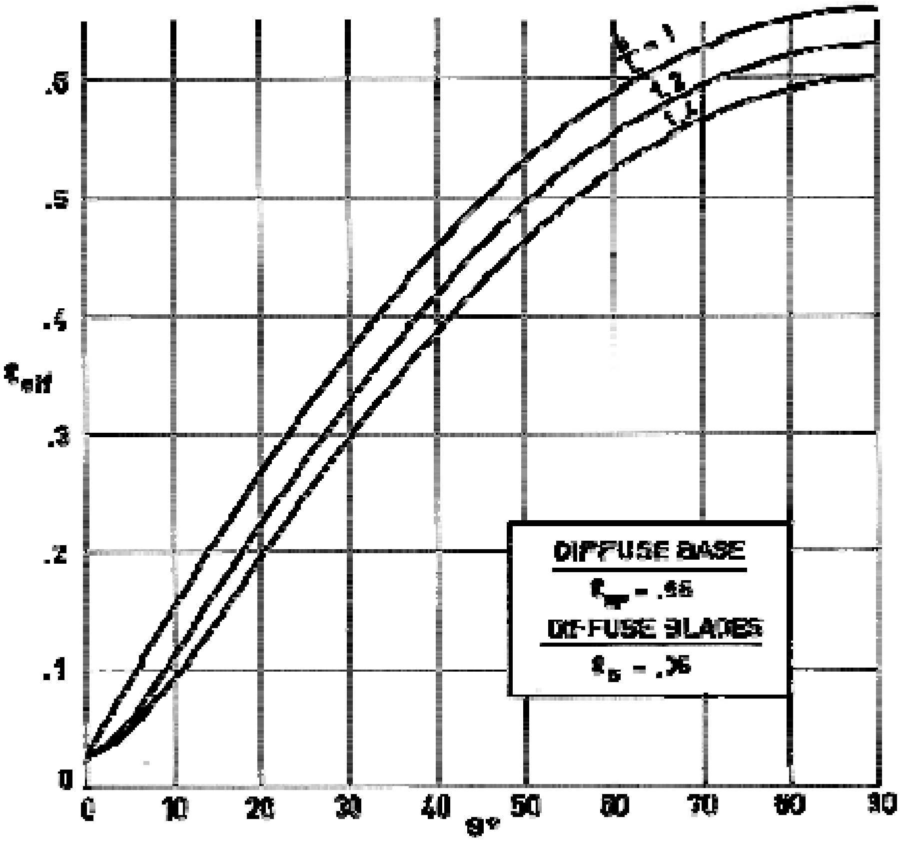

Note: non-si units are used in this figure

Figure 6-10: Effective emittance, ε_{eff}, vs. blade angle, θ, for several b/L values. ε_{eff} has been numerically calculated by using the following expression.

$$\varepsilon_{eff} = \frac{\varepsilon_{BP}}{1-\varepsilon_{BP}} \int_0^1 (1 - B^*) d\beta$$

From Plamondon (1964) [28].

6.2 Shadow operation

6.2.1 Introduction

A diagram of such a louver system is shown in Figure 6-11.

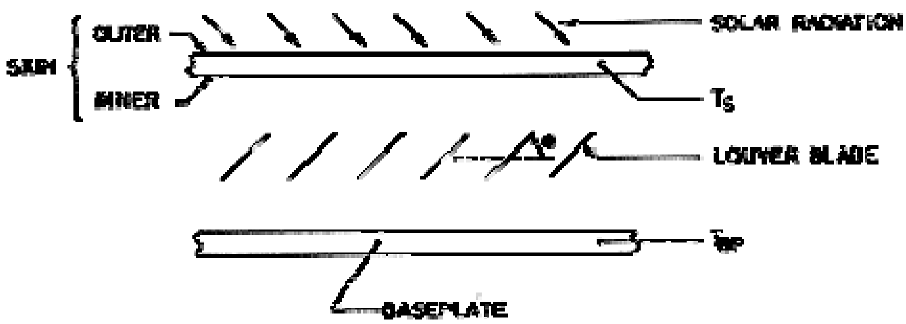

Figure 6-11: Schematic diagram of a louver for shadow operation.

Curves presented in this clause, are based on the following assumptions:

1. All surfaces, skin, blades and baseplate, have uniform, although different, temperatures.
2. All surfaces emit diffusely.
3. Optical properties for solar radiation are different from those corresponding to terrestrial radiation. In addition, $\alpha_\lambda + \rho_\lambda = 1$.
4. The surfaces are thermally coupled by radiation only.
5. The louver system has an infinite number of blades, so that edge effects can be neglected.

6.2.2 Radiosity and temperature field of the blades

Radiosity, B, of a differential area is given by the following expression:

$B = \varepsilon\sigma T^4 + \rho H$

where:

***H*,**	Energy Flux Impinging on the Unit Blade Area. [W.m^{-2}].
***T*,**	Temperature of the Differential Area. [T].
***ε*,**	Emittance of the Differential Area.
***ρ*,**	Reflectance of the Differential Area.
***σ*,**	Stefan-Boltzmann Constant. [W.m^{-2}.K^{-4}]. σ = 5,6697x10^{-8} W.m^{-2}.K^{-4}.

Additional symbols used in the next pages are the following:

B*,	Local Dimensionless Radiosity, defined as: $B^* = B / \sigma T_{BP}^4$
L,	Blade Spacing. [m].

T*,	Local Dimensionless Temperature, defined as: $T^* = T^4 / T_{BP}^4$
b,	Blade Width. [m].
y and z,	Coordinates Along the Outer and Inner Faces of the Blade Respectively. [m].
η and ζ,	Dimensionless Coordinates, $\eta = y/L$, $\zeta = z/L$.

Subscripts:

BI,	Blade Inner Face.
BO,	Blade Outer Face.
BP,	Baseplate.

Since energy is not generated internally in the blades, a heat balance through them gives:

$\sigma\,(\varepsilon_{BO}\,T_{BO}^4 + \varepsilon_{BI}\,T_{BI}^4) = \alpha_{BO}\,H_{BO} + \alpha_{BI} + H_{BI}$

Additional assumptions for calculating radiosity and temperature field of the blades are the following:

Blade temperature is not constant, but at each point of the blade $T_{BO} = T_{BI}$.

1. Emittance and absorptance of each surface are the same. In addition they are constant throughout each surface.
2. Emittance of the inner and outer surfaces of the blades are the same.
3. Both blades and baseplate surface emit and reflect diffusely.

Schematic diagram of the louver array is shown in Figure 6-12.

Figure 6-12: Schematic diagram of the louver array showing the coordinates and the significant geometrical characteristics.

Reference: Plamondon (1964) [28].

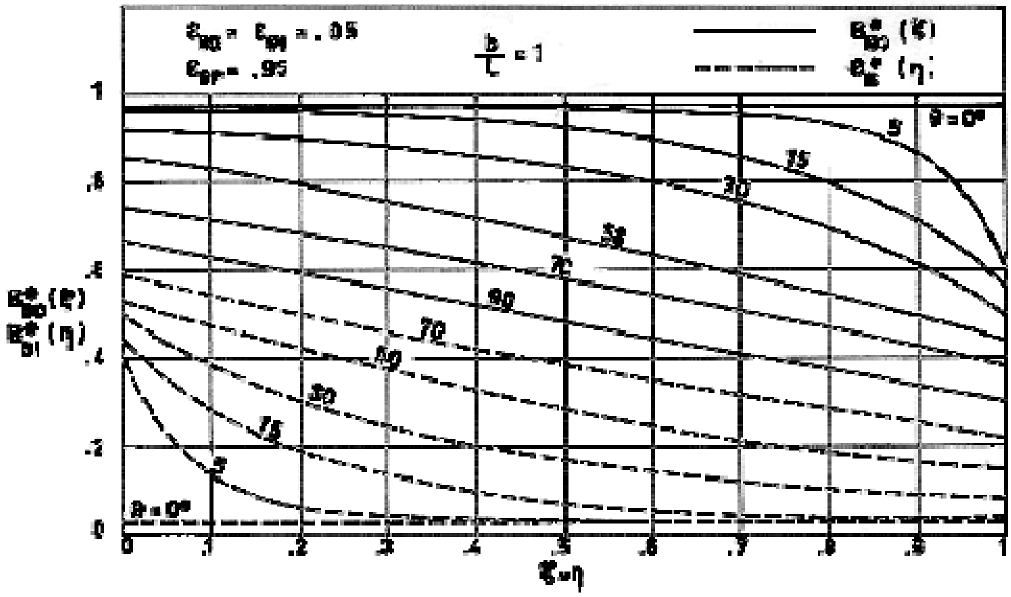

Note: non-si units are used in this figure

Figure 6-13: Dimensionless radiosity, *B, of the blades for several values of the blade angle, *θ*. From Plamondon (1964) [28].**

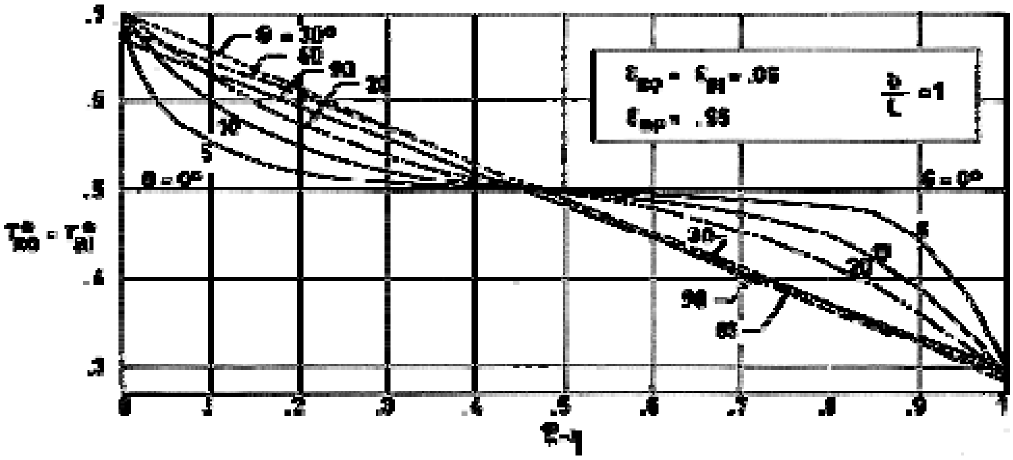

Note: non-si units are used in this figure

Figure 6-14: Dimensionless temperature, *T, of the blades for several values of the blade angle, *θ*. From Plamondon (1964) [28].**

6.2.3 Heat transfer through the louver

Heat transfer can be expressed as

$$q = \frac{\sigma\left(T_{BP}^4 - T_S^4\right)}{R(\theta)} \qquad [6\text{-}1]$$

while equilibrium in the skin requires:

$J + q = \varepsilon_s \sigma T_s^4$

Therefore:

$$q = \frac{\sigma T_{BP}^4 - \dfrac{J+q}{\varepsilon_s}}{R(\theta)} \qquad [6\text{-}2]$$

Introducing $f(\theta)$, defined as indicated in the List of Symbols, one obtains the net heat transfer at the baseplate.

$$q = \frac{\varepsilon_s \sigma T_{BP}^4 - J}{1 + \dfrac{\varepsilon_s}{1 - f(\theta)}} \qquad [6\text{-}3]$$

Figure 6-16 to Figure 6-23 show q as a function of T_{BP} for different values of J and ε_s. To calculate $f(\theta)$, the following emittance values have been taken:

Baseplate, ε_{BP} = 0,87

Blades, ε_B = 0,05

Inner face of the skin, ε_I = 0,87

The values of $f(\theta)$ obtained are plotted in Figure 6-15, and tabulated in the insert of that figure.

It should be noted that J reaches its maximum value when the solar radiation is incoming normally to the skin outer face. In such a case:

J_{max} ~150 W.m^{-2}.

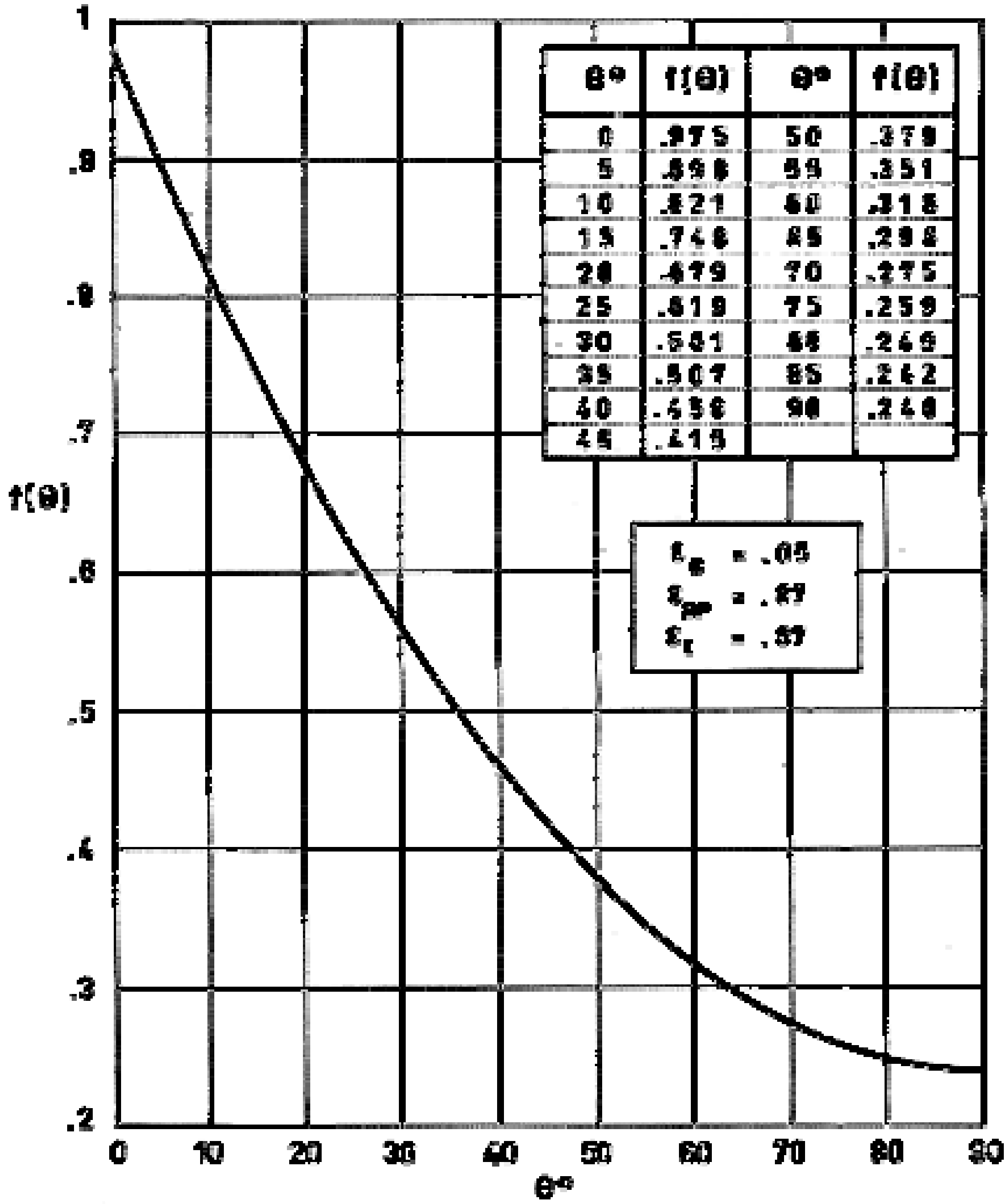

Note: non-si units are used in this figure

Figure 6-15: Function *f(θ)* vs. blade angle *θ*. After Parmer & Buskirk (1967)a [25].

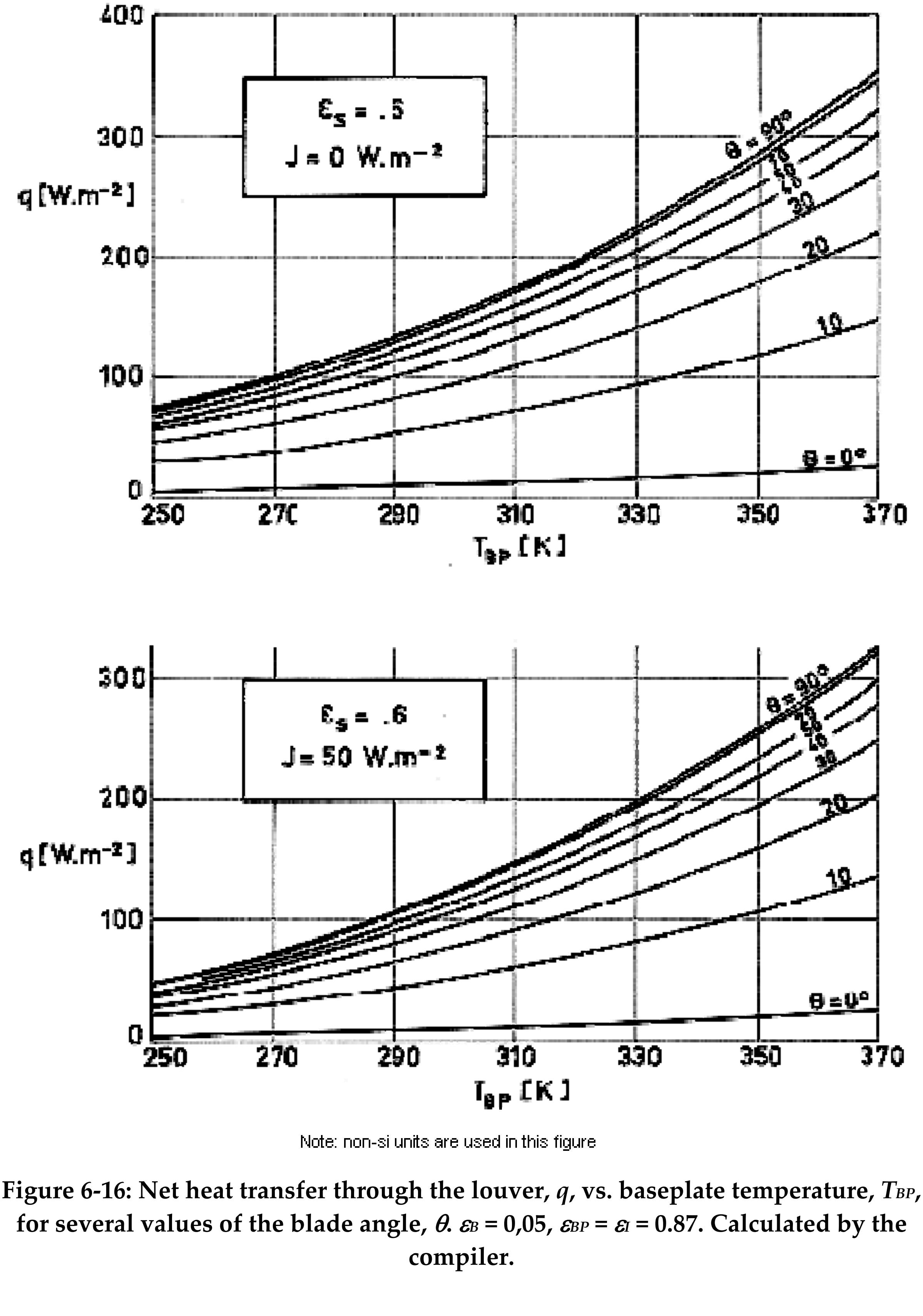

Figure 6-16: Net heat transfer through the louver, *q*, vs. baseplate temperature, T_{BP}, for several values of the blade angle, θ. ε_B = 0,05, $\varepsilon_{BP} = \varepsilon_I$ = 0.87. Calculated by the compiler.

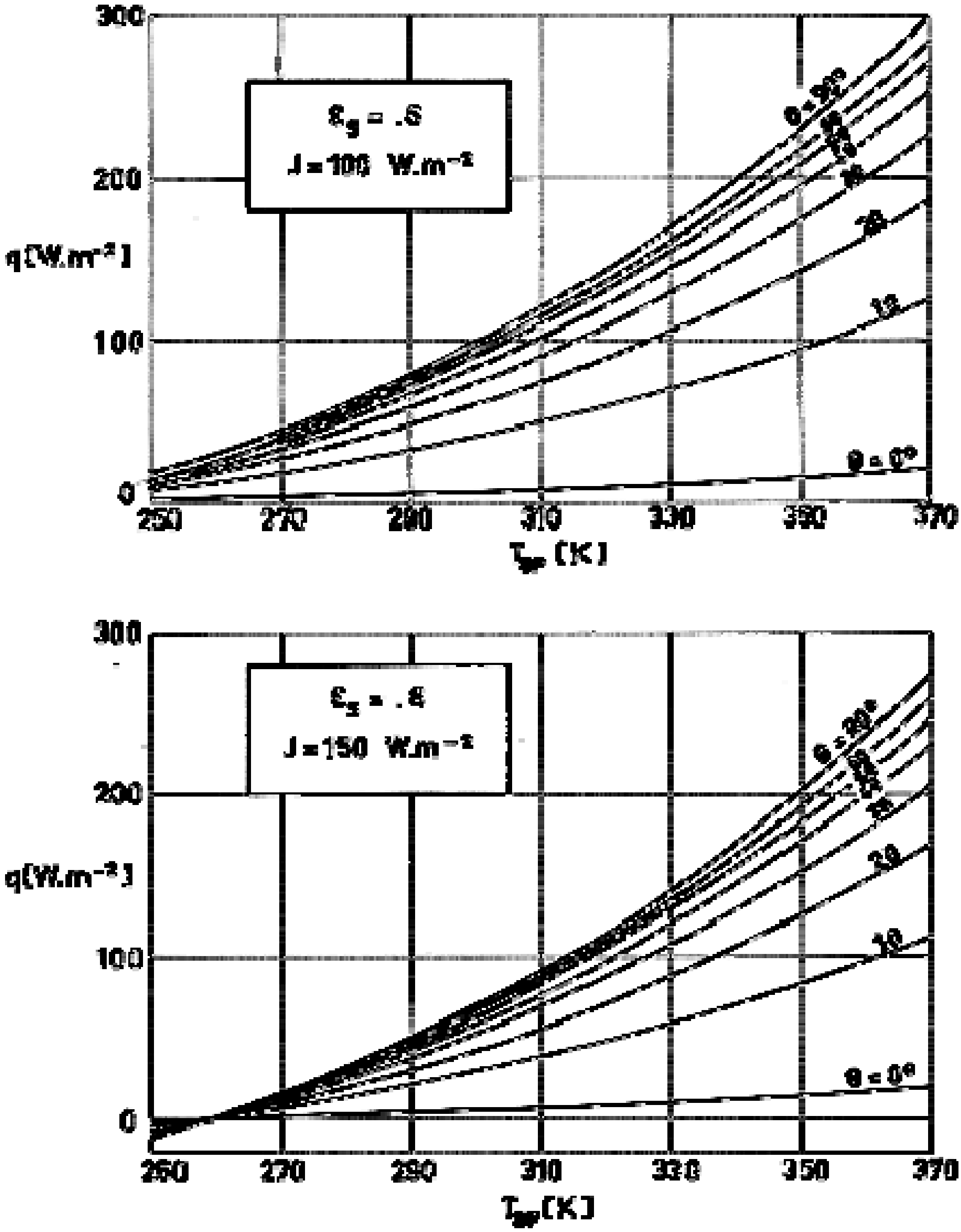

Note: non-si units are used in this figure

Figure 6-17: Net heat transfer through the louver, q, vs. baseplate temperature, T_{BP}, for several values of the blade angle, θ. ε_B = 0,05, ε_{BP} = ε_I = 0,87. Calculated by the compiler.

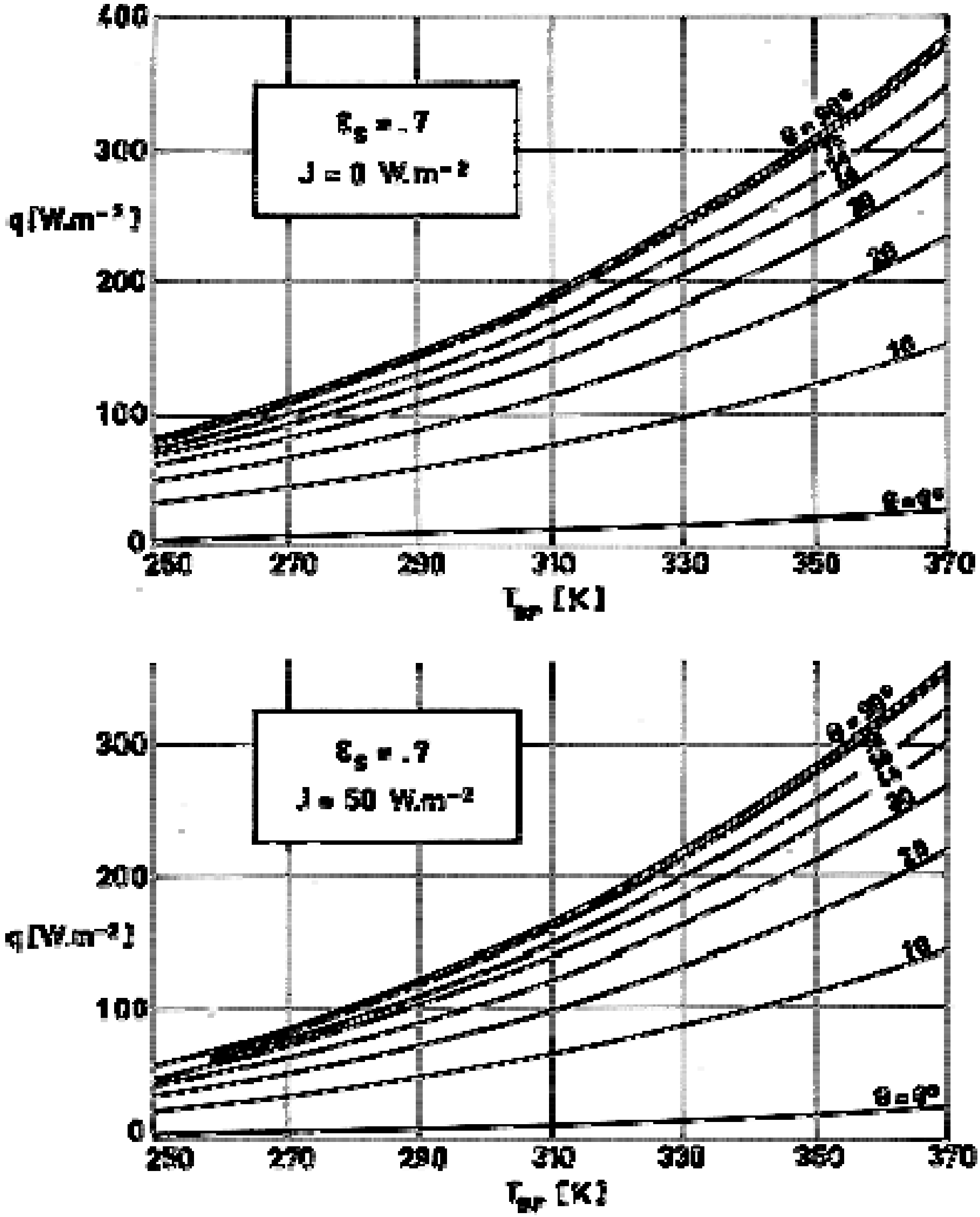

Note: non-si units are used in this figure

Figure 6-18: Net heat transfer through the louver, q, vs. baseplate temperature, T_{BP}, for several values of the blade angle, θ. ε_B = 0,05, ε_{BP} = ε_I = 0,87. Calculated by the compiler.

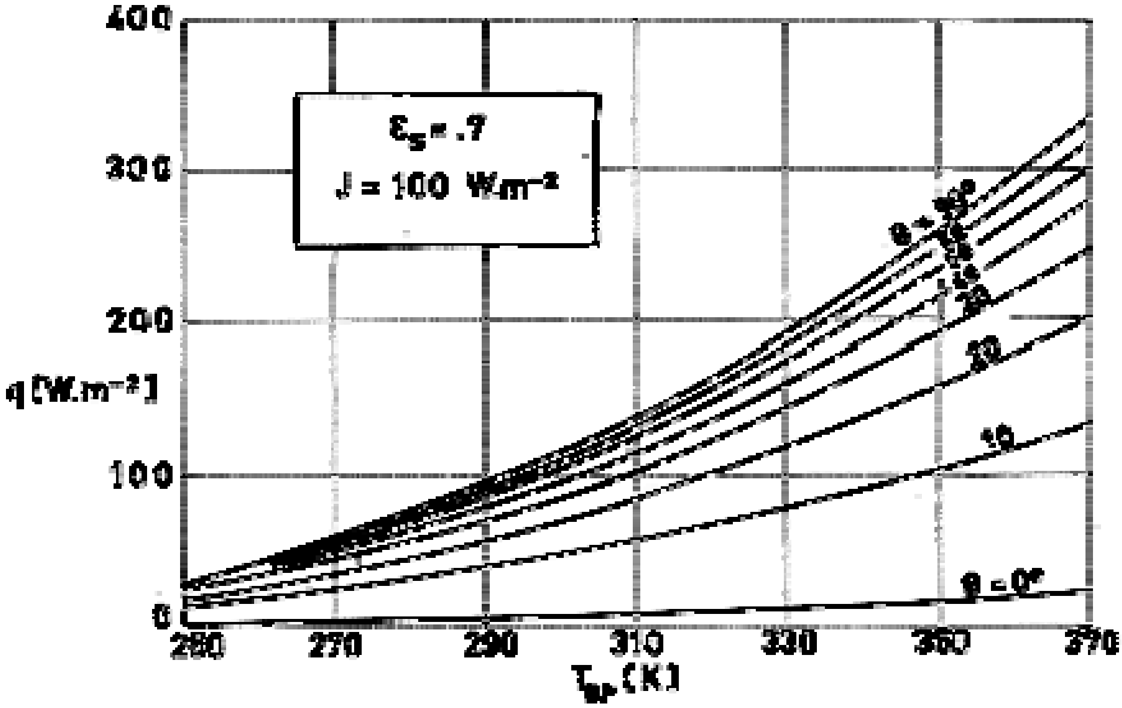

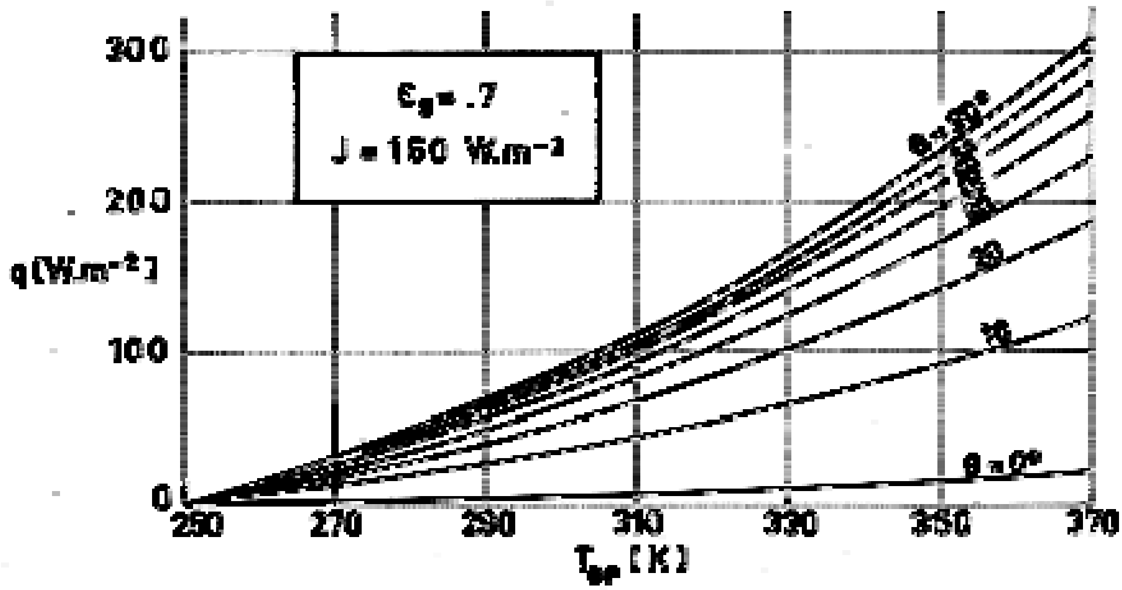

Note: non-si units are used in this figure

Figure 6-19: Net heat transfer through the louver, q, vs. baseplate temperature, T_{BP}, for several values of the blade angle, θ. ε_B = 0,05, ε_{BP} = ε_I = 0,87. Calculated by the compiler.

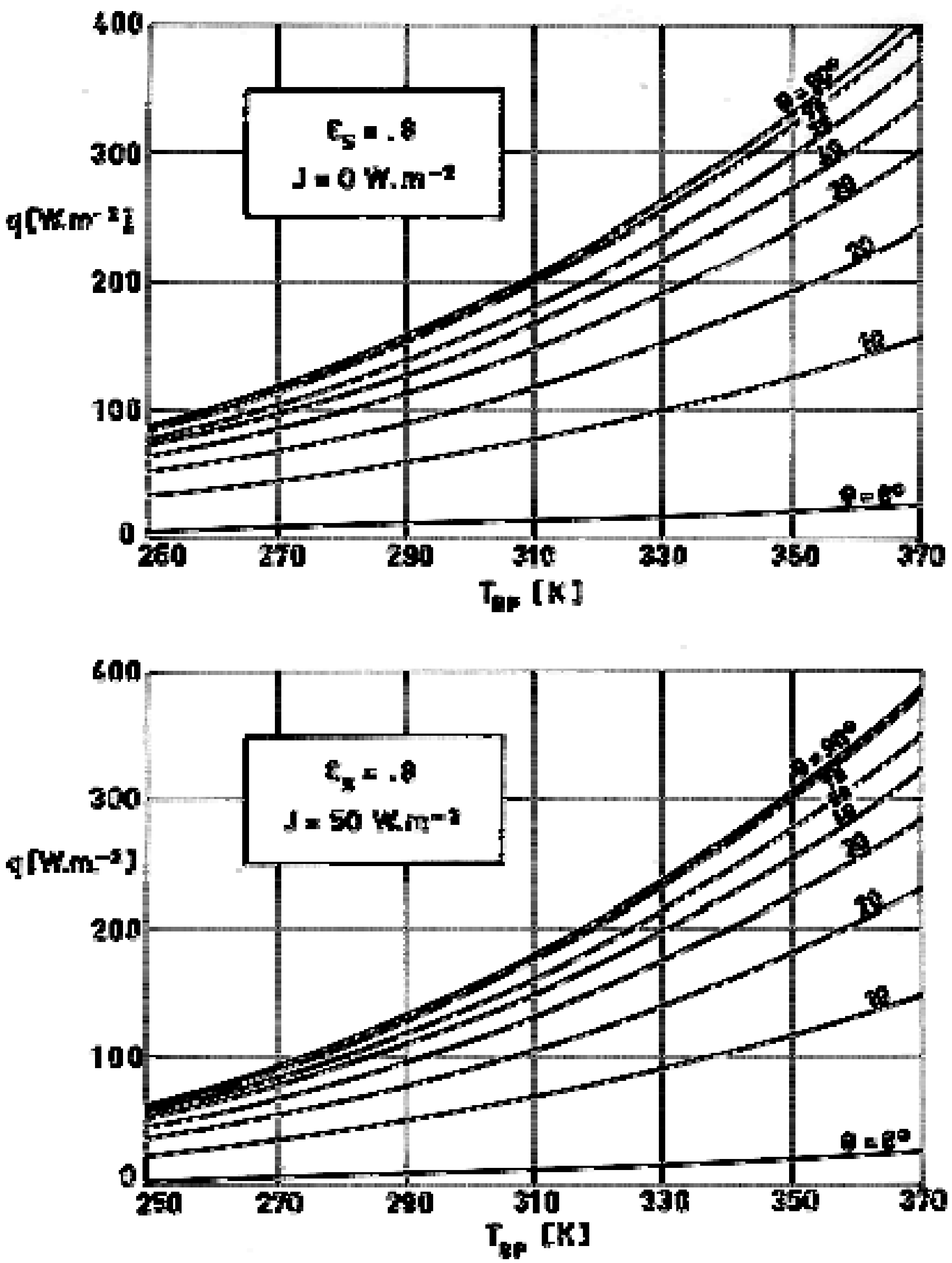

Note: non-si units are used in this figure

Figure 6-20: Net heat transfer through the louver, *q*, vs. baseplate temperature, T_{BP}, for several values of the blade angle, θ. ε_B = 0,05, ε_{BP} = ε_I = 0,87. Calculated by the compiler.

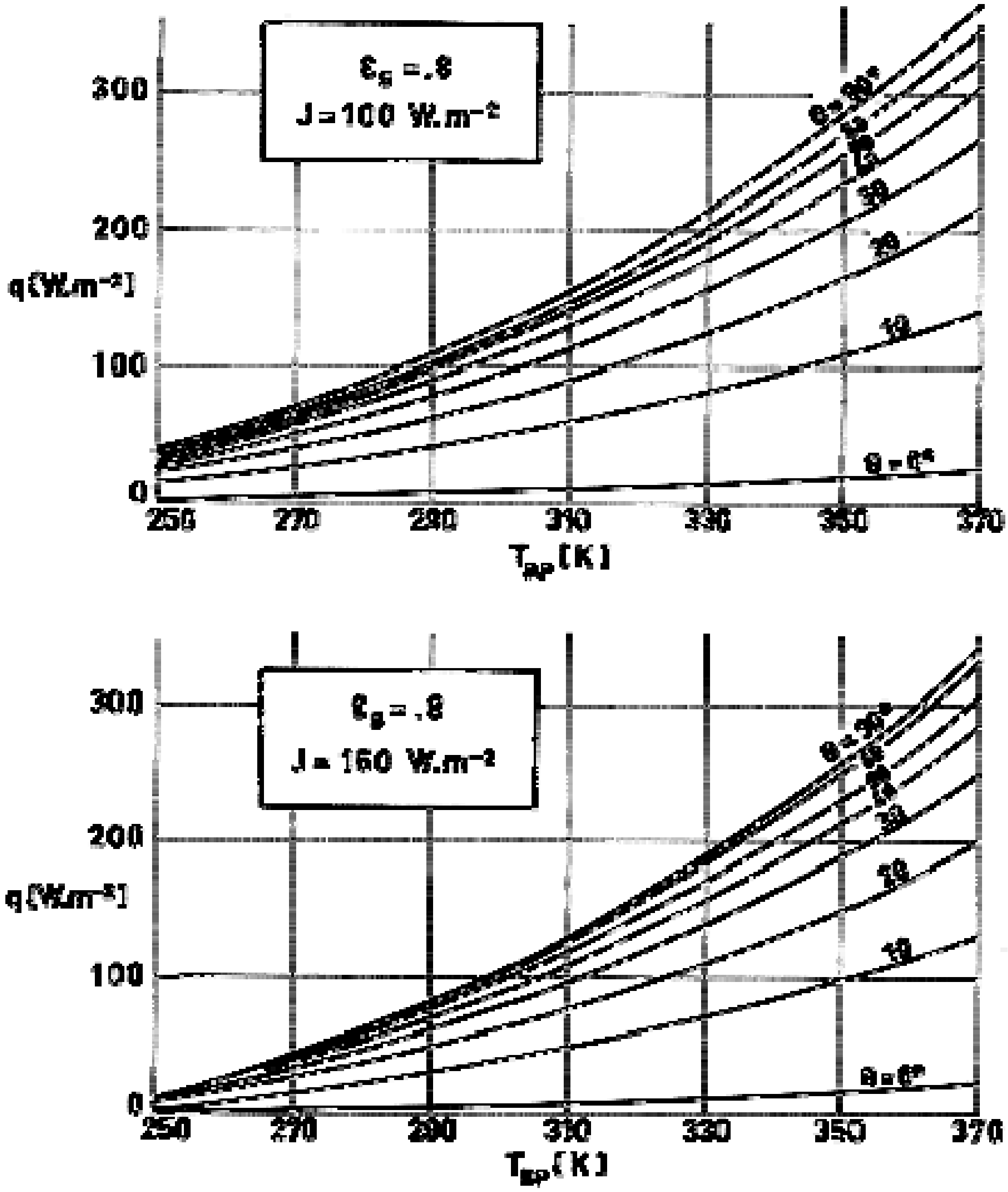

Note: non-si units are used in this figure

Figure 6-21: Net heat transfer through the louver, q, vs. baseplate temperature, T_{BP}, for several values of the blade angle, θ. ε_B = 0,05, ε_{BP} = ε_I = 0,87. Calculated by the compiler.

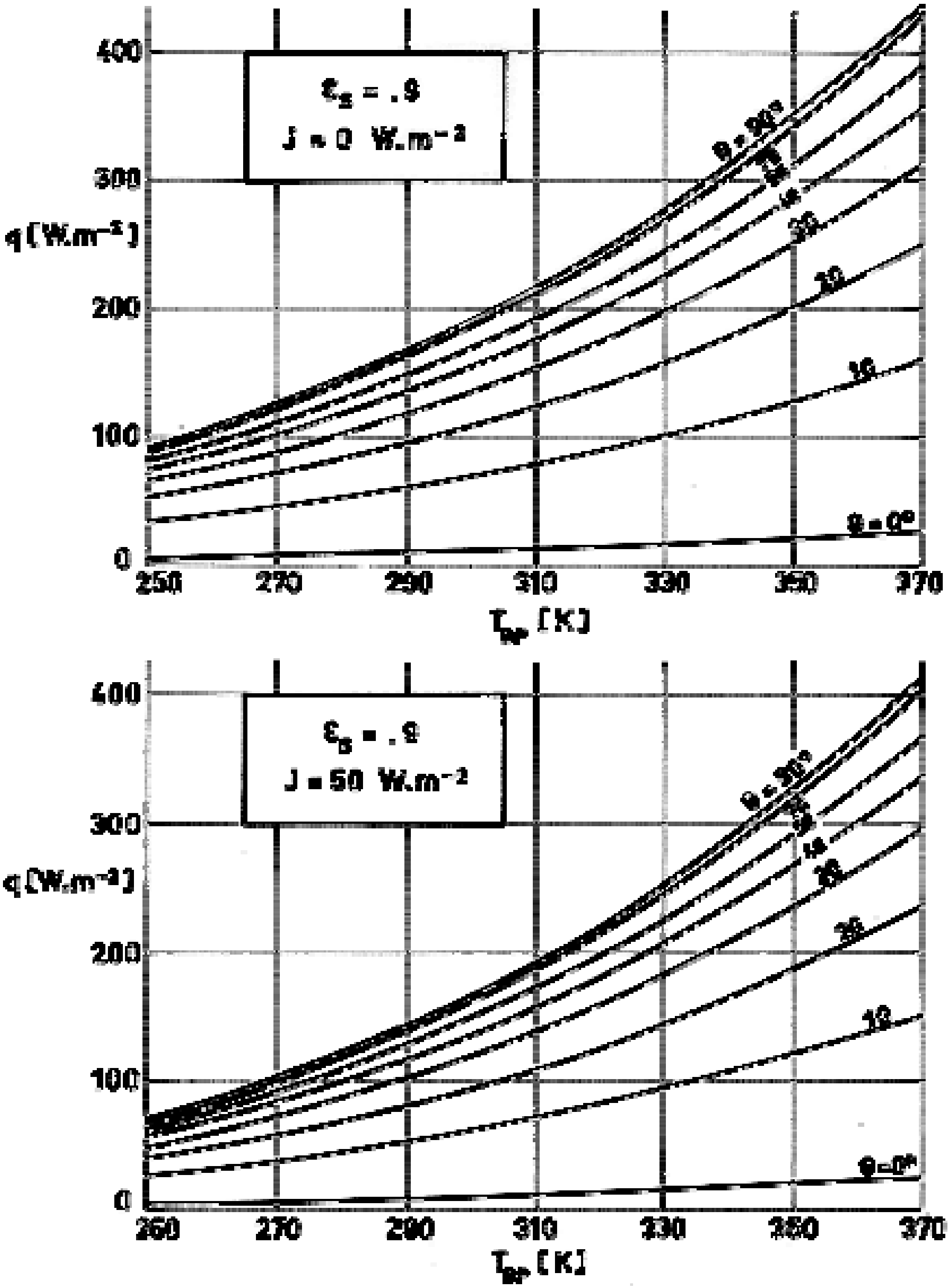

Note: non-si units are used in this figure

Figure 6-22: Net heat transfer through the louver, q, vs. baseplate temperature, T_{BP}, for several values of the blade angle, θ. ε_B = 0,05, ε_{BP} = ε_I = 0,87. Calculated by the compiler.

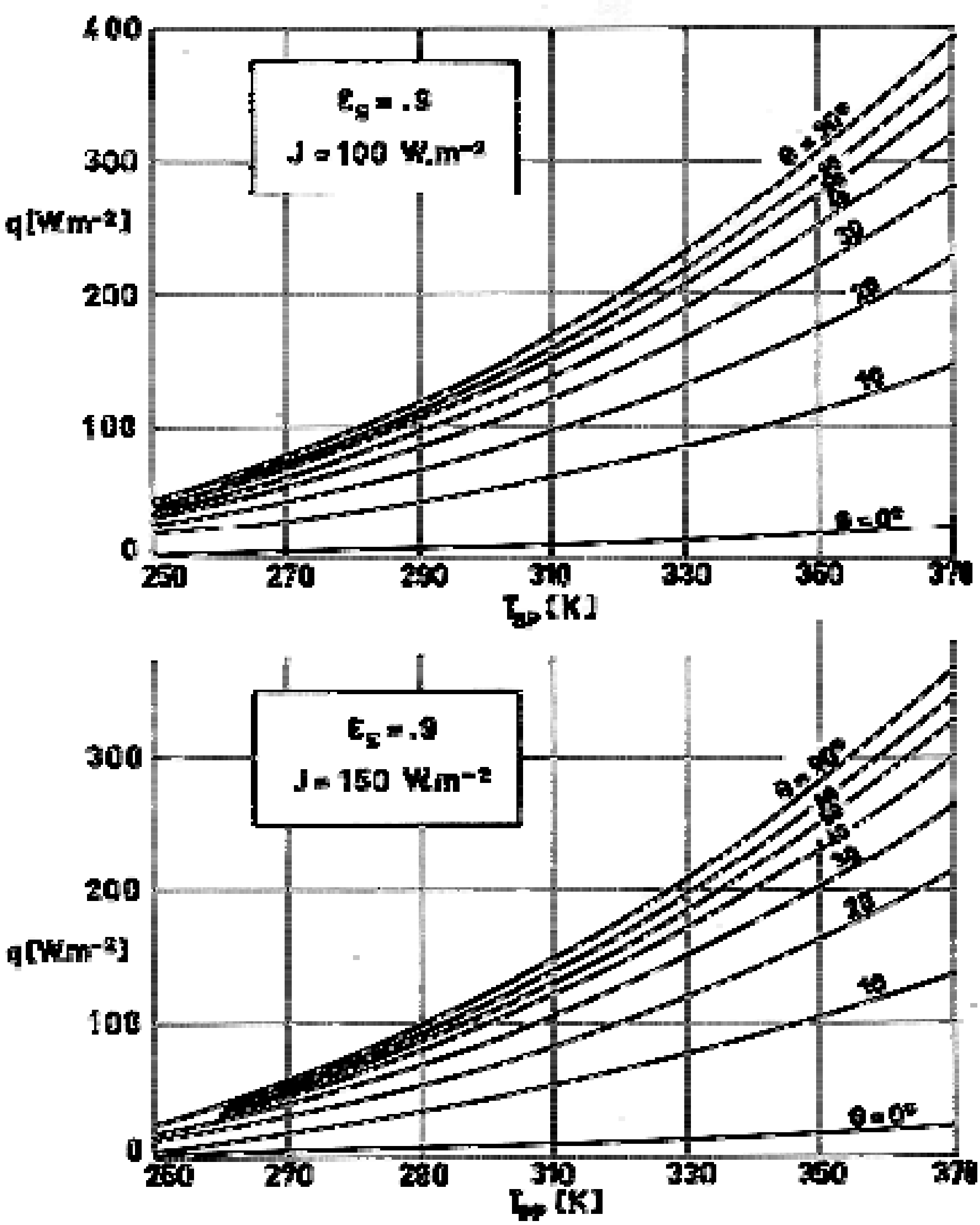

Note: non-si units are used in this figure

Figure 6-23: Net heat transfer through the louver, q, vs. baseplate temperature, T_{BP}, for several values of the blade angle, θ. ε_B = 0,05, $\varepsilon_{BP} = \varepsilon_I$ = 0,87. Calculated by the compiler.

7 Existing systems

7.1 Summary table

EXISTING SYSTEMS	PRODUCER
ATLAS ABLE - 4 LUNAR SATELLITE	
A T S	FAIRCHILD HILLER
HELIOS	ERNO
MARINER	
NIMBUS 1, 2 & 3	GENERAL ELECTRIC
O A O	FAIRCHILD HILLER
OGO 1	
PEGASUS	FAIRCHILD HILLER
PIONEER 4	TRW-SYSTEMS
TELSTAR	
	SNIAS

NOTE For details see the following tables.

		ATLAS ABLE - 4 LUNAR SATELLITE	A T S
PRODUCER			FAIRCHILD HILLER
LAUNCHING DATE		-/-/60	5/30/74
SPACECRAFT EMITTING AREA [m^2]			15,05
SPACECRAFT GENERATED POWER TO EMITTING AREA RATIO [W.m^2]			From 19,91 to 39,86
GEOMETRY OF ARRAY		Circular	Rectangular
LOUVER ARRAYS PER SPACECRAFT		50 Masks	15
MASS TO AREA RATIO PER ARRAY [kg.m^{-2}]			5,57
BLADES	SHAPE	Rotary mask	Rectangular
	DIMENSIONS [mx10^3]		
	MATERIAL		Polished Aluminium with white paint strip (12% area) [a]
	α_s		0,17
	ε		0,05
	NUMBER PER LOUVER ARRAY	4 per mask	
	ANGLE RANGE [Angular Degrees]	± 22,5	90
ACTUATOR	TYPE	Bimetal	Bimetal
	SENSITIVITY [Angular Degrees.K^{-1}]	3,3	5,3
	NUMBER OF BLADES PER ACTUATOR		2
BASEPLATE	AREA PER LOUVER ARRAY [m^2]		0,273 and 0,135 [b]
	COATING		OSR [c]

			ATLAS ABLE - 4 LUNAR SATELLITE		A T S	
	α_s	ε			0,08	0,81
TEMPERATURE RANGE [K]			280–294		ΔT = 17 K	
SET POINT VARIATION RANGE [K]					There are three set points 281, 283, and 292 K	
ε_{eff} RANGE			0,07–0,82		0,12–0,75	
α_{eff} RANGE					Approximately 0,04–0,30	
COST [Local Money per Unit]						
COMMENTS			Maltese cross system		[a] The white paint strip (DC92-007) was added to lower the blade temperature. Values of α_s and ε were measured before the white strip was added. [b] Louvers are made of two different sizes for testing purposes. [c] OSR are placed over a honeycomb-heat pipe structure.	

		HELIOS	MARINER 2 (VENUS)	MARINER 4 (MARS)	MARINER 5 (VENUS)
PRODUCER		ERNO			
LAUNCHING DATE		12/10/74	8/6/62	11/28/64	10/19/67
SPACECRAFT EMITTING AREA [m²]		2,29		3,8	
SPACECRAFT GENERATED POWER TO EMITTING AREA RATIO [W.m²]		78,6		Earth 103,9 Mars 44,7	
GEOMETRY OF ARRAY		Circular	Rectangular		
LOUVER ARRAYS PER SPACECRAFT		15 Segments [a]	1	6	6
MASS TO AREA RATIO PER ARRAY [kg.m⁻²]		4,7	8,6	4	5
BLADES	SHAPE	Trapezoidal	Rectangular		
	DIMENSIONS [mx10³]	220 Length, 100 Max. Width		150x30	
	MATERIAL	Polished Aluminium	Polished Aluminium		
	α_s / ε	/	0,12 / 0,04	0,12 / 0,04	/
	NUMBER PER LOUVER ARRAY	6 per segment	8	22	22
	ANGLE RANGE [Angular Degrees]	90	90		
ACTUATOR	TYPE	Bimetal	Bimetal		
	SENSITIVITY [Angular Degrees.K⁻¹]	3,33	5,4	6,3	
	NUMBER OF BLADES PER ACTUATOR	1	2	2	2
BASEPLATE	AREA PER	0,11 per segment	0,12	0,15	

		HELIOS	MARINER 2 (VENUS)	MARINER 4 (MARS)	MARINER 5 (VENUS)
	LOUVER ARRAY [m^2]				
	COATING	IITRI Z-93 white paint	White paint TiO_2 silicone base	White paint TiO_2/PV-100	PV-100
	α_s				0,2
	ε	0,93			0,85
TEMPERATURE RANGE [K]		283-290	ΔT = 17 K [b]	283-300	
SET POINT VARIATION RANGE [K]					
ε_{eff} RANGE		0,13-0,80	0,08-0,72	0,12-0,76	
α_{eff} RANGE					
COST [Local Money per Unit]					
COMMENTS		a A circular system is formed by eight independent segments with six blades each. • Upper platform has a complete system plus two segments. • Lower platform has five segments.	b Temperature for incipient opening of the louver may be varied.		

<table>
<tr><td colspan="3" rowspan="2"></td><td colspan="4">NIMBUS 1, 2 & 3</td><td colspan="6">O A O</td></tr>
<tr><td colspan="2">CONTROL SUBSYSTEM</td><td colspan="2">SENSORY SUBSYSTEM</td><td colspan="2">2</td><td colspan="2">3</td><td colspan="2">4</td></tr>
<tr><td colspan="3">PRODUCER</td><td colspan="4">GENERAL ELECTRIC</td><td colspan="6">FAIRCHILD HILLER</td></tr>
<tr><td colspan="3">LAUNCHING DATE</td><td colspan="4">8/28/64, 5/15/66 & 1/–/70</td><td colspan="2"></td><td colspan="2"></td><td colspan="2"></td></tr>
<tr><td colspan="3">SPACECRAFT EMITTING AREA [m²]</td><td colspan="2">2</td><td colspan="2">4,95</td><td colspan="2"></td><td colspan="2"></td><td colspan="2"></td></tr>
<tr><td colspan="3">SPACECRAFT GENERATED POWER TO EMITTING AREA RATIO [W.m²]</td><td colspan="2">23,7 (Mean Value)</td><td colspan="2"></td><td colspan="2"></td><td colspan="2"></td><td colspan="2"></td></tr>
<tr><td colspan="3">GEOMETRY OF ARRAY</td><td colspan="2">Rectangular</td><td colspan="2">Cylindrical</td><td colspan="6">Rectangular</td></tr>
<tr><td colspan="3">LOUVER ARRAYS PER SPACECRAFT</td><td colspan="2">2</td><td colspan="2">13, 14 & 17</td><td colspan="2">9</td><td colspan="2"></td><td colspan="2"></td></tr>
<tr><td colspan="3">MASS TO AREA RATIO PER ARRAY [kg.m⁻²]</td><td colspan="2">15,14</td><td colspan="2"></td><td colspan="2">7,32</td><td colspan="2"></td><td colspan="2"></td></tr>
<tr><td rowspan="6">BLADES</td><td colspan="2">SHAPE</td><td colspan="4">Rectangular</td><td colspan="6">Rectangular</td></tr>
<tr><td colspan="2">DIMENSIONS [mx10³]</td><td colspan="2"></td><td colspan="2"></td><td colspan="2"></td><td colspan="2"></td><td colspan="2"></td></tr>
<tr><td colspan="2">MATERIAL</td><td colspan="2">Al-Fiberglass Diffuse</td><td colspan="2">Al-Mylar Specular</td><td colspan="6">Polished Aluminium</td></tr>
<tr><td>α_s</td><td>ε</td><td>0,2</td><td>0,8</td><td>0,15</td><td>0,03</td><td>0,12</td><td></td><td></td><td>0,06</td><td></td><td></td></tr>
<tr><td colspan="2">NUMBER PER LOUVER ARRAY</td><td colspan="2"></td><td colspan="2"></td><td colspan="2">14</td><td colspan="2">26</td><td colspan="2">34</td></tr>
<tr><td colspan="2">ANGLE RANGE [Angular Degrees]</td><td colspan="2">90</td><td colspan="2"></td><td colspan="2">90</td><td colspan="2"></td><td colspan="2"></td></tr>
<tr><td rowspan="3">ACTUATOR</td><td colspan="2">TYPE</td><td colspan="4">Liquid-Vapor Bellows</td><td colspan="2">Bimetal</td><td colspan="2"></td><td colspan="2"></td></tr>
<tr><td colspan="2">SENSITIVITY [Angular Degrees.K⁻¹]</td><td colspan="2"></td><td colspan="2"></td><td colspan="2">8,2</td><td colspan="2"></td><td colspan="2"></td></tr>
<tr><td colspan="2">NUMBER OF BLADES PER ACTUATOR</td><td colspan="2"></td><td colspan="2"></td><td colspan="2"></td><td colspan="2">1</td><td colspan="2"></td></tr>
<tr><td>BASEPLATE</td><td colspan="2">AREA PER LOUVER ARRAY [m²]</td><td colspan="2"></td><td colspan="2"></td><td colspan="2">0,146</td><td colspan="2"></td><td colspan="2"></td></tr>
</table>

	NIMBUS 1, 2 & 3				O A O					
	CONTROL SUBSYSTEM		SENSORY SUBSYSTEM		2		3		4	
COATING	Vitavar PV-100 Paint									
α_s / ε	0,3	0,9	0,3	0,9						
TEMPERATURE RANGE [K]	298-308		292-300		275-292		266-283		280-300	
SET POINT VARIATION RANGE [K]			5 K of Margin		88-533					
ε_{eff} RANGE			0,15-0,65		0,08-0,72					
α_{eff} RANGE										
COST [Local Money per Unit]	Not specified for the complete system [a]									
COMMENTS	[a] The manufacturer quotes 40000 US $.m^{-2} - Fail-Safe bellows are provided.									

		OGO 1	PEGASUS 1	PEGASUS 2	PEGASUS 3
PRODUCER			FAIRCHILD HILLER		
LAUNCHING DATE		9/4/64	2/16/65	5/25/65	8/–/65
SPACECRAFT EMITTING AREA [m²]		7,2			
SPACECRAFT GENERATED POWER TO EMITTING AREA RATIO [W.m²]		34,7			
GEOMETRY OF ARRAY			Rectangular		
LOUVER ARRAYS PER SPACECRAFT			2		
MASS TO AREA RATIO PER ARRAY [kg.m⁻²]		2,93	7,32		
BLADES	SHAPE	Rectangular	Rectangular		
	DIMENSIONS [mx10³]		200x50		
	MATERIAL	Polished Aluminium	Polished Aluminium 5052		
	α_s	0,12	0,11		
	ε	0,04		0,05	
	NUMBER PER LOUVER ARRAY		24		
	ANGLE RANGE [Angular Degrees]	90	90		
ACTUATOR	TYPE	Bimetal	Bimetal		
	SENSITIVITY [Angular Degrees.K⁻¹]	5,3			
	NUMBER OF BLADES PER ACTUATOR	1	1	1	1
BASEPLATE	AREA PER		0,31 (Total)		

<table>
<tr><td colspan="3" rowspan="2"></td><td colspan="2" rowspan="2">OGO 1</td><td colspan="6">PEGASUS</td></tr>
<tr><td colspan="2">1</td><td colspan="2">2</td><td colspan="2">3</td></tr>
<tr><td rowspan="3"></td><td colspan="2">LOUVER ARRAY [m²]</td><td colspan="2"></td><td colspan="2"></td><td colspan="2"></td><td colspan="2"></td></tr>
<tr><td colspan="2">COATING</td><td colspan="2"></td><td colspan="2"></td><td colspan="2"></td><td colspan="2"></td></tr>
<tr><td>α_s</td><td>ε</td><td></td><td></td><td></td><td></td><td></td><td></td><td></td><td></td></tr>
<tr><td colspan="3">TEMPERATURE RANGE [K]</td><td colspan="2">283-300</td><td colspan="2">277-281</td><td colspan="2">278-289</td><td colspan="2">274-281</td></tr>
<tr><td colspan="3">SET POINT VARIATION RANGE [K]</td><td colspan="2"></td><td colspan="2">188-533</td><td colspan="2"></td><td colspan="2"></td></tr>
<tr><td colspan="3">ε_{eff} RANGE</td><td colspan="2"></td><td colspan="2">0,12-0,61</td><td colspan="2">0,13-0,54</td><td colspan="2">0,08-0,50</td></tr>
<tr><td colspan="3">α_{eff} RANGE</td><td colspan="2"></td><td colspan="2"></td><td colspan="2"></td><td colspan="2"></td></tr>
<tr><td colspan="3">COST [Local Money per Unit]</td><td colspan="2"></td><td colspan="6"></td></tr>
<tr><td colspan="3">COMMENTS</td><td colspan="2">Blades are of two formed sheets 1,27x10^{-4} m thick each, welded together along the two edges.</td><td colspan="6">• Extreme values of ε_{eff} are for blade angle opening <5º and >70º respectively.
• Data on temperature range and ε_{eff} are obtained in flight.
• System for shadow operation.</td></tr>
</table>

		PIONEER 4	TELSTAR	
PRODUCER		TRW-SYSTEMS		SNIAS
LAUNCHING DATE		3/3/59	7/10/62	
SPACECRAFT EMITTING AREA [m^2]				
SPACECRAFT GENERATED POWER TO EMITTING AREA RATIO [$W.m^2$]				
GEOMETRY OF ARRAY		Circular	Circular Disk	Rectangular
LOUVER ARRAYS PER SPACECRAFT		1		
MASS TO AREA RATIO PER ARRAY [$kg.m^{-2}$]				10
BLADES	SHAPE	Trapezoidal		Rectangular
	DIMENSIONS [$mx10^3$]	267 Length, 76,2 to 25,4 Width		123x38
	MATERIAL	Aluminium Sheets $2x10^{-4}$ m thick		Polished Aluminium (A9)
	α_s	0,15-0,20		0,10
	ε	0,04		0,04
	NUMBER PER LOUVER ARRAY	30		18
	ANGLE RANGE [Angular Degrees]	90		90
ACTUATOR	TYPE	Bimetal	Liquid-Vapor Bellows	Bimetal or Bourdon
	SENSITIVITY [Angular Degrees.K^{-1}]	3,6		18 [a]
	NUMBER OF BLADES PER ACTUATOR	1		2
BASEPLATE	AREA PER LOUVER ARRAY [m^2]			0,79
	COATING	"CAT-A-LAC" White		OSR

			PIONEER 4		TELSTAR		
	α_s	ε		0,85		0,06	0,77
TEMPERATURE RANGE [K]			278-303		286-292	293-298	
SET POINT VARIATION RANGE [K]							
ε_{eff} RANGE			0,20-0,73			0,13-0,70	
α_{eff} RANGE						0-0,265	
COST [Local Money per Unit]						300000 FF	
COMMENTS						Developed louver use Bimetal as actuator. Bourdon spirals may be also used	
a Average value from tests of a Bourdon actuated unit. From Aalders (1973).							

7.2 Ats louvers

7.2.1 Introduction

The applications Technology Satellite (ATS) is an earth-oriented synchronous altitude platform for advanced communications and specific experimentation.

The spacecraft has two major elements: a precision 9,14 m diameter deployable antenna reflector, and an earth-viewing module (EVM), housing the electronic components and scientific packages.

The EVM is essentially a cube 1,37 m side having a total mass of approximately 816 kg. Four of the six faces of this cube are covered with superinsulations. The two remaining faces are honeycomb panels containing 2,88 m^2 of thermal louver systems. Heat pipes are embedded in the honeycomb panels with the aim of reducing the temperature gradient along them.

7.2.2 Analytical calculations

The thermal performances of the ATS spacecraft were computed using two different programs. The first one is a vehicle illumination program which gives the amount of solar energy absorbed by all parts of the system both through direct input and after a number of reflections not larger than five. The values of the optical properties used in this program are given in Table 7-1.

Table 7-1: Assumed Values of the Optical Properties of the Surfaces for the First Computer program

COMPONENT	α_s	ρ^s (specular)
Blades Baseplate Frames	0,17 0,10 0,10	1 1 1

The second computer program gives the radiation couplings between all parts of the system and between the system and the outer space. the computation has been made taking into account all the reflections, and using the values given in Table 7-2.

Table 7-2: Assumed Values of the Optical Properties of the Surfaces for the Second Computer program

COMPONENT	ε	ρ^s (specular)
Blades Baseplate Frames	0,05 0,82 0,025	0,95 0,81 0,90

Additional assumptions are the following:

1. Optical properties are independent of sun angle.
2. All surfaces emit diffusely.
3. Blades are finite in length, width, and number. In the case under consideration there are four blades 0,158 m long and 0,052 m wide.
4. Blades and baseplate are individually isothermal.
5. Blades are conductively isolated from the remainder of the system.

Analytical predictions of the effective emittance, effective absorptance, and heat rejection capability vs. blade and sun angles are plotted in Figure 7-1, Figure 7-2 and Figure 7-3 respectively. Experimental values of the effective emittance have been also plotted in Figure 7-1.

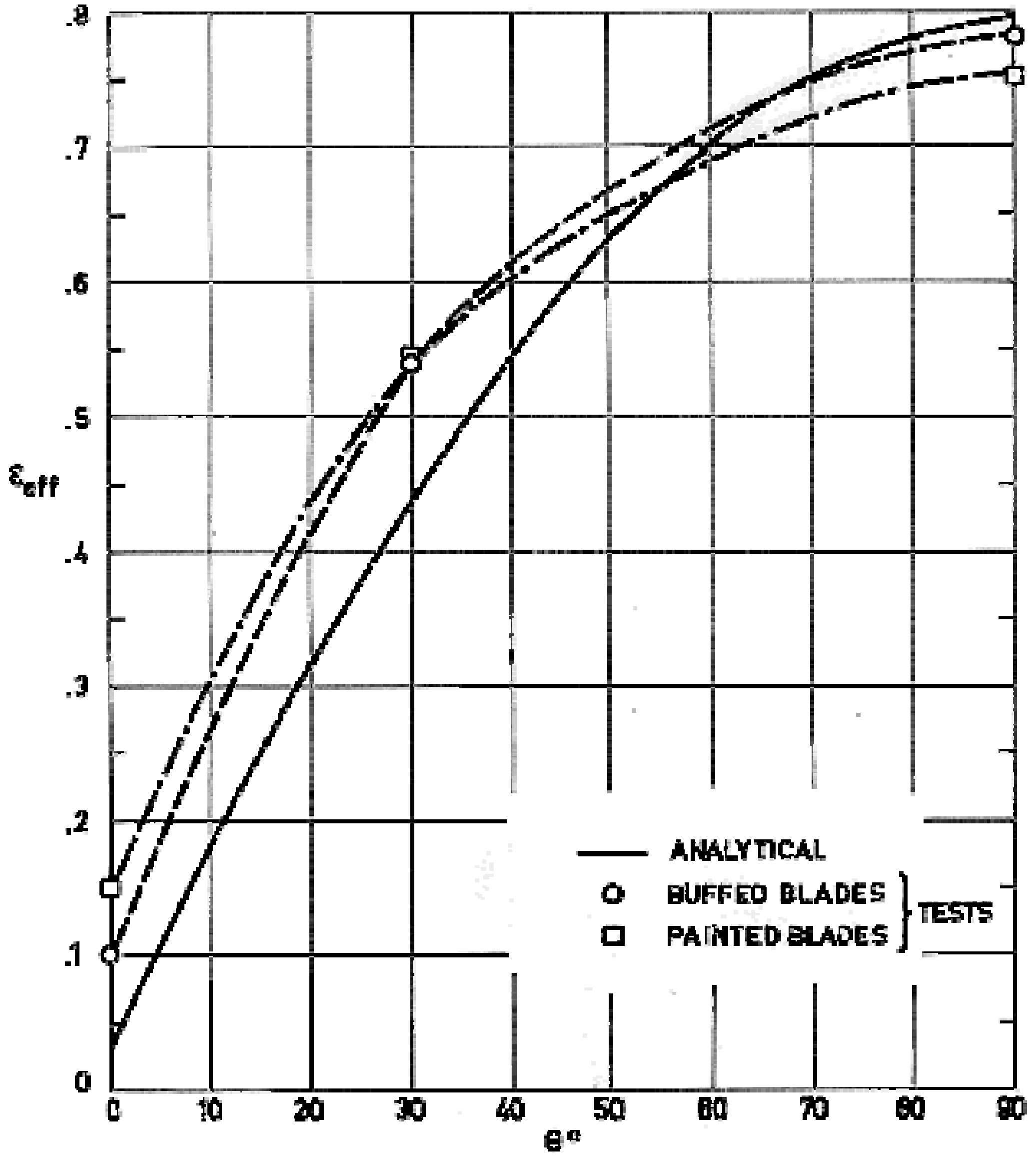

Note: non-si units are used in this figure

Figure 7-1: Effective emittance, ε_{eff}, based on area of the large unit, vs. blade angle, θ, for ATS spacecraft. From Michalek, Stipandic & Coyle (1972) [24].

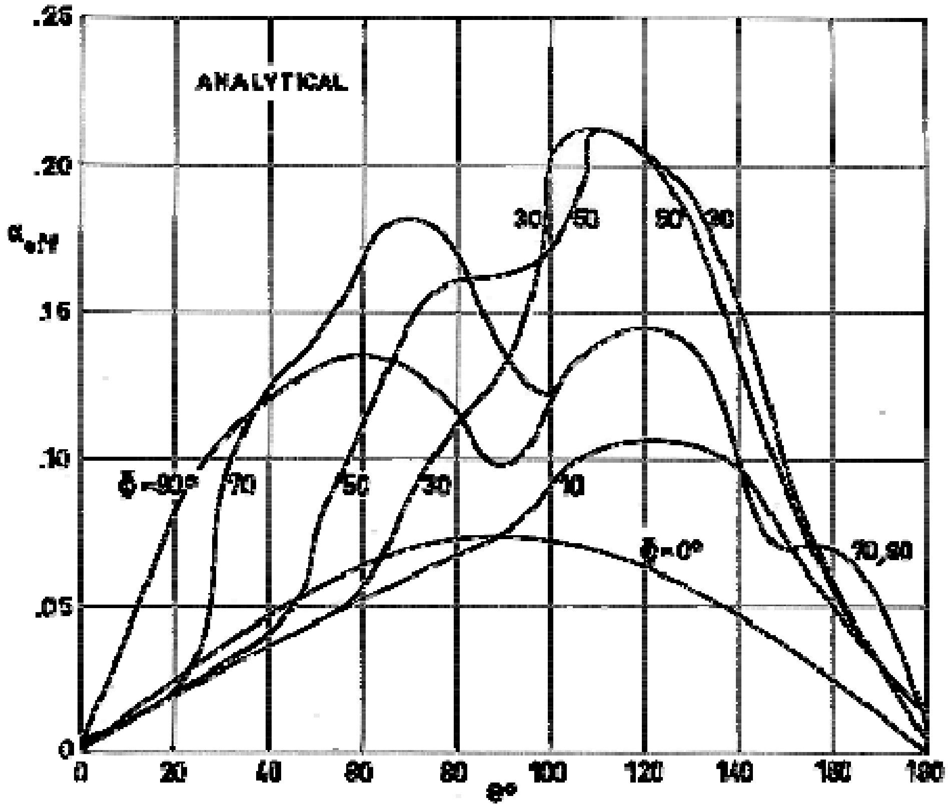

Note: non-si units are used in this figure

Figure 7-2: Effective absorptance, α_{eff}, vs. blade angle, θ, for several values of the sun angle, ϕ, for ATS spacecraft. From Michalek, Stipandic & Coyle (1972) [24].

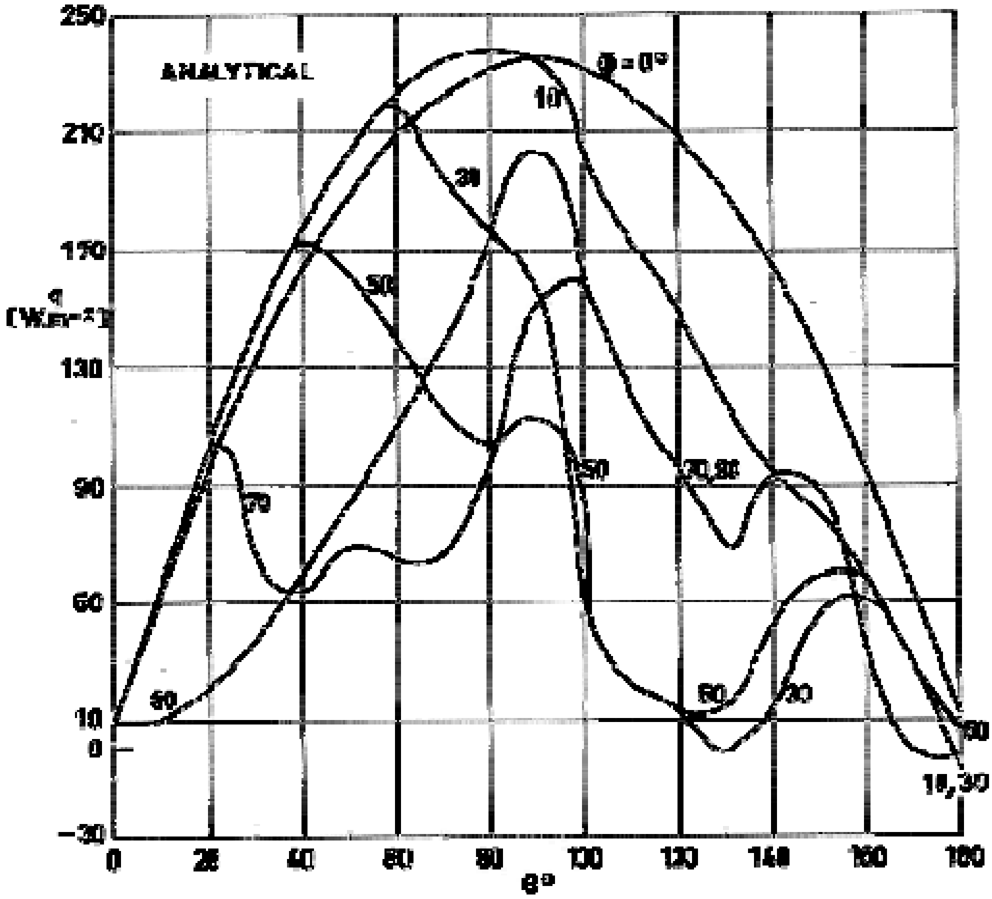

Figure 7-3: Heat rejection capability, *q*, vs. blade angle, *θ*, for several values of the sun angle, *ϕ*, for ATS spacecraft. From Michalek, Stipandic & Coyle (1972) [24].

7.2.3 Tests

Louvers of ATS spacecraft were tested in a solar vacuum chamber. Two separate units, labeled "small unit test" (inner frame dimensions 0,32 x 0,42 m^2) and "large unit test" (inner frame dimensions 0,48 x 0,57 m^2) in Figure 7-4 and Figure 7-5, were mounted on a 6,33 x 10^{-3} m thick aluminium baseplate coated with silvered Teflon second surface mirror. In the louver system which was flown this baseplate coating was substituted by an optical solar reflector (OSR).

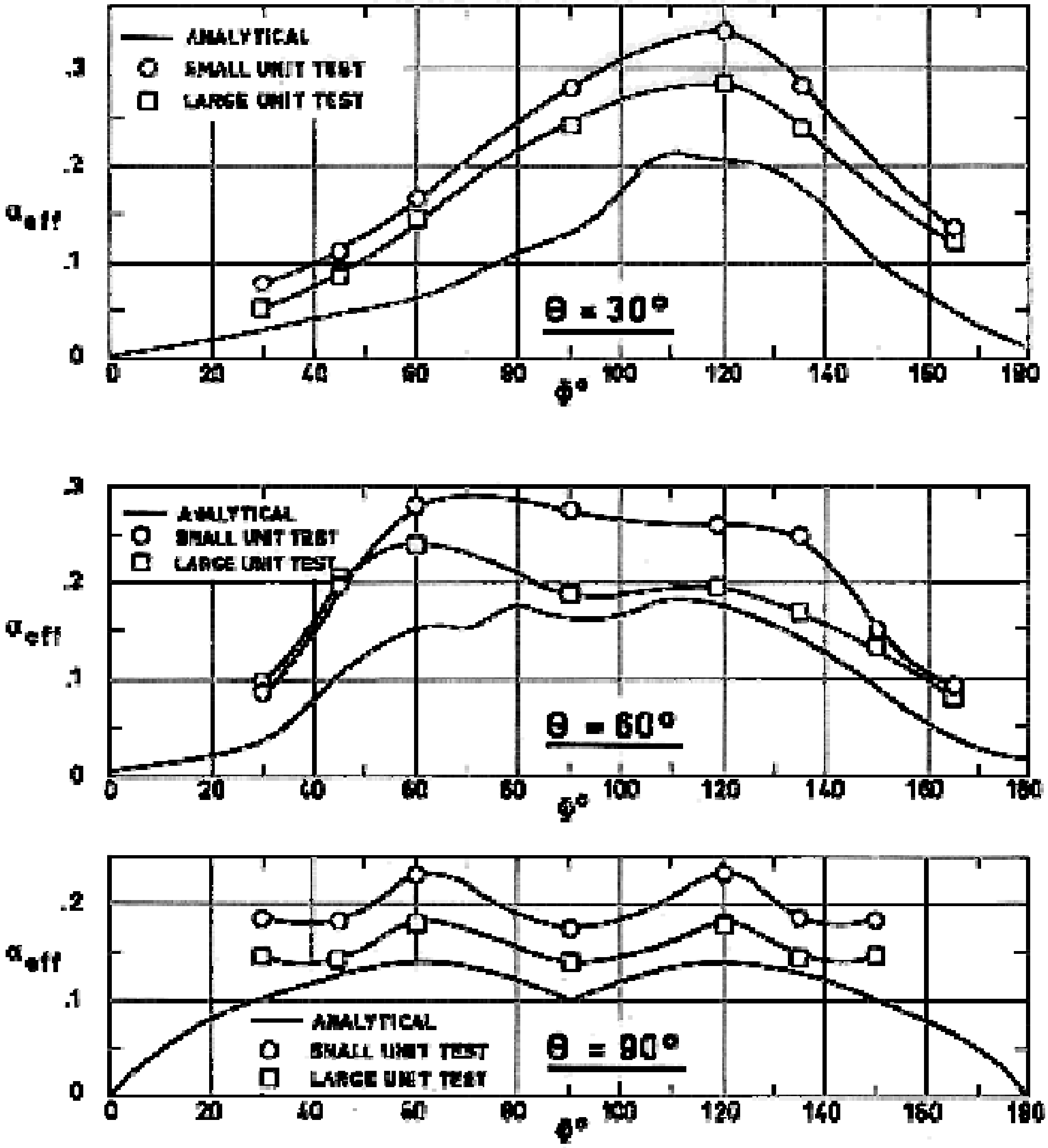

Note: non-si units are used in this figure

Figure 7-4: Effective absorptance, α_{eff}, vs. sun angle, ϕ, for several values of the blade angle, θ, for ATS spacecraft. From Michalek, Stipandic & Coyle (1972) [24].

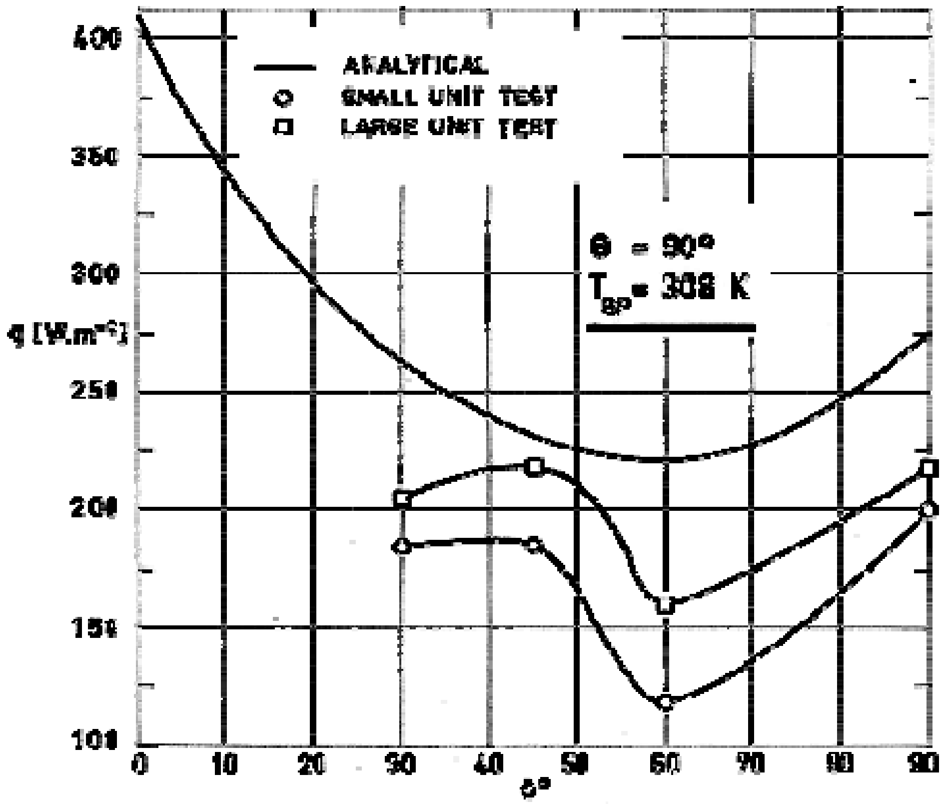

Figure 7-5: Heat rejection capability, q, vs. sun angle, ϕ, for ATS spacecraft. From Michalek, Stipandic & Coyle (1972) [24].

The blades used in the first series of tests were of buffed aluminium sandwich bonded with a BR-34 polyimide adhesive. Measured values of the properties of buffed aluminium were: α_s = 0,17 and ε = 0,05.

In subsequent testing a white paint (DC 92-007) strip (12% of total area) was added to the top of each blade along its entire length. The aim of the white paint was to lower blade temperature.

Experimental values of the effective emittance, for different combinations of louver blade designs, are compared to the analytical predictions in Figure 7-1. These values are based on the effective area of the large unit(0,48 x 0,57 m^2).

Effective absorptances deduced from the tests, for different sun angles, are compared to the numerical results in Figure 7-4.

Both experimentally and numerically obtained values of the heat rejection capability have been plotted in Figure 7-5 as functions of the sun angle for a blade angle of 90° and a baseplate temperature of 308 K.

References: Eby, Kelly & Karam (1971) [9]; Michalek, Stipandic &Coyle (1972) [24]; Hwangbo, Hunter & Kelly (1973) [15].

7.3 Nimbus louvers

7.3.1 Introduction

The basic NIMBUS spacecraft consists of three major structural elements, namely:

1. A toroid-like lower ring of 1,45 m diameter housing the basic sensory subsystem and electronic equipment.
2. A smaller hexagonal upper structure housing the attitude control system.
3. Two solar paddles of 0,91 x 2,44 m^2 each, attached to the upper control housing.

Louvers were mounted in sensory and control subsystems. Louvers of the sensory subsystem have specular blades and baseplate. louvers of the control subsystem have diffuse blades and baseplate. Relevant optical properties are given in Table 7-3.

Table 7-3: Ideal Optical Properties of the NIMBUS Louvers Surfaces

COMPONENT	SENSORY SUBSYSTEM (specular)		CONTROL SUBSYSTEM (Diffuse)	
	α_s	ε	α_s	ε
Blades	0,15	0,03	0,20	0,80
Baseplate	0,30	0,90	0,30	0,90

7.3.2 Louvers of the sensory subsystem

7.3.2.1 Actuator and sensing element

The actuator of the louvers of the sensory subsystem is a spring-loaded bellows containing a liquid-vapor mixture of Freon 114. As the temperature of the fluid filling the bellows increases, the saturation pressure increases. When the saturation pressure exceeds the preload, the bellows is compressed, actuating a linkage connected to the blades.

The liquid-vapor bellows is connected to a sensing plate.

In the event of failure caused by a loss of the actuating fluid, a fail-safe bellows is mounted on the sensing plate.

7.3.2.2 Analytical thermal performance

The thermal performance of this louver has been predicted using known analytical methods to calculate the radiative exchange in specular cavities.

A comparison between analytical and experimental values of the effective emittance is shown in Figure 7-6.

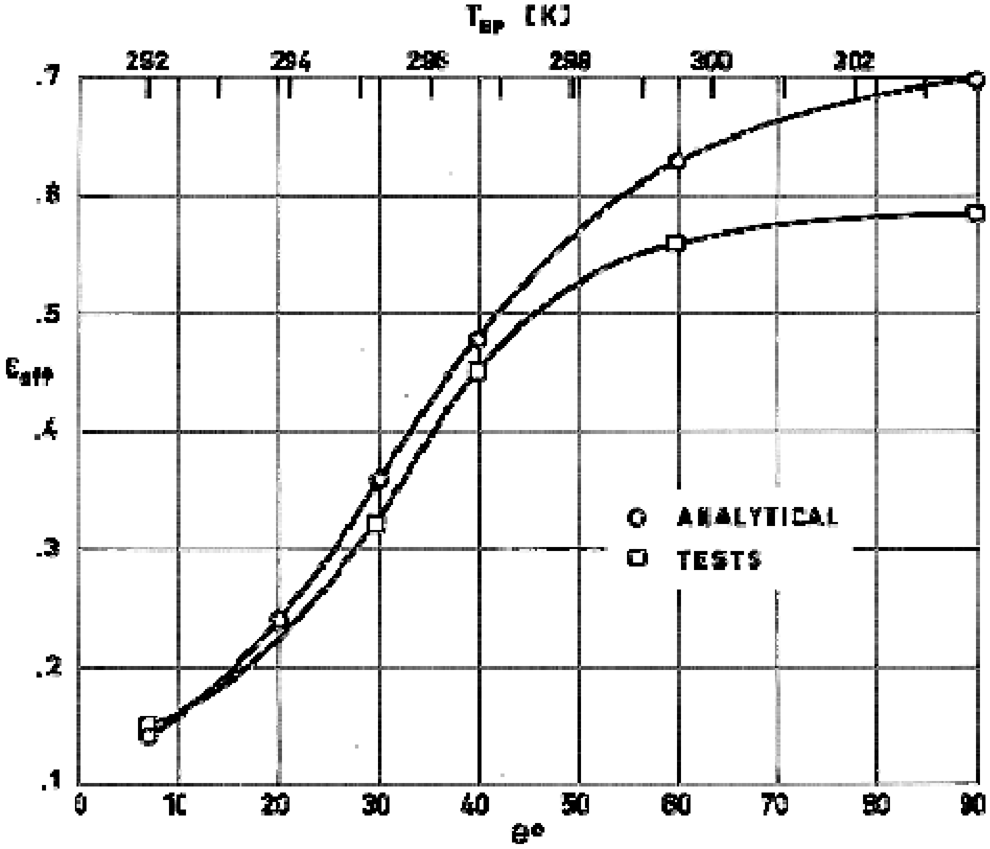

Figure 7-6: Effective emittance vs. blade angle, *θ*, and baseplate temperature, T_{BP}, for sensory subsystem of NIMBUS spacecraft. From London (1967) [20].

7.3.3 Louver of the control subsystem

7.3.3.1 Actuator and sensing element

Actuator of louver of the control subsystem is a beryllium-copper bellows having a spring-loaded return. Motion of the bellows actuates the blades by means of a rack and pinion linkage.

The panel surface temperature is sensed by a tube, which is soldered to a panel and contains a liquid-vapor mixture of Freon 11. One end of the tube is sealed, the other being connected to the bellows.

Liquid-vapor mixture in the tube can be set at a selected pressure by means of the spring-loaded return of the bellows. This pressure can be greater or smaller than the saturation pressure corresponding to maximum operating temperature. in the last case a bubble may appear in the tube.

For the NIMBUS control subsystem, the initial preload of the spring is so small that the preload will just balance the saturation pressure of the fluid at the initial operating temperature (298 K), therefore the system starts out with a small vapor bubble. As the temperature of the mounting plate rises, the temperature of the liquid in the tube also rises, increasing the vapor pressure of the liquid, which displaces the bellows. As in the case of the sensory subsystem, fail-safe bellows are provided.

7.3.3.2 Analytical thermal performance

Thermal performance was predicted analytically. The configuration considered for these analytical results is shown in Figure 7-7. Arrow 4 in this figure points to the blade thickness. Values of the effective emittance have been calculated either taking into account or neglecting blade thickness. The first case is referred to below as blocking and the second one as no blocking.

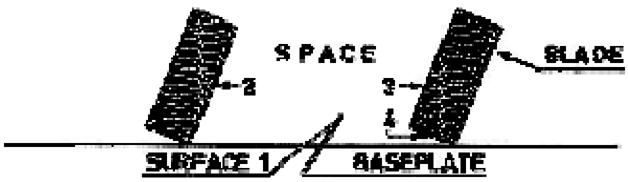

Figure 7-7: Schematic blade geometry for diffuse body radiation analysis. Louvers of the control subsystem. NIMBUS spacecraft. From London (1967) [20].

Analytical tests values of the effective emittance as a function of the blade angle are presented in Figure 7-8. Both static (steady state conditions) and dynamic (transient) tests were made.

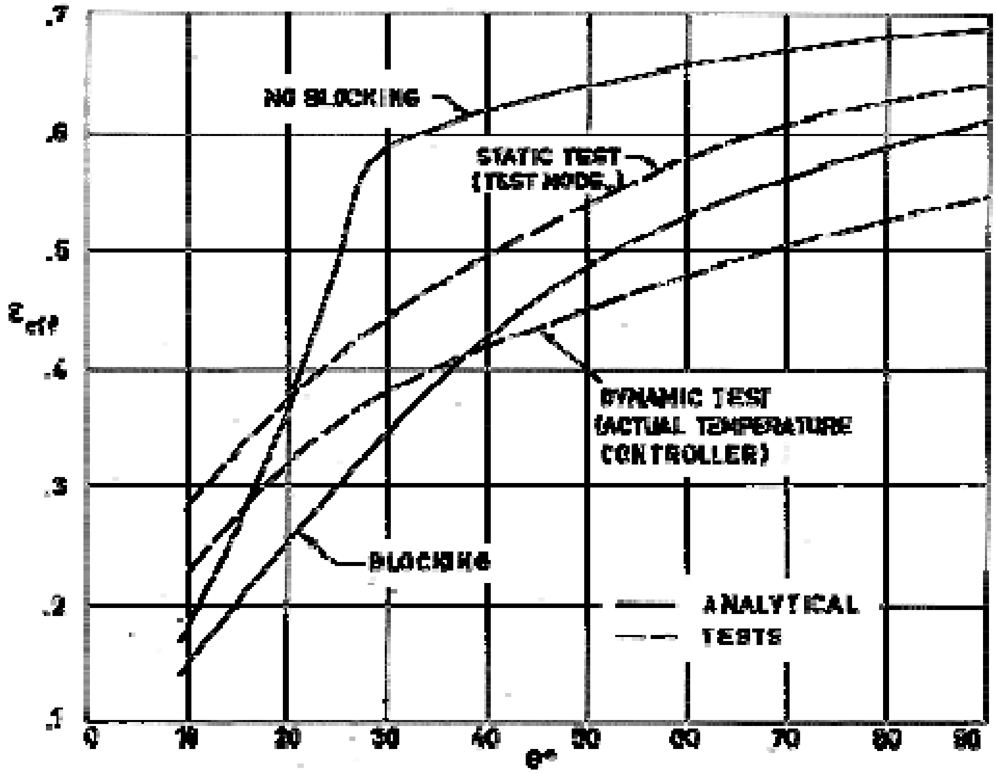

Note: non-si units are used in this figure

Figure 7-8: Effective emittance, ε_{eff}, vs. blade angle, θ, for the control subsystem of NIMBUS spacecraft. From London (1967) [20].

A curve relating effective emittance with the baseplate temperature is plotted in Figure 7-9. These values are based on dynamic tests results.

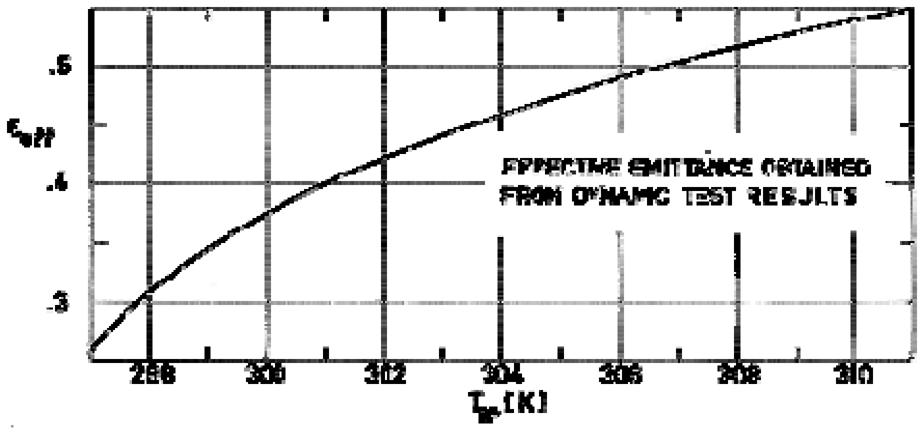

Note: non-si units are used in this figure

Figure 7-9: Effective emittance, ε_{eff}, vs. baseplate temperature, T_{BP}, for the control subsystem of NIMBUS spacecraft. From London (1967) [20].

7.3.4 Flight performance

NIMBUS 1 and NIMBUS 2 were launched in August 28th, 1964 and May 15th, 1966 respectively.

Figure 7-10 presents typical flight data for panel 1 to 6 of the control subsystem as received by telemetry from the spacecraft. The predicted maximum and minimum limits are superimposed on the figures for comparison. The temperature has been measured in each one of the six lateral faces of the hexagonal structure which houses the attitude control system.

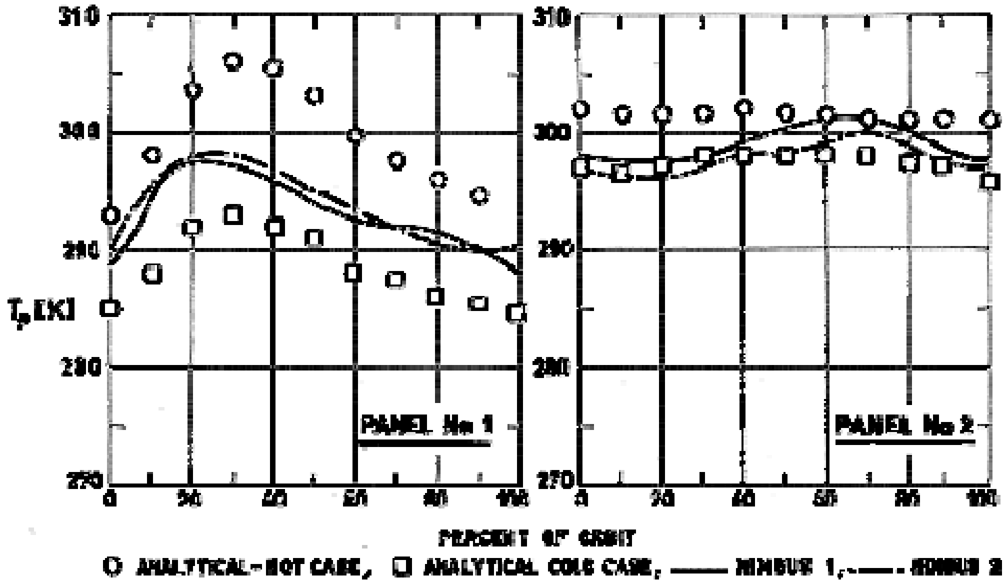

Figure 7-10: Comparison of NIMBUS 1 and 2 control subsystem panel temperatures, T_p, vs. orbital position. From London (1967) [20].

The louvers of the control subsystem are placed onto two opposite faces of this hexagonal structure. It is suspected that louvers are placed in panels 2 and 5, although precise details have not been reported.

References: London & Drummond (1966) [19]; London (1967) [20].

7.4 Snias louvers

7.4.1 Introduction

A louver system has been developed by SNIAS (Société Nationale Industrielle Aérospatiale. Cannes (France)). Dimensions are given in Figure 7-11. The baseplate is divided by the central housing in two parts having an area of 0,0765 m² each. The complete system has 18 blades. Each pair of blades is driven by a bimetal spring, although Bourdon spirals have been also considered.

Optical characteristics of the surface are summarized in Table 7-4.

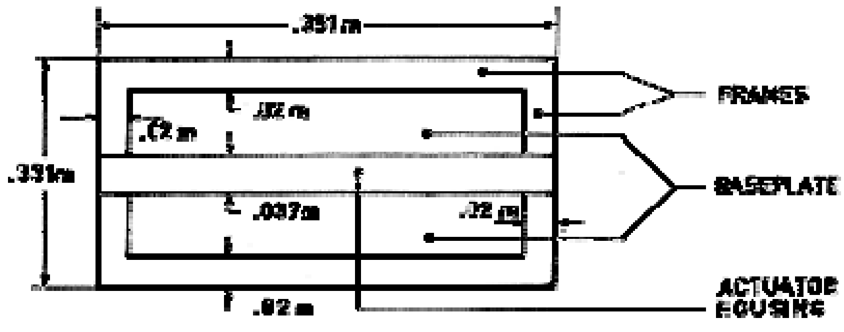

Figure 7-11: Overall dimensions of SNIAS louver. Not to scale.

Table 7-4: Optical Characteristics of the Surfaces of SNIAS Louver.

COMPONENT	ε	α_s
BLADES (Polished aluminium A9)	0,04	0,10
BASEPLATE (Coated with OSR squares of 0,03x0,03 m²)	0,713	0,08
FRAMES and ACTUATOR HOUSING (Covered with polished aluminium A4, on the parts looking towards the base, and with aluminized Kapton (Kapton outside) on the other parts)		
POLISHED ALUMINIUMA4	0,05	0,17
ALUMINIZED KAPTON	0,63	0,39

7.4.2 Analytical calculations

The analytical prediction of the performances have been made by use of the following assumptions:

1. Optical properties of all surfaces are independent of the solar angle.
2. Blades, baseplate, frames, and the part of the actuator housing covered with polished aluminium are 100% specular for all wavelengths.
3. All surfaces emit diffusely.
4. The system is finite (nine blades of 0,123 m length).
5. The solar vector is always normal to the blade axis.
6. The temperature of the baseplate is fixed at 294 K.

Relevant steps in the computation procedure are the following:

1. The number of reflections taken into account in the computation of radiative coupling and of incident solar energy is only limited by a criterion based on the amount of energy remaining after reflection. The reflected energy threshold is low enough to practically take into account all the reflections, and practically all the rays leave the system before having reached that value.
2. Both solar and infrared exchanges are computed with ray tracing programs, each emitting surface being divided into small segments ($2{,}5 \times 10^{-4}$ m width for the solar flux and 2×10^{-3} m width for the infrared). For infrared calculations the 180º angle of emission has been divided into 30 elementary angles each containing the same amount of energy.
3. Once the fluxes have been computed, they are introduced in a 29 nodes model whose steady state temperatures are computed by matrix inversion.
4. All the inter-nodal conductive couplings have been taken into account.

Results obtained by using this analytical model are summarized in Figure 7-12 to Figure 7-15, and in Table 7-5 to Table 7-7. The effective thermal emittance, ε_{eff},is related to blade angle, θ, in Figure 7-12. The effective absorptance, α_{eff},appears in Table 7-5 and in Figure 7-13 for several values of the sun angle, ϕ,and blade angle, θ. The heat rejection capability, q, is tabulated in Table 7-6 and plotted in Figure 7-14. Finally, the maximum blade temperature, T_B, is given in Table 7-7 and Figure 7-15.

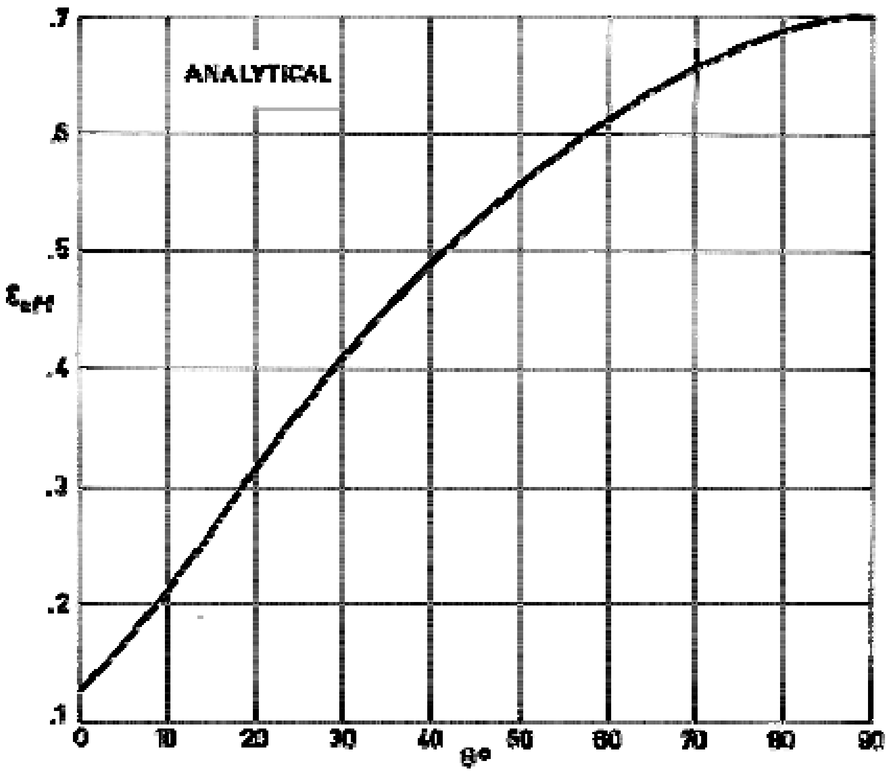

Note: non-si units are used in this figure

Figure 7-12: Effective emittance, ε_{eff}, vs. blade angle, θ, for the SNIAS louver system. From Redor (1972) [29].

Table 7-5: Effective Absorptance α_{eff}, for Several Values of Sun Angle, ϕ, and Blade Angle, θ.

	α_{eff}									
ϕ(°) θ(°)	**0**	**10**	**20**	**30**	**40**	**45**	**50**	**60**	**70**	**80**
0	0	0,0296	0,0414	0,0511	0,0682	0,0756	0,0830	0,0859	0,1079	0,1104
10	0	0,0297	0,0485	0,0490	0,0545	0,0576	0,0606	0,0646	0,0800	0,0969
20	0	0,0284	0,0391	0,0504	0,0534	0,0582	0,0584	0,0695	0,0706	0,1014
30	0	0,0204	0,0339	0,0464	0,0516	0,0530	0,0577	0,0614	0,1099	0,1365
40	0	0,0212	0,0321	0,0411	0,0459	0,0549	0,0545	0,1040	0,1329	0,1494
45	0	0,0193	0,0293	0,0415	0,0481	0,0506	0,0794	0,1136	0,1415	0,1621
50	0	0,0176	0,0286	0,0393	0,0466	0,0835	0,0923	0,1240	0,1613	0,1695
60	0	0,0170	0,0269	0,0396	0,1061	0,1281	0,1330	0,1612	0,1770	0,1930
70	0	0,0180	0,0319	0,1075	0,1576	0,1763	0,1778	0,1964	0,2145	0,1779
80	0	0,0171	0,1008	0,1436	0,1607	0,1815	0,1824	0,1656	0,1767	0,1509
90	0	0,0621	0,1167	0,1347	0,1439	0,1443	0,1414	0,1585	0,1541	0,1323

ϕ(°) θ(°)	**90**	**100**	**110**	**120**	**130**	**135**	**140**	**150**	**160**	**170**
0	0,0765	0,0971	0,0962	0,0886	0,0914	0,0808	0,0731	0,0643	0,0521	0,0334
10	0,0876	0,0884	0,0997	0,1284	0,1605	0,1551	0,1704	0,1797	0,1186	0,0531
20	0,1027	0,1791	0,1441	0,1929	0,1873	0,2416	0,2079	0,1588	0,1190	0,0450
30	0,1224	0,1874	0,2286	0,2087	0,2351	0,2049	0,1987	0,1235	0,0975	0,0364
40	0,1566	0,2559	0,2634	0,2325	0,1650	0,1562	0,1376	0,1074	0,0746	0,0375
45	0,1697	0,2487	0,2407	0,2280	0,1851	0,1421	0,1425	0,1106	0,0896	0,0292
50	0,1716	0,2041	0,2219	0,2336	0,2048	0,1850	0,1303	0,1107	0,0672	0,0281
60	0,1713	0,2057	0,1960	0,1677	0,1639	0,1431	0,1314	0,0937	0,0486	0,0360
70	0,1342	0,1346	0,1460	0,1352	0,1431	0,1176	0,1044	0,0731	0,0634	0,0494
80	0,1011	0,1101	0,1250	0,1188	0,1187	0,1156	0,1341	0,1070	0,0864	0,0468
90	0,0874	0,1197	0,1242	0,1474	0,1443	0,1354	0,1234	0,1171	0,0945	0,0681

NOTE From Redor (1972) [29].

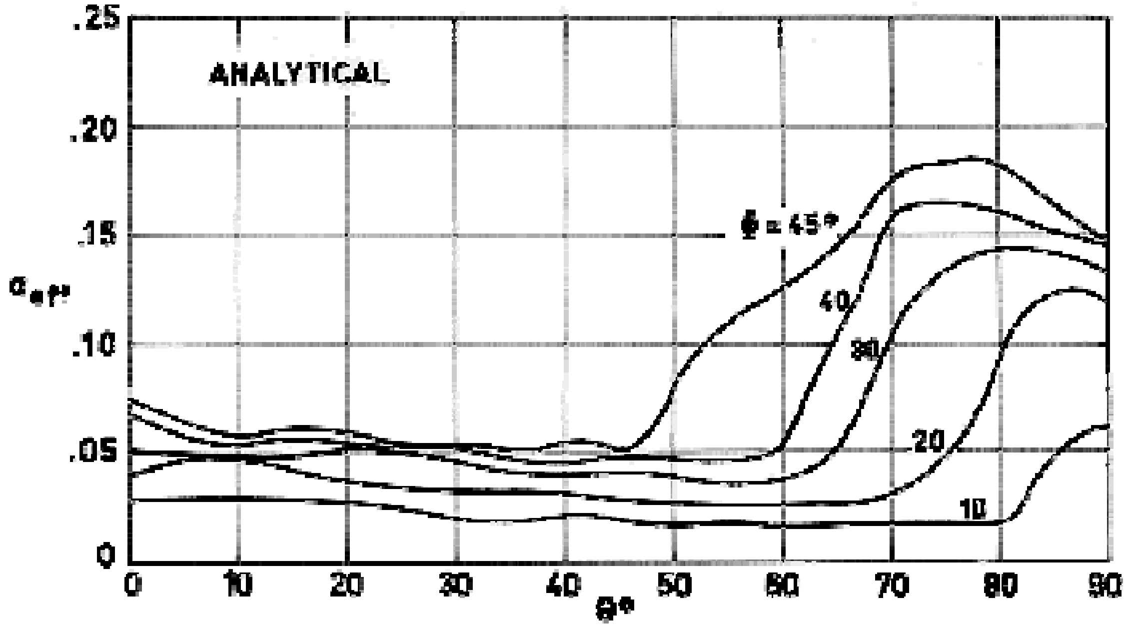

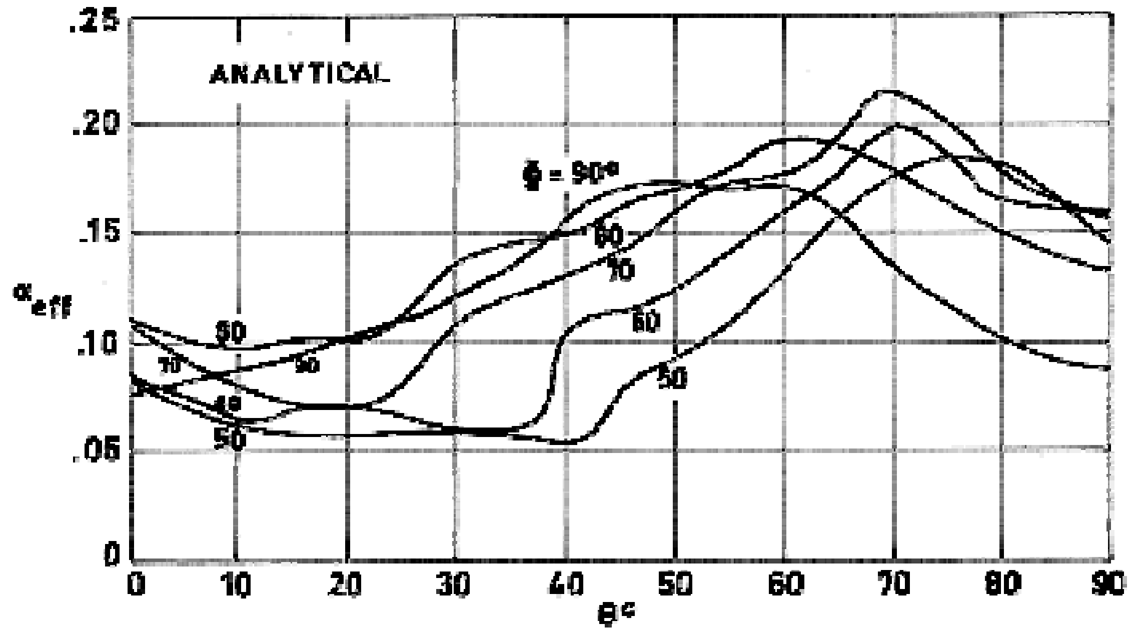

Note: non-si units are used in this figure

Figure 7-13: Effective absorptance, α_{eff}, vs. blade angle, θ, for several values of the sun angle, ϕ. SNIAS louver system. From Redor (1972) [29].

Table 7-6: Heat Rejection Capability, q, for Several Values of Sun Angle, ϕ, and Blade Angle, θ.

	q [W.m^{-2}]									
ϕ(°) θ(°)	0	10	20	30	40	45	50	60	70	80
0	54,7	13,3	-3,3	-16,8	-40,8	-51,1	-61,5	-65,5	-96,4	-99,9
10	88,7	47,1	20,8	20,1	12,4	8,1	3,9	-1,8	-23,3	-46,9
20	131,9	92,2	77,1	61,4	57,1	50,4	50,2	34,6	33,0	-10,0
30	173,9	145,4	126,5	108,9	101,6	99,7	93,1	87,9	20,0	-17,2
40	208,8	179,1	163,9	151,3	144,6	131,9	132,5	63,2	22,7	-0,4
45	223,3	196,3	182,3	165,2	156,0	152,4	112,2	64,2	25,2	-3,6
50	235,3	210,7	195,2	180,3	170,1	118,4	106,1	61,7	9,5	-2,0
60	256,9	233,1	219,3	201,5	108,4	77,6	70,7	31,2	9,1	-13,3
70	279,2	254,0	234,5	128,7	58,6	32,4	30,3	4,2	-21,1	30,1
80	291,3	267,3	150,2	90,2	66,3	37,2	36,0	59,5	43,9	80,1
90	299,1	212,1	135,7	110,5	97,6	97,1	101,2	77,2	83,4	113,9

ϕ(°) θ(°)	90	100	110	120	130	135	140	150	160	170
0	-52,4	-81,3	-80,0	-69,4	-73,3	-58,4	-47,7	-35,3	-18,3	8,0
10	-34,0	-35,1	-50,9	-91,0	-136,0	-128,4	-149,8	-162,9	-77,3	14,4
20	-11,9	-118,9	-69,8	-138,2	-130,3	-206,4	-159,1	-90,4	-34,7	68,9
30	2,5	-88,5	-146,2	-118,3	-155,2	-112,9	-104,3	1,0	-37,4	123,0
40	-10,5	-149,4	-160,0	-116,7	-22,2	-9,9	16,2	58,4	104,4	156,3
45	-14,3	-114,9	-113,7	-95,9	-35,87	24,4	23,8	68,4	97,9	182,4
50	-5,0	-50,4	-75,4	-91,7	-51,4	-23,7	52,9	80,3	141,2	196,0
60	17,1	-31,1	-17,5	22,1	27,5	56,5	73,0	125,7	188,9	206,5
70	91,3	90,8	74,8	89,9	78,8	114,5	133,0	176,9	190,5	210,0
80	149,8	137,2	116,3	125,0	125,1	129,5	103,6	141,5	170,4	225,8
90	176,7	131,5	125,2	92,8	97,1	109,5	126,3	135,1	166,8	203,8

NOTE From Redor (1972) [29].

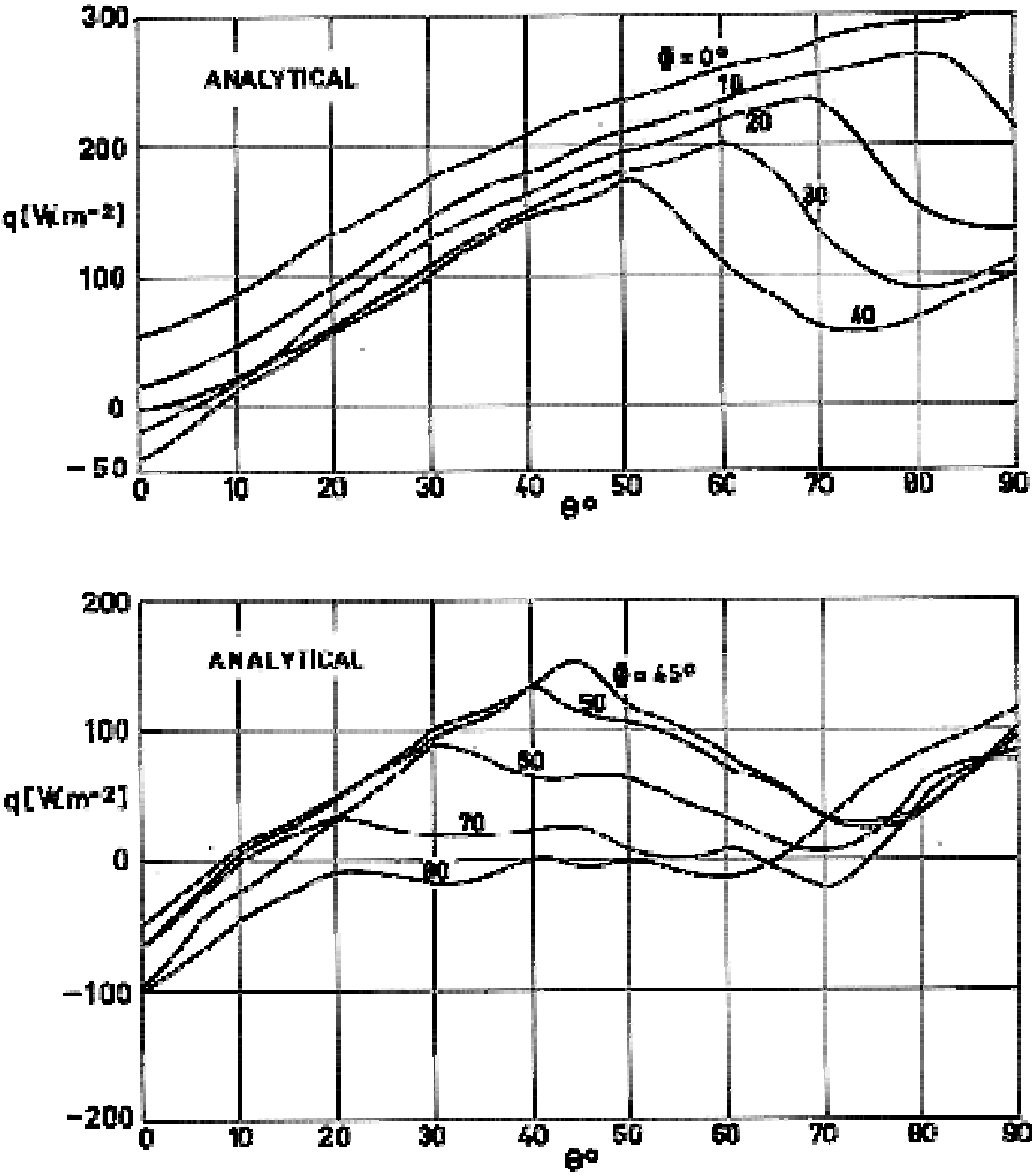

Figure 7-14: Heat rejection capability, *q*, vs. blade angle, *θ*, for several values of the sun angle, *ϕ*. SNIAS louver system. From Redor (1972) [29].

Table 7-7: Maximum Blade Temperature, T_B, for Several Values of Sun Angle, ϕ, and Blade Angle, θ.

	T_B [K]									
ϕ(°) θ(°)	0	10	20	30	40	45	50	60	70	80
0	258,5	343,4	380,1	390,6	404,5	412,8	425,8	432,3	455,6	455,3
10	260,0	327,9	388,3	395,1	392,8	400,1	417,1	429,2	427,6	441,0
20	261,9	345,8	364,5	395,6	416,5	405,3	410,9	443,0	420,1	448,3
30	262,5	340,1	353,7	380,1	402,3	407,3	402,4	415,1	457,0	479,6
40	261,3	349,3	376,4	393,2	388,3	409,4	401,8	464,0	482,4	485,5
45	260,9	339,1	364,5	401,8	390,8	395,7	449,1	456,0	482,5	489,2
50	260,2	326,2	357,8	386,3	390,8	438,1	469,5	471,1	483,8	501,3
60	260,1	322,5	351,0	392,5	467,0	483,7	485,9	491,2	490,6	500,8
70	258,0	327,7	376,4	469,0	509,7	507,5	502,8	503,1	502,2	482,0
80	254,4	326,2	481,9	482,3	484,1	506,9	516,1	473,4	467,2	412,9
90	246,9	415,5	463,0	472,5	468,6	462,6	435,5	449,1	437,5	392,3

ϕ(°) θ(°)	90	100	110	120	130	135	140	150	160	170
0	430,1	468,0	456,7	446,3	439,1	427,9	418,2	405,1	386,9	336,8
10	439,4	446,5	445,0	457,1	471,6	476,5	478,0	484,3	484,0	343,1
20	454,6	492,9	465,7	486,2	477,5	511,9	522,9	485,2	462,9	379,3
30	468,7	490,7	508,9	507,6	506,2	507,4	502,2	443,2	420,7	365,8
40	490,0	541,1	518,3	497,3	435,3	440,8	424,9	439,8	424,6	350,6
45	500,9	520,2	509,4	461,1	452,7	422,3	448,6	440,1	426,2	340,2
50	489,5	496,1	486,0	487,7	480,6	483,0	450,3	432,3	398,5	335,3
60	458,4	476,2	484,6	467,0	450,6	469,3	464,3	432,0	366,5	327,2
70	408,1	401,4	431,0	434,1	450,6	463,9	454,7	416,1	368,7	367,8
80	337,3	351,5	416,8	423,3	433,9	436,6	458,6	439,6	438,0	376,4
90	275,7	393,3	425,4	455,8	459,1	452,4	456,3	461,1	438,1	426,0

NOTE From Redor (1972) [29].

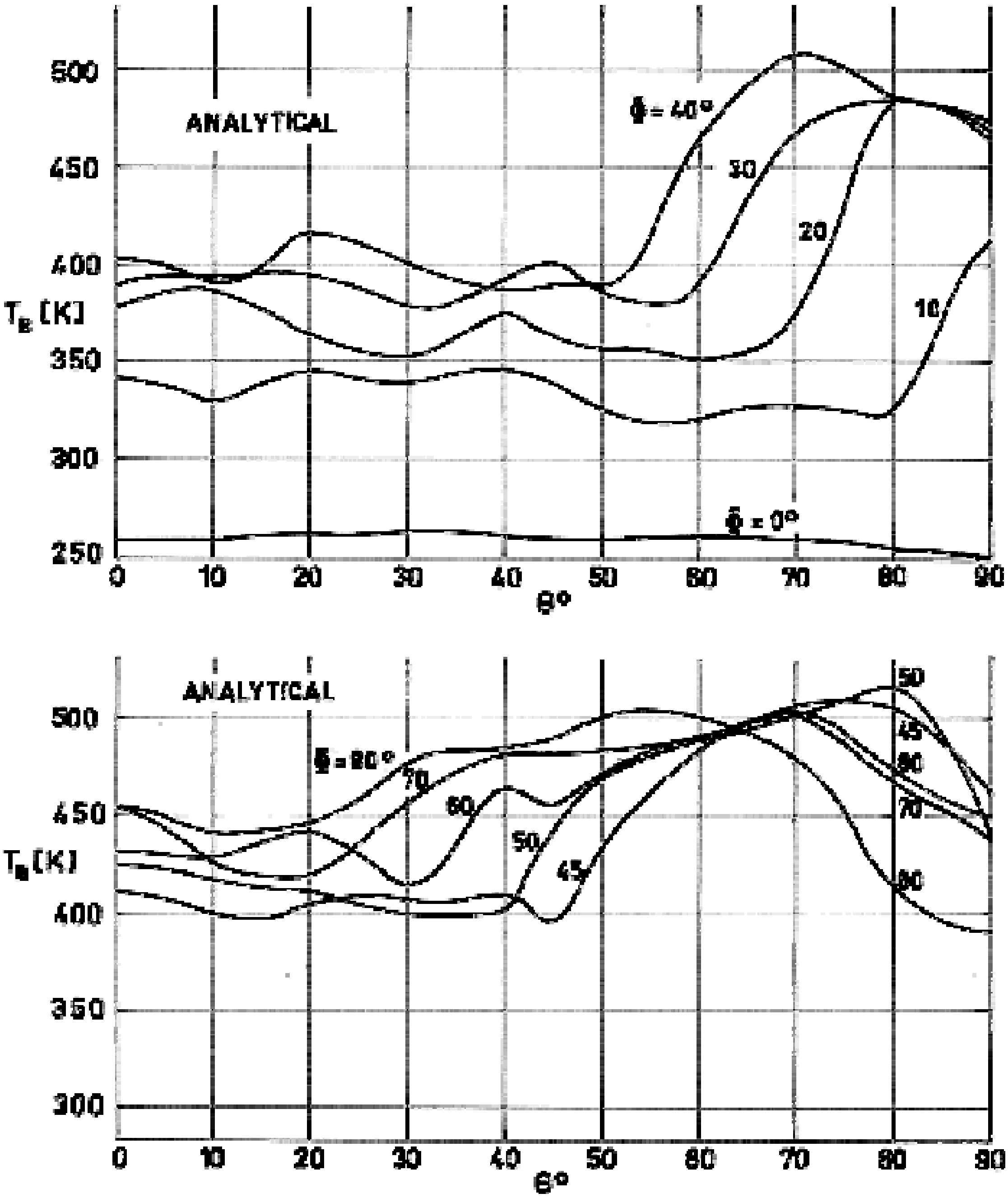

Figure 7-15: Maximum blade temperature, T_B, vs. blade angle, θ, for several values of the sun angle, ϕ. SNIAS louver system. From Redor (1972) [29].

7.4.3 Tests

The results, which have been just mentioned, can be modified to account for several effects not considered in the analytical model, such as: conduction through the supports, heat leaks, and so.

The modified results, which fairly agree with the results of the simulation tests, have been plotted in Figure 7-16, which concerns the effective emittance, ε_{eff}, and in Figure 7-17. The last figure presents values of the heat rejection capability, q, deduced, 1) from the simplified analytical model, 2) from the modified model and 3) from the simulation tests.

References: Redor (1972) [29], Croiset & Leroy (1973) [8].

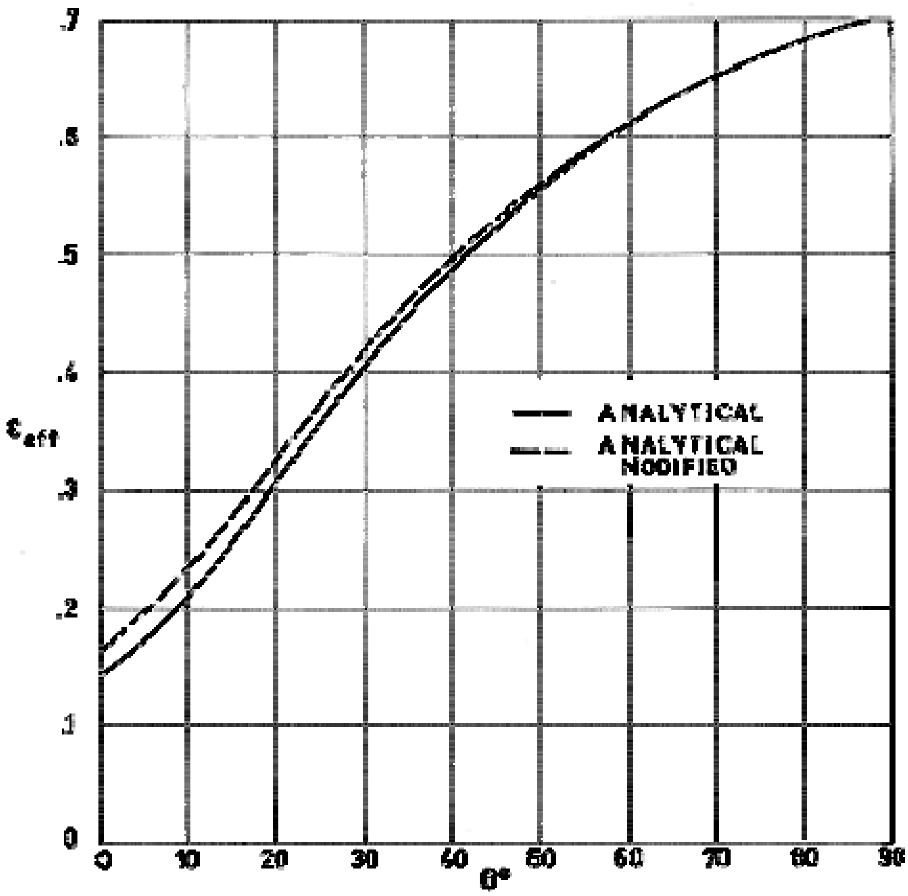

Note: non-si units are used in this figure

Figure 7-16: Effective emittance, ε_{eff}, vs. blade angle, θ, for the louver system of SNIAS. Solid line: From Redor (1972) [29]. Dashed line: From Croiset & Leroy (1973) [8].

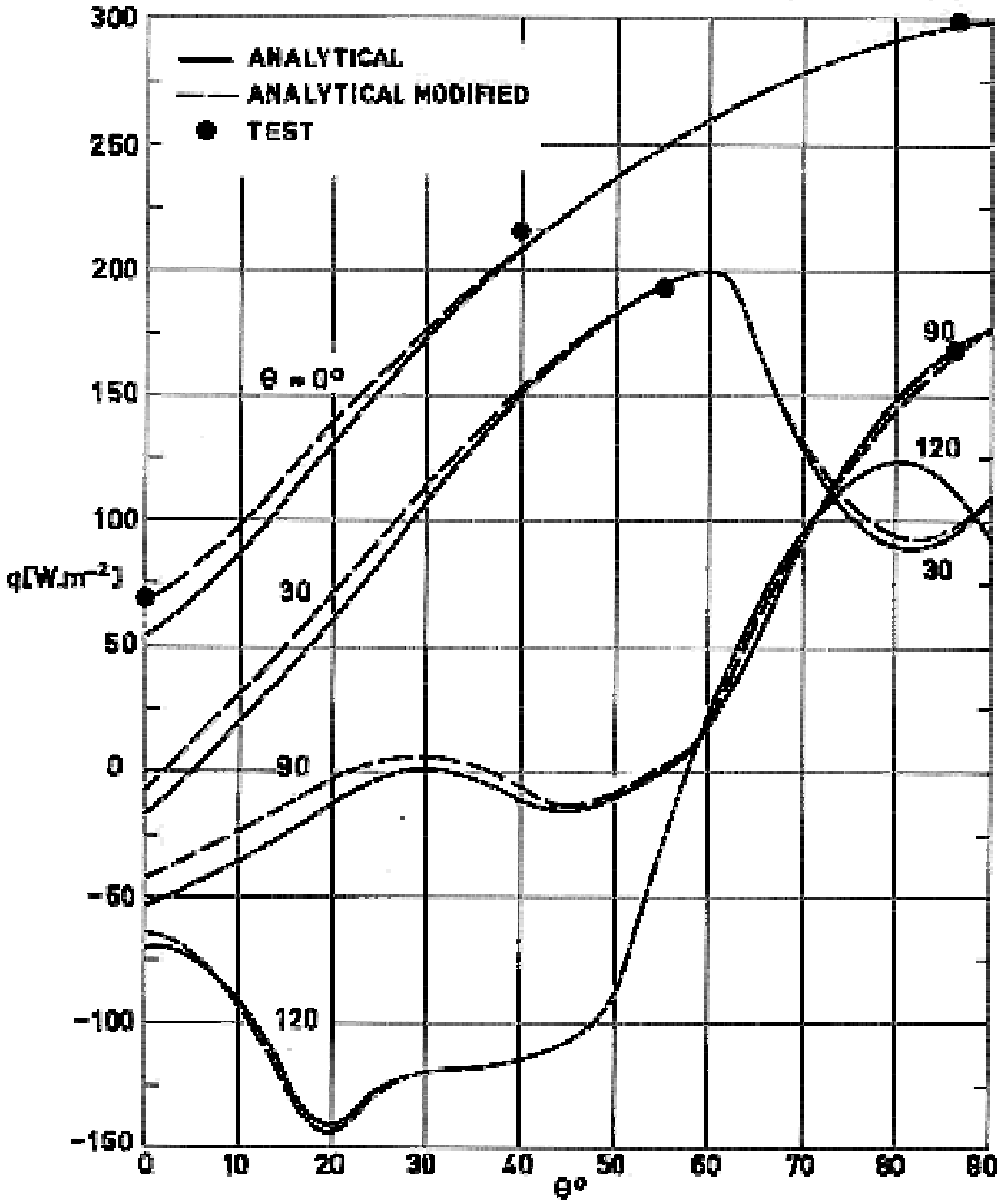

Figure 7-17: Heat rejection capability, q, vs. blade angle, θ, for several values of the sun angle, ϕ. SNIAS louver system. Solid line: From Redor (1972) [29]. Dashed line: From Croiset & Leroy (1973) [8].

7.4.4 The Bourdon tube used as an actuator in the SNIAS Louver system

7.4.4.1 Summary

A Bourdon spiral was developed by REUSSER (Zürich (Switzerland)) to activate the blades of the SNIAS louver.

The complete actuating and sensing system consists of a tank containing ether, a Bourdon spiral with an overpressure compensator, and a capillary tube connecting Bourdon and tank. The sensing element is the tank, while the actuator is the Bourdon.

When the tank temperature increases, the pressure of the liquid increases and is transmitted through the capillary tube of the Bourdon spiral. The angle of rotation of the end of the Bourdon spiral is proportional to the pressure and, therefore, proportional to the mean temperature of the liquid inside the tank.

7.4.4.2 Characteristics of the Bourdon spiral

Table 7-8: Several Characteristics of the Bourdon Spiral

	MATERIAL	MASS [kg]	VOLUMEX10^6 [m^3]	INNER FLUID
BOURDON SPIRAL ONLY	Cu-4Sn-4Zn	$9x10^{-3}$	0,447	DIMETHYL ETHER $C_4H_{10}O$
TANK OF SINGLE BLADE ACTUATION SYSTEM	STAINLESS STEEL (AlSl 304) (Fe-18Cr-8Ni)	$1{,}25x10^{-1}$ INCLUDING FLUID	4,7	
TANK OF MULTIPLE BLADE ACTUATION SYSTEM	STAINLESS STEEL (AlSl 304) (Fe-18Cr-8Ni)	$9{,}2X10^{-1}$ INCLUDING FLUID	42,3	

NOTE From Reusser et al. (1973) [30].

Table 7-9: Several Parameters of the Bourdon Spiral

Linear Range Angle Corresponding Linear Range Temperature Corresponding Linear Range Pressure	0 to 210 10 K 0 to 1,9x10^{6}Pa
Operating Range Angle Corresponding Temperature Range	0 to 90 5 K
Rupture Pressure (Without Retainer) Corresponding Temperature Range Corresponding Angle of Rotation	2,33x10^{6}Pa 16,7 K 300
Highest Permissible Pressure (Non Operating, with Retainer) Highest Permissible Temperature	3.65.10^{6}Pa 323 K

NOTE From Reusser et al (1973) [30].

In order to increase the highest non-operating pressure, a special retainer for the spiral was developed. The development test showed that the highest permissible pressure of 3,65x10^6 Pa is reached at about 318 K, depending on the tank rigidity. In order to extend the non-operating temperature, an overpressure compensator was developed. The overpressure compensator is a spring-preloaded bellows which extends the non-operating temperature up to 343 K.

Other relevant data are:

Contact Area of Tank Bottom	A = 8x10^{-4} m^2
Density of Ether	ρ = 714 kg.m^{-3}
Mass of Ether	m = 3,35x10^{-3} kg
Specific Heat of Ether	c = 2,38x10^3 J.kg^{-1}.K^{-1}
Thermal Conductance (mean value)	h = 100 W.m^{-2}.K^{-1}.

7.4.4.3 Set point and temperature ranges

The basic set point temperature of the system can be changed by changing the mechanical preload angle and the corresponding filling temperature of the fluid.

With an initial coiling angle of 30° and a filling temperature of 291,5 K there are two temperature ranges within the linear range of pressure variation: 293 K to 298 K and 298 K to 303 K. The corresponding set point being 293 K and 298 K respectively. Additional temperature ranges do not fall within the pressure linear range.

The temperature-pressure characteristics of the Bourdon spiral for three different filling temperatures of the ether (T_C = 286,5; 291,5 and 296,5 K) are shown in Figure 7-18. Figure 7-19 shows the different set point temperature ranges, in the pressure linear range, for the same three filling temperatures.

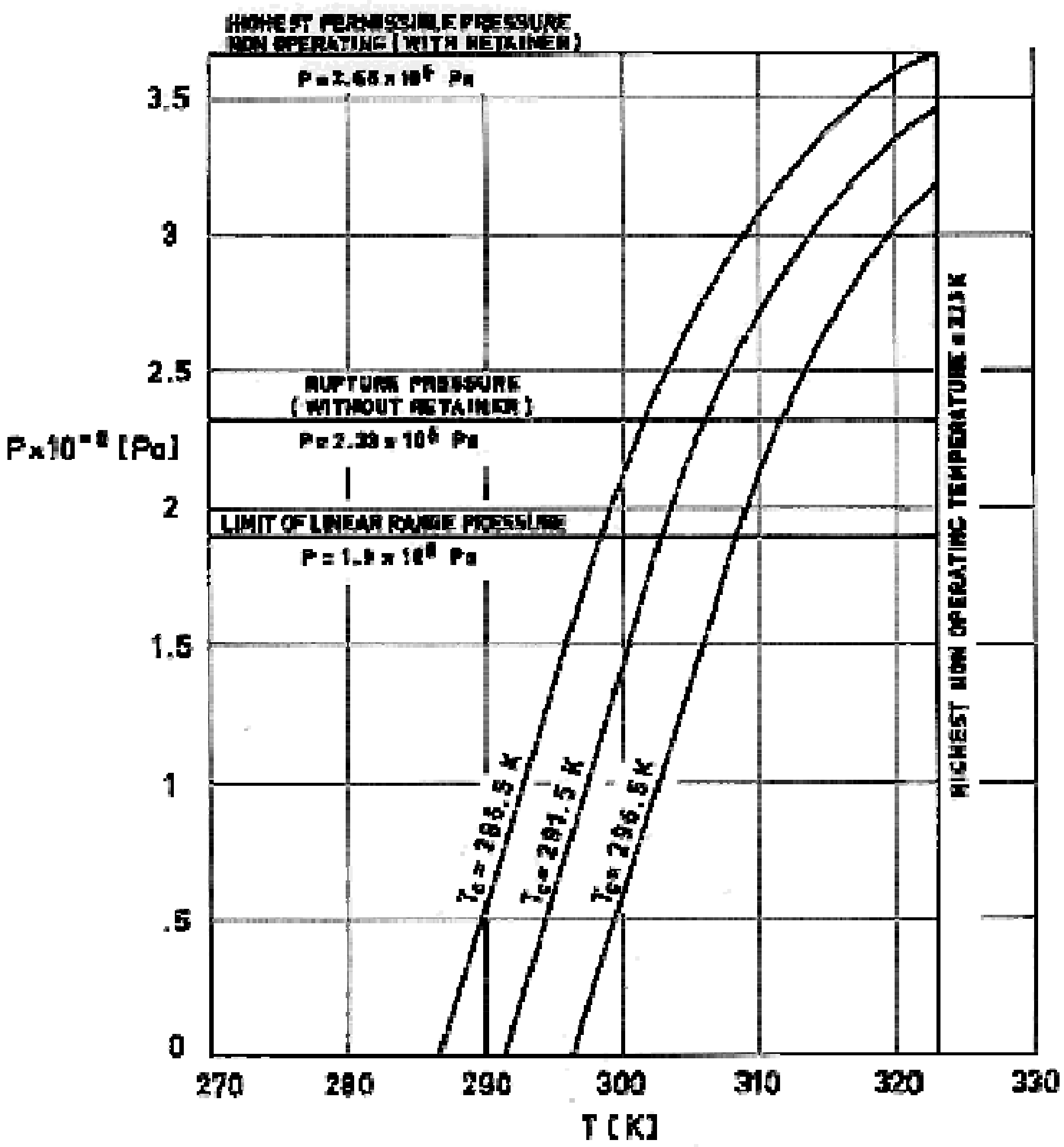

Note: non-si units are used in this figure

Figure 7-18: Temperature-pressure characteristic of the Bourdon spiral. From Reusser et al. (1973) [30].

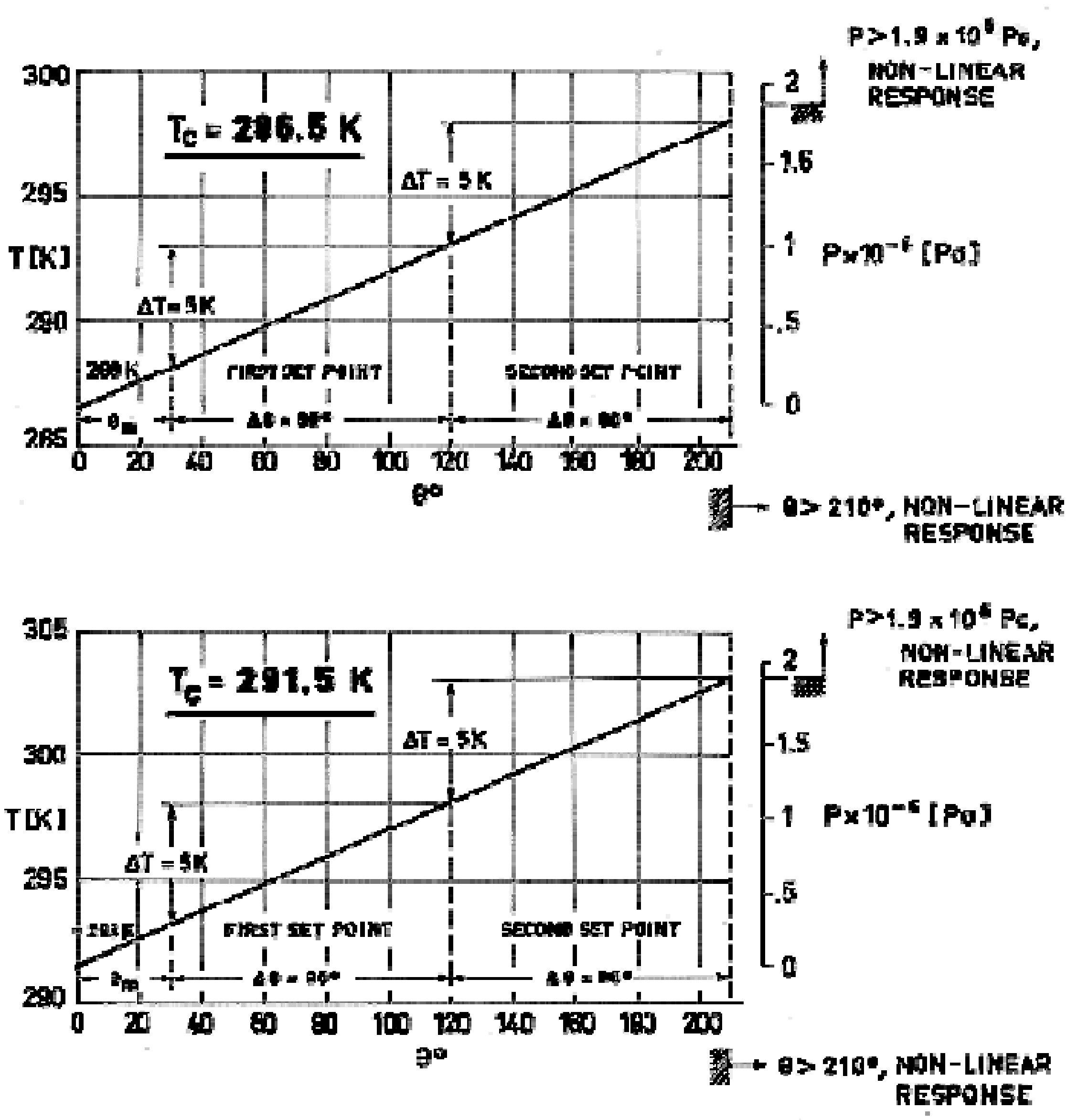

Note: non-si units are used in this figure

Figure 7-19: Performance of a Bourdon actuating a single blade. After Reusser et al. (1973) [30].

7.4.4.4 Response time of the sensing element

The response of the sensing element is controlled by the time required to heat the liquid of the tank from the starting temperature, T_{OL}, to a temperature T.

Assuming that the baseplate temperature is constant, the time needed to heat the liquid inside the tank from the starting temperature, T_{OL}, to the temperature T is given by the expression:

$$\tau = -\frac{mc}{hA}\ln\left(\frac{T_{BP}-T}{T_{BP}-T_{OL}}\right) \qquad [7\text{-}1]$$

The ratio $(T_{BP}-T)/(T_{BP}-T_{0L})$ corresponding to the Bourdon spiral developed by REUSSER is plotted in Figure 7-20 as a function of the time, τ, for mc/hA = 99,84 s. The heat transfer to the liquid after time τ is given by the expression:

$$Q = Q_0\left[1 - e^{-\frac{hA}{mc}\tau}\right] \qquad [7\text{-}2]$$

where Q_0 is the heat transferred from the baseplate to the liquid after an infinite time. For an increment in temperature of 5 K (operating temperature range of the Bourdon) the value of Q_0 is 40 J. The ratio Q/Q_0 as a function of τ for the value of mc/hA quoted above has been also plotted in Figure 7-20.

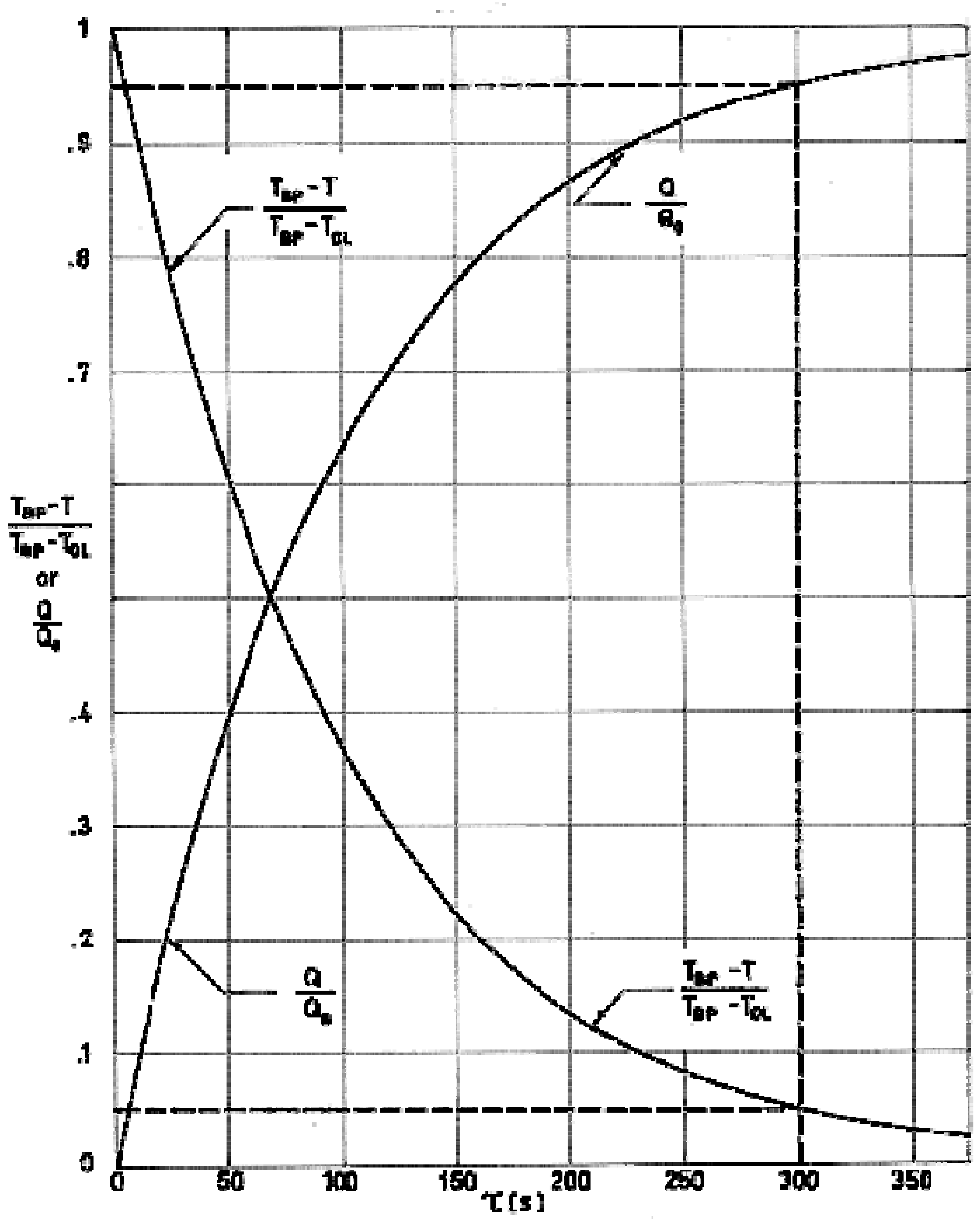

Note: non-si units are used in this figure

Figure 7-20: Ratios (T_{BP}–T)/(T_{BP}–T_{OL}) and Q/Q_0 vs. time, τ. After Reusser et al. (1973) [30].

It is deduced from Figure 7-20 that for a time of 300 s the heat received by the liquid is 95% of the total value. Also, the increment of temperature T_{BP}–T is only a 5% of the initial increment T_{BP}–T_{OL}. It should be pointed out that the real time is surely smaller than the 300 s calculated above, since it is assumed that heating only takes place at the baseplate, neglecting the heat transfer at the other surfaces of the tank. In addition liquid convection has also been neglected.

Bibliography

[1] Aalders, B.G.M., "Performance Test of the Reusser Actuation System for Use with a Louver Array", ESTEC Internal Working Paper No. 743, April 1973.

[2] Anon., "Advanced Planetary Probe Study", NASA CR-79502, pp. 490-510.

[3] Baldwin, Jr., W.M., "The Selection and Application of Wrought Copper and Copper Alloys", in "Metals Handbook, Vol. 1, Properties and Selection of Metals", 8th Ed., T. Lyman Ed., American Society for Metals (ASM), Cleveland, Ohio, 1961, pp. 1016-1021.

[4] Bannister, T.C., "Active Thermal Control of the Micrometeoroid Capsule Electronics", Proceedings of Conference on Active Temperature Control, NASA TM X-56165, April 1964.

[5] Burton, W.E., "Engineering with Rubber", 1st Ed., McGraw-Hill Book Company, Inc., New York, 1949, pp. 13-42.

[6] Caroll, W., Coyle, G.G., Delden, H., "Mariner Mars 1964 Active Temperature Control Hardware Design and Development", NASA TR 32-955, Engineering Report, JPL, Pasadena, Cal.

[7] Clausen, O.W., Kirkpatrick, J.P., "Thermal Tests of an Improved Louver System for Spacecraft Thermal Control", AIAA Paper No. 69-627, June 1969.

[8] Croiset, P., Leroy, L., "Volets pour Controle Thermique de Satellite", ESRO CR-208, Dec. 1973.

[9] Eby, R.J., Kelly, W.H., Karam, R.D., "Thermal Control of ATS F & G", ASME Paper 71-Av-28, April 1971.

[10] FAIRCHILD HILLER, "Louver Assembly for Satellite Thermal Control", Fairchild Space and Electronics Division, Germantown, Maryland, 1972.

[11] FAIRCHILD HILLER, "Installation. Orbiting Astronomical Observatory Thermal Control Louver Assemblies", Fairchild Hiller Space and Electronics Systems Division, Germantown, Maryland.

[12] FIAT, "Prototype Development Proposal", Fiat Divisione Aviazione, ESRO RFQ/1006, ESTEC CO/950/70, Sep. 1970.

[13] Gram, M., "Temperature Control Louvers for the Mariner Venus and Mariner Mars Spacecrafts", Proceedings of Conference on Active Temperature Control, NASA TM X-56165, April 1964.

[14] Hodgman, Ch.D., "Handbook of Chemistry and Physics", 35th Ed., Chemical Rubber Publishing Company, Cleveland, Ohio, 1953, pp. 690-1229.

[15] Hwangbo, H., Hunter, J.H., Kelly, W.H., "Analytical Modeling of Spacecraft with Active Thermal Control Systems", AIAA Paper No. 73-773, July 1973.

[16] KAMMERER, "Deflectherm Thermostatic Bimetals", Fr. Kammerer GmbH, Edition April 1971.

[17] Lewis, J.G., Kenkare, A.S., "Assessment of an Active Thermal Control Louver Array for Spacecraft", Journal of Spacecraft and Rockets, Vol. 11, No. 5, May 1974, pp. 342-344.

[18] Linton, R., "Thermal Design Evaluation of Pegasus", NASA TN D-3642, 1966.

[19] London, A., Drummond, Jr., F.O., "Thermal System Design of the Nimbus Spacecraft", in "Spacecraft Systems", Proceedings of XVIIth International Astronautical Congress, Madrid, 1966, Dunod Editeur, Paris, pp. 387-403.

[20] London, A., "Shutter System Design for the Nimbus Spacecraft", in "Progress in Astronautics and Aeronautics", Vol. 20, G.B. Heller, Ed., Academic Press, New York, 1967, pp. 725-757.

[21] Martin, P., Yarworth, N., "An Introduction to the Theory and Use of Thermostatic Bimetals", Telcon Metals, Ltd., Manor Royal, Crawley. Sussex, Sep. 1961, Also published in Engineering, 22 Sep. 1961.

[22] Mauroy, P., "Système de Contrôle Thermique par Volets Mobiles", Centre National d'Etudes Spatiales, Centre Spatial de Toulouse, France, Mars 1968.

[23] MBB, "Conceptual Study on Movable Louver Systems for Satellite Thermal Control in Solar Environment", Messerschmitt-Bölkow-Blohm GmbH, Space Division, Munich, Germany, Sep. 1970.

[24] Michalek, T.J., Stipandic, E.A., Coyle, M.J., "Analytical and Experimental Studies of an all Specular Thermal Control Louver System in a Solar Vacuum Environment", AIAA Paper No. 72-268, April 1972.

[25] Parmer, J.F., Buskirk, D.L., "Thermal Control Aspects of Spacecraft Louvers", NASA CR-88876, 1967.

[26] Parmer, J.F., Buskirk, D.L., "The Thermal Radiation Characteristics of Spacecraft Temperature Control Louvers in the Solar Space Environment", in "Progress in Astronautics and Aeronautics", Vol. 20, G.B. Heller, Ed., Academic Press, New York, 1967, pp. 695-708.

[27] Parmer, J.F., Stipandic, E.L., "Thermal Control Characteristics of a Diffuse Bladed, Specular Base Louver System", AIAA Paper No. 68-764, June 1968.

[28] Plamondon, J.A., "Analysis of Movable Louvers for Temperature Control", Journal of Spacecraft and Rockets, Vol. 1, No. 5, Sep.-Oct. 1964, pp. 492-497.

[29] Redor, J.F., "Performance on the ESRO Louver Array", Working Paper No. 686, May 1972, ESTEC, Noordwijk.

[30] Reusser, P.U., Coebergh, J.A.F., Meister, J., "Development of a High Performing Actuation System for a Louver Array for Satellite", Reusser Engineers and Management Consultants, Meilen-Zurich, Switzerland, April 1973.

[31] Rosenberg, M.J., "Thermal Considerations of Spacecraft External Panel Effects on Specular Louver Systems", AIAA Paper No. 69-26, Jan. 1969.

[32] Russell, L.W., Linton, R.C., "Experimental Studies of the Pegasus Thermal Control Louver System", in "Progress in Astronautics and Aeronautics", Vol. 20, G.B. Heller, Ed., Academic Press, New York, 1967, pp. 709-724.

[33] Shyffer, B., Shev, O., Brown, T., Lewis, D.W., "Mariner Mars 1969 Solar Panel Effect on Louver Assembly Thermal Performance", JPL, Pasadena, Cal., July 1968.

[34] Stern, H.J., "Rubber: Natural and Synthetic", Maclaren & Sons, Ltd., London, 1954, pp. 91-99.

[35] THE MOND NICKEL Co., "The Physical Properties of the Nickel-Iron Alloys", The Mond Nickel Co., Ltd., Sunderland House, Curzon St., London, W.I.

[36] TRW, "Bellows. -Aerospace Fluid Component Designers' Handbook", Technical Documentary Report No. R.PL-TDR-64-25, TRW-Systems Group, Feb. 1970.

[37] Trylinski, W., "Fine Mechanisms and Precission Instruments", Translated from the Polish by A. Voellnagel, Pergamon Press, Oxford, 1971, pp. 189-221.

[38] WIGGIN & Co., "Nimonic Alloys, Physical and Mechanical Properties", Publication No. 3270, Henry Wiggin & Co., Ltd., Hereford, England, March 1967, p. C3.

[39] Zapffe, C.A., "Wrought Stainless Steels", in "Metals Handbook, Properties and Selection of Metals", 8th Ed., T. Lyman Ed., American Society for Metals (ASM), Cleveland, Ohio, 1961, pp. 422-423.